THE EUROPEAN
PHYSICAL JOURNAL C

CrossMark

Regular Article - Experimental Physics

Search for new phenomena in events containing a same-flavour opposite-sign dilepton pair, jets, and large missing transverse momentum in $\sqrt{s} = 13$ TeV pp collisions with the ATLAS detector

ATLAS Collaboration[*]

CERN, 1211 Geneva 23, Switzerland

Abstract Two searches for new phenomena in final states containing a same-flavour opposite-sign lepton (electron or muon) pair, jets, and large missing transverse momentum are presented. These searches make use of proton–proton collision data, collected during 2015 and 2016 at a centre-of-mass energy $\sqrt{s} = 13$ TeV by the ATLAS detector at the large hadron collider, which correspond to an integrated luminosity of 14.7 fb^{-1}. Both searches target the pair production of supersymmetric particles, squarks or gluinos, which decay to final states containing a same-flavour opposite-sign lepton pair via one of two mechanisms: a leptonically decaying Z boson in the final state, leading to a peak in the dilepton invariant-mass distribution around the Z boson mass; and decays of neutralinos (e.g. $\tilde{\chi}_2^0 \rightarrow \ell^+\ell^-\tilde{\chi}_1^0$), yielding a kinematic endpoint in the dilepton invariant-mass spectrum. The data are found to be consistent with the Standard Model expectation. Results are interpreted in simplified models of gluino-pair (squark-pair) production, and provide sensitivity to gluinos (squarks) with masses as large as 1.70 TeV (980 GeV).

Contents

1 Introduction

Supersymmetry (SUSY) [1–7] is an extension of the Standard Model (SM) that introduces partner particles (called *sparticles*) that differ by half a unit of spin from their SM counterparts. The squarks ($\tilde{q}$) and sleptons ($\tilde{\ell}$) are the scalar partners of the quarks and leptons, respectively, and the gluinos ($\tilde{g}$) are the fermionic partners of the gluons. The charginos ($\tilde{\chi}_i^{\pm}$) and neutralinos ($\tilde{\chi}_i^0$) are the mass eigenstates (where the index i is ordered from the lightest to the heaviest) formed from the linear superpositions of the SUSY partners of the Higgs bosons (higgsinos) and electroweak gauge bosons.

If the masses of the gluino, higgsinos, and top squarks are close to the TeV scale, SUSY may offer a solution to the SM hierarchy problem [8–11]. In this case, strongly interacting sparticles should be produced at a high enough rate to be detected by the experiments at the large hadron collider (LHC). For models with R-parity conservation [12], such sparticles would be pair-produced and are expected to decay into jets, perhaps leptons, and the lightest stable SUSY particle (LSP). The LSP is assumed to be only weakly interacting and therefore escapes the detector, resulting in events with potentially large missing transverse momentum (p_T^{miss}, with magnitude E_T^{miss}). In such a scenario the LSP could be a dark-matter candidate [13,14].

[*] e-mail: atlas.publications@cern.ch

Springer

Final states containing pairs of leptons may arise from the cascade decays of squarks and gluinos via several mechanisms. In this paper, two search channels are considered that target scenarios with same-flavour (SF) opposite-sign (OS) lepton (electron or muon) pairs. The first channel requires a lepton pair with an invariant mass $m_{\ell\ell}$ that is consistent with the Z boson mass m_Z ("on-shell Z" channel), while the second channel considers all SFOS lepton pairs ("edge" channel). The presence of two leptons in the final state suppresses large SM backgrounds from, e.g., QCD multijet and W + jets production, providing a clean environment in which to search for new physics. As discussed further below, in such events the distribution of dilepton mass $m_{\ell\ell}$ may be used to characterise the nature of the SUSY particle decay and constrain mass differences between SUSY particles.

The SFOS lepton pairs may be produced in the decay $\tilde{\chi}_2^0 \rightarrow \ell^+\ell^-\tilde{\chi}_1^0$ (or, in models of generalised gauge mediation with a gravitino LSP [15–17], via $\tilde{\chi}_1^0 \rightarrow \ell^+\ell^-\tilde{G}$). The properties of the $\tilde{\chi}_2^0$ decay depend on the mass difference $\Delta m_\chi \equiv m_{\tilde{\chi}_2^0} - m_{\tilde{\chi}_1^0}$, the mixing of the charginos and neutralinos, and on whether there are additional sparticles with masses less than $m_{\tilde{\chi}_2^0}$ that may be produced in the decay of the $\tilde{\chi}_2^0$ particle. For $\Delta m_\chi > m_Z$, SFOS lepton pairs may be produced in the decay $\tilde{\chi}_2^0 \rightarrow Z\tilde{\chi}_1^0 \rightarrow \ell^+\ell^-\tilde{\chi}_1^0$, leading to a peak in the invariant-mass distribution near $m_{\ell\ell} \approx m_Z$. Such models are the target of the on-shell Z search. For $\Delta m_\chi < m_Z$, the decay $\tilde{\chi}_2^0 \rightarrow Z^*\tilde{\chi}_1^0 \rightarrow \ell^+\ell^-\tilde{\chi}_1^0$ leads to a rising $m_{\ell\ell}$ distribution that is truncated at a kinematic endpoint, whose position is given by $m_{\ell\ell}^{\max} = \Delta m_\chi < m_Z$, below the Z boson mass peak. If there are sleptons with masses less than $m_{\tilde{\chi}_2^0}$, the $\tilde{\chi}_2^0$ particle may decay as $\tilde{\chi}_2^0 \rightarrow \tilde{\ell}^\pm\ell^\mp \rightarrow \ell^+\ell^-\tilde{\chi}_1^0$, also leading to a kinematic endpoint but with a different shape and $m_{\ell\ell}$ endpoint position, given by $m_{\ell\ell}^{\max} = \sqrt{(m_{\tilde{\chi}_2^0}^2 - m_{\tilde{\ell}}^2)(m_{\tilde{\ell}}^2 - m_{\tilde{\chi}_1^0}^2)/m_{\tilde{\ell}}^2}$, which may occur below, on, or above the Z boson mass peak. The latter two scenarios are targeted by the "edge" search channel, which considers the full $m_{\ell\ell}$ range.

This paper reports on a search for SUSY in the same-flavour dilepton final state with 14.7 fb^{-1} of pp collision data at $\sqrt{s} = 13$ TeV recorded in 2015 and 2016 by the ATLAS detector at the LHC. Searches for SUSY in the Z + jets + E_T^{miss} final state have previously been performed at $\sqrt{s} = 8$ TeV by the CMS [18,19] and ATLAS [20] collaborations using Run-1 LHC data. In the ATLAS analysis performed with 20.3 fb^{-1} of $\sqrt{s} = 8$ TeV data reported in Ref. [20], an excess of events above the SM background with a significance of 3.0 standard deviations was observed. The event selection criteria for the on-shell Z search in this paper are almost identical, differing only in the details of the analysis object definitions and missing transverse momentum. CMS performed

a search with $\sqrt{s} = 13$ TeV data in a similar kinematic region but did not observe evidence to corroborate this excess [21].

Searches for an edge in the $m_{\ell\ell}$ distribution in events with 2ℓ + jets + E_T^{miss} have been performed by the CMS [19,22] and ATLAS [20] collaborations. In Ref. [19], CMS reported an excess above the SM prediction with a significance of 2.6 standard deviations. In a similar search region, however, the Run-1 ATLAS analysis [20] and Run-2 CMS analysis [21] observed results consistent with the SM prediction.

2 ATLAS detector

The ATLAS detector [23] is a general-purpose detector with almost 4π coverage in solid angle.[1] The detector comprises an inner tracking detector, a system of calorimeters, and a muon spectrometer.

The inner tracking detector (ID) is immersed in a 2 T magnetic field provided by a superconducting solenoid and allows charged-particle tracking out to $|\eta| = 2.5$. It includes silicon-pixel and silicon-strip tracking detectors inside a straw-tube tracking detector. In 2015 the detector received a new innermost layer of silicon pixels, which improves the track impact parameter resolution by almost a factor of two in both the transverse and longitudinal directions [24].

High-granularity electromagnetic and hadronic calorimeters cover the region $|\eta| < 4.9$. All the electromagnetic calorimeters, as well as the endcap and forward hadronic calorimeters, are sampling calorimeters with liquid argon as the active medium and lead, copper, or tungsten as the absorber. The central hadronic calorimeter is a sampling calorimeter with scintillator tiles as the active medium and steel as the absorber.

The muon spectrometer uses several detector technologies to provide precision tracking out to $|\eta| = 2.7$ and triggering in $|\eta| < 2.4$, making use of a system of three toroidal magnets.

The ATLAS detector incorporates a two-level trigger system, with the first level implemented in custom hardware and the second level implemented in software. This trigger system selects events of interest at an output rate of about 1 kHz.

---

[1] ATLAS uses a right-handed coordinate system with its origin at the nominal interaction point (IP) in the centre of the detector and the z-axis along the beam pipe. The x-axis points from the IP to the centre of the LHC ring, and the y-axis points upward. Cylindrical coordinates (r, ϕ) are used in the transverse plane, ϕ being the azimuthal angle around the z-axis. The pseudorapidity is defined in terms of the polar angle θ as $\eta = -\ln\tan(\theta/2)$ and the rapidity is defined as $y = 1/2 \cdot \ln[(E + p_z)/(E - p_z)])$, where E is the energy and p_z the longitudinal momentum of the object of interest. The opening angle between two analysis objects in the detector is defined as $\Delta R = \sqrt{(\Delta y)^2 + (\Delta\phi)^2}$.
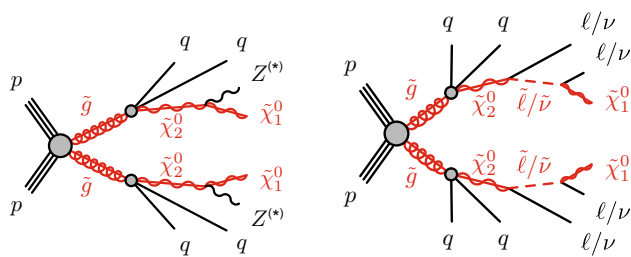
Fig. 1 Example decay topologies for two of the simplified models considered, involving gluino-pair production, with the gluinos following an effective three-body decay for $\tilde{g} \to q\bar{q}\tilde{\chi}_2^0$, with $\tilde{\chi}_2^0 \to Z^{(*)}\tilde{\chi}_1^0$ (*left*) and $\tilde{\chi}_2^0 \to \tilde{\ell}^{\mp}\ell^{\pm}/\tilde{\nu}\nu$ (*right*). For simplicity, no distinction is made between particles and antiparticles

3 SUSY signal models

SUSY-inspired simplified models are considered as signal scenarios for these analyses. In all of these models, squarks or gluinos are directly pair-produced, decaying via an intermediate neutralino, $\tilde{\chi}_2^0$, into the LSP ($\tilde{\chi}_1^0$). All sparticles not directly involved in the decay chains considered are effectively decoupled. Two example decay topologies are shown in Fig. 1. For all models with gluino-pair production, a three-body decay for $\tilde{g} \to q\bar{q}\tilde{\chi}_2^0$ is used. Signal models are generated in a grid over a two-dimensional space, varying the gluino or squark mass and the mass of either the $\tilde{\chi}_2^0$ or the $\tilde{\chi}_1^0$.

Three models, one with squark-pair production and two with gluino-pair production, which result exclusively in events with two on-shell Z bosons in the final state are considered for the on-shell search. For two of these models, signal mass points are generated across the $\tilde{g}-\tilde{\chi}_2^0$ (or $\tilde{q}-\tilde{\chi}_2^0$) plane. These models are produced following the decays $\tilde{g} \to q\bar{q}\tilde{\chi}_2^0$ or $\tilde{q} \to q\tilde{\chi}_2^0$, with the $\tilde{\chi}_1^0$ (LSP) mass set to 1 GeV, inspired by SUSY scenarios with a low-mass LSP (e.g. generalised gauge mediation). These two models are referred to here as the $\tilde{g}-\tilde{\chi}_2^0$ on-shell and $\tilde{q}-\tilde{\chi}_2^0$ on-shell grids, respectively, and are summarised in Table 1. The third model is based on MSSM-inspired topologies [25–27] with potentially higher mass LSPs. Signal points are generated

across the $\tilde{g}-\tilde{\chi}_1^0$ plane, and this model is thus referred to as the $\tilde{g}-\tilde{\chi}_1^0$ on-shell grid. In this case the $\tilde{\chi}_2^0$ mass is set to be 100 GeV above the $\tilde{\chi}_1^0$ mass, which in many models maximises the branching fraction of the $\tilde{\chi}_2^0$ decay to Z bosons. For the two models with gluino-pair production, since the gluino coupling to $q\tilde{q}$ is flavour independent and the corresponding flavours of squarks are assumed to be mass degenerate, the branching fractions for $q = u, d, c, s$ are each 25%. Other ATLAS searches are dedicated to final states with two leptons and heavy flavour jets [28,29]. For the model involving squark-pair production, the superpartners of the u, d, c and s quarks have the same mass, with the superpartners of the b and t quarks being decoupled.

The edge search considers two scenarios, both of which involve the direct pair production of gluinos and differ by the decay mode of the $\tilde{\chi}_2^0$. These signal models are also summarised in Table 1. In the $Z^{(*)}$ model the $\tilde{\chi}_2^0$ decays as $\tilde{\chi}_2^0 \to Z^{(*)}\tilde{\chi}_1^0$. For $\Delta m_\chi = m(\tilde{\chi}_2^0) - m(\tilde{\chi}_1^0) > m_Z$, the Z boson is on-shell, leading to a peak in the $m_{\ell\ell}$ distribution at m_Z, while for $\Delta m_\chi < m_Z$, the Z boson is off-shell, leading to an edge in the dilepton mass distribution with a position below m_Z. The slepton model assumes that the sleptons are lighter than the $\tilde{\chi}_2^0$, which decays as $\tilde{\chi}_2^0 \to \tilde{\ell}^{\mp}\ell^{\pm}$ with $\tilde{\ell} \to \ell\tilde{\chi}_1^0$ or as $\tilde{\chi}_2^0 \to \tilde{\nu}\nu$ with $\tilde{\nu} \to \nu\tilde{\chi}_1^0$, each with a branching fraction of 50%, where $\tilde{\ell} = \tilde{e}, \tilde{\mu}, \tilde{\tau}$ and $\tilde{\nu} = \tilde{\nu}_e, \tilde{\nu}_\mu, \tilde{\nu}_\tau$. The endpoint position can occur at any mass, highlighting the need to search over the full dilepton mass distribution. The gluino decays as $\tilde{g} \to q\bar{q}\tilde{\chi}_2^0$, and both models have equal branching fractions for $q = u, d, c, s, b$. The $\tilde{\chi}_2^0$ mass is set to the average of the gluino and $\tilde{\chi}_1^0$ masses. For the slepton model, the masses of the superpartners of the left-handed leptons are set as the average of the $\tilde{\chi}_2^0$ and $\tilde{\chi}_1^0$ masses, while the superpartners of the right-handed leptons are decoupled. The three slepton flavours are mass-degenerate. In both these models the $\tilde{g}$ and $\tilde{\chi}_1^0$ masses are free parameters that are varied to produce the two-dimensional signal grid. The mass splittings are chosen to maximise the differences between these simplified models and other models with only one intermediate particle between the gluino and the LSP [30].

Table 1 Summary of the simplified signal model topologies used in this paper. Here x and y denote the $x-y$ plane across which the signal model masses are varied to construct the signal grid. For the slepton model, the masses of the superpartners of the left-handed leptons are given by $[m(\tilde{\chi}_2^0)+m(\tilde{\chi}_1^0)]/2$, while the superpartners of the right-handed leptons are decoupled

Model	Production mode	Quark flavours	$m(\tilde{g})/m(\tilde{q})$	$m(\tilde{\chi}_2^0)$	$m(\tilde{\chi}_1^0)$
$\tilde{g}-\tilde{\chi}_2^0$ on-shell	$\tilde{g}\tilde{g}$	u, d, c, s	x	y	1 GeV
$\tilde{g}-\tilde{\chi}_1^0$ on-shell	$\tilde{g}\tilde{g}$	u, d, c, s	x	$m(\tilde{\chi}_1^0) + 100$ GeV	y
$\tilde{q}-\tilde{\chi}_2^0$ on-shell	$\tilde{q}\tilde{q}$	u, d, c, s	x	y	1 GeV
$Z^{(*)}$	$\tilde{g}\tilde{g}$	u, d, c, s, b	x	$[m(\tilde{g}) + m(\tilde{\chi}_1^0)]/2$	y
slepton	$\tilde{g}\tilde{g}$	u, d, c, s, b	x	$[m(\tilde{g}) + m(\tilde{\chi}_1^0)]/2$	y

4 Data and Monte Carlo samples

The data used in this analysis were collected by ATLAS during 2015 and 2016, with a mean number of additional pp interactions per bunch crossing (*pile-up*) of approximately 14 in 2015 and 21 in 2016, and a centre-of-mass collision energy of 13 TeV. Following requirements based on beam and detector conditions and data quality, the data set corresponds to an integrated luminosity of 14.7 fb^{-1}. The uncertainty in the combined 2015 and 2016 integrated luminosity is $\pm 2.9\%$. It is derived, following a methodology similar to that detailed in Refs. [31] and [32], from a preliminary calibration of the luminosity scale using x–y beam-separation scans performed in August 2015 and May 2016.

Data events are collected using a combination of single-lepton and dilepton triggers [33], in order to maximise the signal acceptance. The dielectron, dimuon, and electron–muon triggers have leading-lepton p_T thresholds in the range 12–24 GeV. Additional single-electron (single-muon) triggers are also used, with trigger p_T thresholds of 60 (50) GeV, to increase the trigger efficiency for models with high-p_T leptons. Events are required to contain at least two selected leptons with $p_T > 25$ GeV, making the selection fully efficient with respect to the trigger p_T thresholds.

An additional control sample of events containing photons is collected using a set of single-photon triggers with p_T thresholds in the range 20–140 GeV. All triggers except for the one with threshold $p_T = 120$ GeV in 2015, or the one with $p_T = 140$ GeV in 2016, are prescaled. Events are required to contain a selected photon with $p_T > 37$ GeV, so that they are selected efficiently by the lowest available p_T trigger in 2015, which had a threshold of $p_T^\gamma = 35$ GeV.

Simulated event samples are used to aid in the estimation of SM backgrounds, validate the analysis techniques, optimise the event selection, and provide predictions for SUSY signal processes. All SM background samples used are listed in Table 2, along with the parton distribution function (PDF) set, the configuration of underlying-event and hadronisation parameters (underlying-event tune) and the cross-section calculation order in α_S used to normalise the event yields for these samples.

Samples simulated using MG5_AMC@NLO v2.2.2 [34], interfaced with PYTHIA 8.186 [35] with the A14 underlying-event tune [36] to simulate the parton shower and hadronisation, are generated at leading order in α_S (LO) with the NNPDF23LO PDF set [37]. For samples generated using POWHEG BOX V2 [38–40], PYTHIA 6.428 [41] is used to simulate the parton shower, hadronisation, and the underlying event. The CTEQ6L1 PDF set is used with the corresponding PERUGIA2012 [42] tune. In the case of both the MG5_AMC@NLO and POWHEG samples, the EVTGEN v1.2.0 program [43] is used for properties of the bottom and charm hadron decays. SHERPA 2.1.1 [44] simulated samples use the CT10 PDF set with SHERPA's own internal parton shower [45] and hadronisation methods, as well as the SHERPA default underlying-event tune. Diboson processes with four charged leptons, three charged leptons and a neutrino or two charged leptons and two neutrinos are simulated using the SHERPA 2.1.1 generator. Matrix elements contain all diagrams with four electroweak vertices. They are calculated for up to one (4ℓ, $2\ell + 2\nu$) or zero ($3\ell + 1\nu$) partons at next-to-leading order in α_S (NLO) and up to three partons at LO using the Comix [46] and OpenLoops [47] matrix element generators and merged with the SHERPA parton shower using the ME+PS@NLO prescription [48]. For the Z/γ^* + jets background, SHERPA 2.1.1 is used to generate a sample with up to two additional partons at NLO and up to four at LO. For Monte Carlo (MC) closure studies, γ + jets events are generated at LO with up to four additional partons using SHERPA 2.1.1. Additional MC simulation samples of events with a leptonically decaying vector boson and photon ($V\gamma$, where $V = W, Z$) are generated at LO using SHERPA 2.1.1. Matrix elements including all diagrams with three electroweak couplings are calculated with up to three partons. These samples are used to estimate backgrounds with real E_T^{miss} in γ + jets event samples.

Table 2 Simulated background event samples used in this analysis with the corresponding matrix element and parton shower generators, cross-section order in α_S used to normalise the event yield, underlying-event tune and PDF set

Physics process	Generator	Parton shower	Cross section	Tune	PDF set
$t\bar{t} + W$ and $t\bar{t} + Z$ [60,61]	MG5_AMC@NLO	PYTHIA 8.186	NLO [62,63]	A14	NNPDF23LO
$t\bar{t} + WW$ [60]	MG5_AMC@NLO	PYTHIA 8.186	LO [34]	A14	NNPDF23LO
$t\bar{t}$ [64]	POWHEG BOX V2 r3026	PYTHIA 6.428	NNLO+NNLL [65,66]	PERUGIA2012	NLO CT10
Single-top (Wt) [64]	POWHEG BOX V2 r2856	PYTHIA 6.428	Approx. NNLO [67]	PERUGIA2012	NLO CT10
WW, WZ and ZZ [68]	SHERPA 2.1.1	SHERPA 2.1.1	NLO [69,70]	SHERPA default	NLO CT10
$Z/\gamma^*(\to \ell\ell)$ + jets [71]	SHERPA 2.1.1	SHERPA 2.1.1	NNLO [72,73]	SHERPA default	NLO CT10
γ + jets	SHERPA 2.1.1	SHERPA 2.1.1	LO [44]	SHERPA default	NLO CT10
$V(= W, Z)\gamma$	SHERPA 2.1.1	SHERPA 2.1.1	LO [44]	SHERPA default	NLO CT10

The SUSY signal samples are produced at LO using MG5_AMC@NLO with the NNPDF2.3LO PDF set, interfaced with PYTHIA 8.186. The scale parameter for CKKW-L matching [49,50] is set at a quarter of the mass of the gluino. Up to one additional parton is included in the matrix element calculation. The underlying event is modelled using the A14 tune for all signal samples, and EVTGEN is adopted to describe the properties of bottom and charm hadron decays. Signal cross sections are calculated at NLO in α_S. This includes the resummation of soft gluon emission at next-to-leading-logarithm accuracy (NLO+NLL) [51–55].

All of the SM background MC samples are subject to a full ATLAS detector simulation [56] using GEANT4 [57]. A fast simulation [56], which uses a combination of a parameterisation of the response of the ATLAS electromagnetic and hadronic calorimeters and GEANT4, is used in the case of signal MC samples. This fast simulation is validated by comparing a few chosen signal samples to some fully simulated points. Minimum-bias interactions are generated and overlaid on the hard-scattering process to simulate the effect of multiple pp interactions occurring during the same (in-time) or a nearby (out-of-time) bunch-crossing (pile-up). These are produced using PYTHIA 8.186 with the A2 tune [58] and MSTW 2008 PDF set [59]. The pile-up distribution in MC samples is simulated to match that in data during 2015 and 2016 pp data-taking.

5 Analysis object identification and selection

All analysis objects are categorised as either "baseline" or "signal" based on various quality and kinematic requirements. *Baseline* objects are used in the calculation of missing transverse momentum and to disambiguate between the analysis objects in the event, while the jets and leptons entering the final analysis selection must pass more stringent *signal* requirements. The selection criteria for both the baseline and signal objects differ from the requirements used in the Run-1 ATLAS Z+jets+E_T^{miss} search reported in Ref. [20], owing to the new silicon-pixel tracking layer and significant changes to the reconstruction software since 2012 data-taking. In particular, improvements in the lepton identification criteria have reduced the background due to hadrons misidentified as electrons. The primary vertex in each event is defined as the reconstructed vertex [74] with the highest $\sum p_T^2$, where the summation includes all particle tracks with $p_T > 400$ MeV associated with the vertex.

Electron candidates are reconstructed from energy clusters in the electromagnetic calorimeter matched to ID tracks. Baseline electrons are required to have transverse energy $E_T > 10$ GeV, satisfy the "loose likelihood" criteria described in Ref. [75] and reside within the region $|\eta| < 2.47$. Signal electrons are further required to have $p_T > 25$ GeV,

satisfy the "medium likelihood" criteria of Ref. [75], and be consistent with originating from the primary vertex. The signal electrons must originate from within $|z_0 \sin \theta| = 0.5$ mm of the primary vertex along the direction of the beamline.[2] The transverse-plane distance of closest approach of the electron to the beamline, divided by the corresponding uncertainty, must be $|d_0/\sigma_{d_0}| < 5$. These electrons must also be isolated with respect to other objects in the event, according to a p_T-dependent isolation requirement. The isolation uses calorimeter- and track-based information to obtain 95% efficiency at $p_T = 25$ GeV, rising to 99% efficiency at $p_T = 60$ GeV.

Baseline muons are reconstructed from either ID tracks matched to muon segments (collections of hits in a single muon spectrometer layer) or combined tracks formed from the ID and muon spectrometer [76]. They must satisfy the "medium" selection criteria described in Ref. [76], and to satisfy $p_T > 10$ GeV and $|\eta| < 2.5$. Signal muon candidates are further required to have $p_T > 25$ GeV, be isolated, and have $|z_0 \sin \theta| < 0.5$ mm and $|d_0/\sigma_{d_0}| < 3$. Calorimeter- and track-based isolation criteria are used to obtain 95% efficiency at $p_T = 25$ GeV, rising to 99% efficiency at $p_T = 80$ GeV [76]. Further, the relative uncertainties in the q/p of each of the ID track alone and muon spectrometer track alone are required to be less than 80% of the uncertainty in the q/p of the combined track. This reduces the already low rate of grossly mismeasured muons. The combined isolation and identification efficiency for single leptons, after the trigger requirements, is about 70% (80%) for electrons (muons) with $p_T \sim 25$ GeV, rising to about 90% for $p_T > 200$ GeV.

Jets are reconstructed from topological clusters of energy [77] in the calorimeter using the anti-k_t algorithm [78,79] with a radius parameter of 0.4. Calibration corrections are applied to the jets based on a comparison to jets made of stable particles (those with lifetimes $\tau > 0.3 \times 10^{-10}$ s) in the MC simulation. A residual correction is applied to jets in data, based on studies of p_T balance between jets and well-calibrated objects in the MC simulation and data [80,81]. Baseline jet candidates are required to have $p_T > 20$ GeV and reside within the region $|\eta| < 4.5$. Signal jets are further required to satisfy $p_T > 30$ GeV and reside within the region $|\eta| < 2.5$. Jets with $p_T < 60$ GeV and $|\eta| < 2.4$ must meet additional criteria designed to select jets from the hard-scatter interaction and reject those originating from pile-up. This is enforced by using the jet vertex tagger described in Ref. [82]. Finally, events containing a jet that does not pass specific jet quality requirements are vetoed from the analysis selection in order to remove events impacted by detector noise and

---

[2] The distance of closest approach between a particle object and the primary vertex (beamline) in the longitudinal (transverse) plane is denoted by z_0 (d_0).

non-collision backgrounds [83,84]. The MV2c10 boosted decision tree algorithm [85,86] identifies jets with $|\eta| < 2.5$ containing b-hadrons (b-jets) based on quantities such as the impact parameters of associated tracks and any reconstructed secondary vertices. A selection that provides 77% efficiency for tagging b-jets in simulated $t\bar{t}$ events is used. These tagged jets are called b-tagged jets.

Photon candidates must satisfy "tight" selection criteria described in Ref. [87], have $p_T > 25$ GeV and reside within the region $|\eta| < 2.37$, excluding the transition region $1.37 < |\eta| < 1.6$ where there is a discontinuity in the calorimeter. Signal photons are further required to have $p_T > 37$ GeV and to be isolated from other objects in the event, using p_T-dependent requirements on both track- and calorimeter-based isolation.

To avoid the duplication of analysis objects in more than one baseline selection, an overlap removal procedure is applied. Any baseline jet within $\Delta R = 0.2$ of a baseline electron is removed, unless the jet is b-tagged, in which case the electron is identified as originating from a heavy-flavour decay and is removed instead. Remaining electrons residing within $\Delta R = 0.4$ of a baseline jet are then removed from the event. Subsequently, any baseline muon residing within $\Delta R = 0.2$ of a remaining baseline b-tagged jet is discarded. If such a jet is not b-tagged then the jet is removed instead. Any remaining muon found within $\min(0.04 + (10\text{ GeV})/p_T, 0.4)$ of a jet is also discarded. This stage of the overlap removal procedure differs from that used in Ref. [20]. It was improved to retain muons near jet candidates mostly containing calorimeter energy from final-state radiation from muons, while still rejecting muons from heavy-flavour decays. Finally, to remove electron candidates originating from muon bremsstrahlung, any baseline electron within $\Delta R = 0.01$ of any remaining baseline muon is removed from the event. Photons are removed if they reside within $\Delta R = 0.4$ of a baseline electron, and any jet within $\Delta R = 0.4$ of any remaining photon is discarded.

The E_T^{miss} is defined as the magnitude of the negative vector sum, $\boldsymbol{p}_T^{miss}$, of the transverse momenta of all baseline electrons, muons, jets, and photons [88,89]. Low-momentum contributions from particle tracks from the primary vertex that are not associated with reconstructed analysis objects are included in the calculation of E_T^{miss}. This contribution to the E_T^{miss} is referred to as the "soft term".

Models with large hadronic activity are targeted by placing additional requirements on the quantity H_T, defined as the scalar sum of the p_T values of all signal jets, or on H_T^{incl}, the scalar sum of the p_T values of all signal jets and the two leptons with largest p_T.

All MC samples have correction factors applied to take into account small differences between data and MC simulation in identification, reconstruction and trigger efficiencies

for leptons. The p_T values of leptons in MC samples are additionally smeared to match the momentum resolution in data.

6 Event selection

For each search channel, signal regions (SRs) are designed to target events from specific SUSY signal models. Control regions (CRs) are defined to be depleted in SUSY signal events and enriched in specific SM backgrounds, and they are used to assist in estimating these backgrounds in the SRs. To validate the background estimation procedures, various validation regions (VRs) are defined to be analogous to the CRs and SRs, but with less stringent requirements than the SRs on E_T^{miss}, H_T^{incl} or H_T. Other VRs with additional requirements on the number of leptons are used to validate the modelling of backgrounds in which more than two leptons are expected.

Events in SRs are required to contain at least two signal leptons (electrons or muons). If more than two signal leptons are present in a given event, the selection process continues based on the two leptons with the highest p_T values in the event.

The selected events must pass at least one of the leptonic triggers. If an event is selected by a dilepton trigger, the two leading, highest p_T, leptons must be matched to one of the objects that triggered the event. These leptons must also have p_T higher than the threshold of the trigger in question. For events selected by a single-lepton trigger, at least one of the two leading leptons must be matched to the trigger object in the same way. The leading two leptons in the event must have $p_T > 25$ GeV, and form an SFOS pair.

As at least two jets are expected in all signal models studied, selected events are further required to contain at least two signal jets. Furthermore, events in which the azimuthal opening angle between either of the leading two jets and the E_T^{miss} satisfies $\Delta\phi(\text{jet}_{12}, \boldsymbol{p}_T^{miss}) < 0.4$ are rejected so as to remove events with E_T^{miss} from jet mismeasurements. This requirement also suppresses $t\bar{t}$ events in which the top quark, the anti-top quark, or the entire $t\bar{t}$ system has a large Lorentz boost.

The various methods used predict the background in the SRs are discussed in Sect. 7. The selection criteria for the CRs, VRs, and SRs are summarised in Tables 3 and 4. The most important of these regions are shown graphically in Fig. 2.

For the on-shell Z search, the leading-lepton p_T threshold is raised to 50 GeV to increase the sensitivity to signal models with final-state Z bosons. This is an increased leading-lepton p_T threshold relative to Ref. [20] and is found to better reject fake-lepton candidates from misidentified jets, photon conversions and b-hadron decays, while retaining high efficiency for signal events, which tend to produce boosted Z

Table 3 Overview of all signal (SR), control (CR) and validation regions (VR) used in the on-shell Z search. The flavour combination of the dilepton pair is denoted as either "SF" for same-flavour or "DF" for different-flavour. All regions require at least two leptons, unless otherwise indicated. In the case of CRγ, VR-WZ, VR-ZZ, and VR-3L the number of leptons, rather than a specific flavour configuration, is indicated. The main requirements that distinguish the control and validation regions from the signal region are indicated in bold. The kinematic quantities used to define these regions are discussed in the text. The quantity $m_T(\ell_3, E_T^{miss})$ indicates the transverse mass formed by the E_T^{miss} and the lepton which is not assigned to either of the Z-decay leptons

On-shell Z regions	E_T^{miss} (GeV)	H_T^{incl} (GeV)	n_{jets}	$m_{\ell\ell}$ (GeV)	SF/DF	$\Delta\phi(jet_{12}, p_T^{miss})$	$m_T(\ell_3, E_T^{miss})$ (GeV)	n_b-jets
Signal region								
SRZ	>225	>600	≥2	$81 < m_{\ell\ell} < 101$	SF	>0.4	–	–
Control regions								
CRZ	**<60**	>600	≥2	$81 < m_{\ell\ell} < 101$	SF	>0.4	–	–
CR-FS	>225	>600	≥2	**$61 < m_{\ell\ell} < 121$**	**DF**	>0.4	–	–
CRT	>225	>600	≥2	**$>45, m_{\ell\ell} \notin [81, 101]$**	SF	>0.4	–	–
CRγ	–	>600	≥2	–	**0ℓ, 1γ**	–	–	–
Validation regions								
VRZ	**<225**	>600	≥2	$81 < m_{\ell\ell} < 101$	SF	>0.4	–	–
VRT	**100–200**	>600	≥2	**$>45, m_{\ell\ell} \notin [81, 101]$**	SF	>0.4	–	–
VR-S	**100–200**	>600	≥2	$81 < m_{\ell\ell} < 101$	SF	>0.4	–	–
VR-FS	**100–200**	>600	≥2	**$61 < m_{\ell\ell} < 121$**	**DF**	>0.4	–	–
VR-WZ	**100–200**	–	–	–	**3ℓ**	–	<100	0
VR-ZZ	**<100**	–	–	–	**4ℓ**	–	–	0
VR-3L	**60–100**	**>200**	≥2	$81 < m_{\ell\ell} < 101$	**3ℓ**	>0.4	–	–

Table 4 Overview of all signal (SR), control (CR) and validation regions (VR) used in the edge search. The flavour combination of the dilepton pair is denoted as either "SF" for same-flavour or "DF" for different-flavour. The charge combination of the leading lepton pairs are given as "SS" for same-sign or "OS" for opposite-sign. All regions require *at least* two leptons, with the exception of CR-real, which requires *exactly* two leptons, and the three γ CRs, which require no leptons and one photon. More details are given in the text. The main requirements that distinguish the control and validation regions from the signal regions are indicated in bold. The kinematic quantities used to define these regions are discussed in the text

Edge regions	E_T^{miss} (GeV)	H_T (GeV)	n_{jets}	$m_{\ell\ell}$ (GeV)	SF/DF	OS/SS	$\Delta\phi(\text{jet}_{12}, p_T^{\text{miss}})$	$m_{\ell\ell}$ ranges
Signal regions								
SR-low	>200	–	≥2	>12	SF	OS	>0.4	9
SR-medium	>200	>400	≥2	>12	SF	OS	>0.4	8
SR-high	>200	>700	≥2	>12	SF	OS	>0.4	7
Control regions								
CRZ-low	**<60**	–	≥2	>12	SF	OS	>0.4	–
CRZ-medium	**<60**	>400	≥2	>12	SF	OS	>0.4	–
CRZ-high	**<60**	>700	≥2	>12	SF	OS	>0.4	–
CR-FS-low	>200	–	≥2	>12	**DF**	OS	>0.4	–
CR-FS-medium	>200	>400	≥2	>12	**DF**	OS	>0.4	–
CR-FS-high	>200	>700	≥2	>12	**DF**	OS	>0.4	–
CRγ-low	–	–	≥2	–	**0ℓ, 1γ**	–		–
CRγ-medium	–	>400	≥2	–	**0ℓ, 1γ**	–		–
CRγ-high	–	>700	≥2	–	**0ℓ, 1γ**	–		–
CR-real	–	**>200**	≥2	81–101	2ℓ SF	OS	–	–
CR-fake	**<125**	–	–	**∈ [12, ∞], ∉ [81, 101](SF)**	2ℓ **SF/DF**	**SS**	–	–
Validation regions								
VR-low	**100–200**	–	≥ 2	> 12	SF	OS	>0.4	–
VR-medium	**100–200**	>400	≥2	> 12	SF	OS	>0.4	–
VR-high	**100–200**	>700	≥2	> 12	SF	OS	>0.4	–
VR-fake	**>50**	–	≥2	**∈ [12, ∞], ∉ [81, 101](SF)**	**SF/DF**	**SS**	–	–
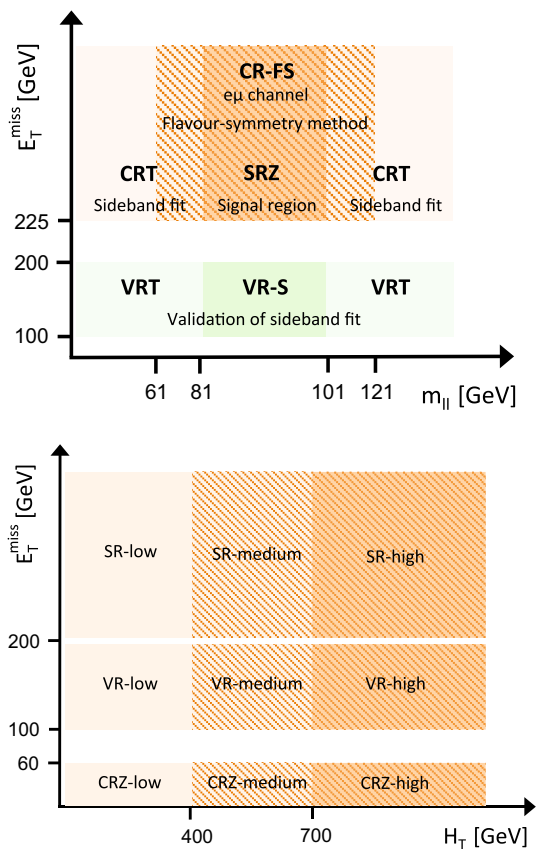
Fig. 2 Schematic diagrams of the control (CR), validation (VR) and signal regions (SR) for the on-shell Z (*top*) and edge (*bottom*) searches. For the on-shell Z search the various regions are shown in the $m_{\ell\ell}$–E_T^{miss} plane, whereas in the case of the edge search the signal and validation regions are depicted in the H_T–E_T^{miss} plane. The flavour-symmetry and sideband-fit background estimation methods are described further in Sect. 7.1

bosons. To select events containing a leptonically decaying Z boson, the invariant mass of the dilepton system is required to be $81 < m_{\ell\ell} < 101$ GeV. In the CRs and VRs that use the Z mass sidebands, only events with $m_{\ell\ell} > 45$ GeV are used to reject the lower $m_{\ell\ell}$ region dominated by Drell–Yan (DY) production. In Ref. [20] an "on-Z" SR, denoted SRZ, is defined requiring $E_T^{\text{miss}} > 225$ GeV and $H_T^{\text{incl}} > 600$ GeV. The region is motivated by SUSY signals with high gluino or squark mass and high jet activity. Since b-jets are not always expected in the simplified models considered here, no requirement is placed on b-tagged jet multiplicity ($n_{b-\text{jets}}$) so as to be as inclusive as possible and to be consistent with Ref. [20]. Dedicated CRs are defined, with selection criteria similar to those of SRZ, to estimate the contribution from the dominant SM backgrounds in SRZ. These CRs are discussed in more detail in Sect. 7.

The edge selection requires at least two leptons with $p_T > 25$ GeV. The search is performed across the full $m_{\ell\ell}$ spectrum, with the exception of the region with $m_{\ell\ell} <$

12 GeV, which is vetoed to reject low-mass DY events and the J/ψ and Υ resonances. Three regions are defined to target signal models with low, medium and high values of $\Delta m_{\tilde{g}} = m(\tilde{g}) - m(\tilde{\chi}_1^0)$, denoted SR-low, SR-medium, and SR-high, respectively. All these regions require $E_T^{\text{miss}} > 200$ GeV. SR-medium and SR-high also include the requirements $H_T > 400$ GeV and $H_T > 700$ GeV, respectively, to further isolate high-$\Delta m_{\tilde{g}}$ events. Here the leptons are not included in the H_T definition to avoid introducing any bias in the $m_{\ell\ell}$ distribution. Events selected in SR-low, SR-medium and SR-high are further grouped into non-orthogonal $m_{\ell\ell}$ windows, which represent the search regions used in the edge analysis. The dilepton mass ranges of these are chosen to maximise sensitivity to the targeted signal models, with the window boundaries being motivated by the dilepton mass endpoints of generated signal points. In total, 24 $m_{\ell\ell}$ windows are defined by selecting ranges with the best expected sensitivity to signal models. Of these windows, nine are in SR-low, eight are in SR-medium and seven are in SR-high. Details of the $m_{\ell\ell}$ definitions in these regions are given along with the results in Sect. 9. Models without light sleptons are targeted by windows with $m_{\ell\ell} < 60$ GeV or $m_{\ell\ell} < 80$ GeV for $\Delta m_{\chi} < m_Z$ leading to off-shell Z bosons, and by the window with $81 < m_{\ell\ell} < 101$ GeV for $\Delta m_{\chi} > m_Z$ leading to on-shell Z bosons. Models with light sleptons are targeted by the remaining $m_{\ell\ell}$ windows, which cover the full $m_{\ell\ell}$ range. The edge selection and on-shell Z selection are not orthogonal. In particular, SR-medium in the range $81 < m_{\ell\ell} < 101$ GeV overlaps significantly with SRZ.

For the combined $ee + \mu\mu$ channels, the typical signal acceptance times efficiency values for the signal models considered in SRZ are 2–8%. They are 8–40%, 3–35%, and 1–35%, inclusively in $m_{\ell\ell}$, for SR-low, SR-medium and SR-high, respectively. The on-shell Z and edge analyses are each optimised for different signal models. There are models in which signal contamination in CRs or VRs can become significant. For example, CRT in Table 3 is used to normalise the $t\bar{t}$ MC sample to data as a cross-check in the on-shell Z search, but it is a region where the signal contamination from signal models targeted by the edge search can be up to 80% relative to the expected background. In addition, the contamination from on-shell Z signals in the region used to validate the Z/γ^* + jets and flavour-symmetric estimates, VR-S, is up to 60% for models with $m(\tilde{g}) < 1$ TeV. The signal contamination from the slepton models in the DF regions used to estimate the flavour-symmetric backgrounds in the edge search, CR-FS-low/medium/high in Table 4, is less than 20% for models with $m(\tilde{g}) > 600$ GeV. It is only the contamination in these $e\mu$ CRs that is relevant in terms of the model-dependent interpretation of the results, and its impact is further discussed in Sect. 10. In general, for models giving substantial

contamination in the CRs, the signal-to-background ratio in the SRs is found to be large enough for this contamination to have negligible impact on the sensitivity of the search.

7 Background estimation

The dominant background processes in the SRs are "flavour-symmetric" (FS) backgrounds, where the ratio of ee, $\mu\mu$ and $e\mu$ dileptonic branching fractions is 1:1:2 because the two leptons originate from independent $W \to \ell\nu$ decays. This background is dominated by $t\bar{t}$ (50–70%) and also includes WW, Wt, and $Z \to \tau\tau$ processes. The FS background constitutes 60–90% of the expected background in the SRs, and is estimated using control samples of $e\mu$ events.

As all the SRs have a high-E_T^{miss} requirement, Z/γ^*+jets events only enter the SRs when there is large E_T^{miss} originating from instrumental effects or from neutrinos in jet fragments. This background is generally small, but it is difficult to model with MC simulation and can mimic signal, particularly for the on-shell Z search. This background is estimated using a control sample of γ + jets events in data, which are kinematically similar to Z/γ^*+jets and have similar sources of E_T^{miss}.

The production of WZ/ZZ dibosons contributes approximately 30% of the SM background in SRZ and up to 20% of the background in the edge SR $m_{\ell\ell}$ windows. These backgrounds are estimated from MC simulation, after validation in dedicated 3ℓ (WZ) and 4ℓ (ZZ) VRs. Rare top backgrounds, which include $t\bar{t}W$, $t\bar{t}Z$ and $t\bar{t}WW$ processes, constitute <5% of the expected SM background in all SRs, and are estimated from MC simulation. The contribution from events with fake or misidentified leptons is at most 15% (in one of the edge $m_{\ell\ell}$ ranges in SR-low), but is generally <5% of the expected SM background in most SRs.

7.1 Flavour-symmetric backgrounds

The flavour-symmetric background is dominant in all SRs. To estimate the contribution of this background to each SR, the so-called "flavour-symmetry" method, detailed in Ref. [20], is used. In this method, data events from a DF control sample, which is defined with the same kinematic requirements as the SR, are used to determine the expected event yields in the SF channels. In the on-shell Z analysis, the method is used to predict the background yield in the Z mass window, defined as $81 < m_{\ell\ell} < 101$ GeV. In the edge analysis, the method is extended to predict the full dilepton mass shape, such that a prediction can be extracted in any of the predefined $m_{\ell\ell}$ windows.

For the edge search, the flavour-symmetric contribution to each $m_{\ell\ell}$ bin of the signal regions is predicted using data from the corresponding bin in an $e\mu$ control region. All edge CR-FS regions (definitions can be seen in Table 4) are 88–97% pure in flavour-symmetric processes (this purity is calculated from MC simulation).

For the on-shell search, this method is complicated slightly by a widening of the $m_{\ell\ell}$ window used in CR-FS, the $e\mu$ control region (defined in Table 3). The window is enlarged to $61 < m_{\ell\ell} < 121$ GeV to approximately triple the amount of data in the control region and thus increase the statistical precision of the method. This results in a region that is ~95% pure in flavour-symmetric processes (the expected composition of this 95% is ~80% $t\bar{t}$, ~10% Wt, ~10% WW and <1% $Z \to \tau\tau$).

Apart from the $m_{\ell\ell}$ widening in CR-FS, the method used is identical for the on-shell and edge regions. Events in the control regions are subject to lepton p_T- and η-dependent correction factors measured in data and MC simulation. Because the triggers used are not identical in 2015 and 2016, these factors are measured separately for each year and account for the different identification and reconstruction efficiencies for electrons and muons, as well as the different trigger efficiencies for the dielectron, dimuon and electron–muon selections. The estimated numbers of events in the SF channels, $N_{ee/\mu\mu}^{\text{est}}$, are given by:

$$N_{ee}^{\text{est}} = \frac{1}{2} \cdot f_{\text{FS}} \cdot f_{\text{Z-mass}} \cdot \sum_i^{N_{e\mu}^{\text{data}}} k_e(p_T^{i,\mu}, \eta^{i,\mu}) \cdot \alpha(p_T^{i,\mu}, \eta^{i,\mu}),$$
(1)

$$N_{\mu\mu}^{\text{est}} = \frac{1}{2} \cdot f_{\text{FS}} \cdot f_{\text{Z-mass}} \cdot \sum_i^{N_{e\mu}^{\text{data}}} k_\mu(p_T^{i,e}, \eta^{i,e}) \cdot \alpha(p_T^{i,e}, \eta^{i,e}),$$
(2)

where $N_{e\mu}^{\text{data}}$ is the number of data events observed in a given control region, $\alpha(p_T^i, \eta^i)$ accounts for the different trigger efficiencies for SF and DF events, and $k_e(p_T^{i,\mu}, \eta^{i,\mu})$ and $k_\mu(p_T^{i,e}, \eta^{i,e})$ are electron and muon selection efficiency factors for the kinematics of the lepton being replaced, in event i. The trigger and selection efficiency correction factors are derived from the events in an inclusive on-Z selection ($81 < m_{\ell\ell} < 101$ GeV, ≥ 2 jets), according to:

$$k_e(p_T, \eta) = \sqrt{\frac{N_{ee}^{\text{meas}(p_T, \eta)}}{N_{\mu\mu}^{\text{meas}(p_T, \eta)}}}$$
(3)

$$k_\mu(p_T, \eta) = \sqrt{\frac{N_{\mu\mu}^{\text{meas}(p_T, \eta)}}{N_{ee}^{\text{meas}(p_T, \eta)}}}$$
(4)

$$\alpha(p_T, \eta) = \frac{\sqrt{\epsilon_{ee}^{\text{trig}}(p_T^{\ell_1}, \eta^{\ell_1}) \times \epsilon_{\mu\mu}^{\text{trig}}(p_T^{\ell_1}, \eta^{\ell_1})}}{\epsilon_{e\mu}^{\text{trig}}(p_T^{\ell_1}, \eta^{\ell_1})}$$
(5)

where $\epsilon_{ee/\mu\mu}^{\mathrm{trig}}$ is the trigger efficiency and $N_{ee/\mu\mu}^{\mathrm{meas}}$ is the number of $ee/\mu\mu$ events in the inclusive on-Z region outlined above. Here $k_e(p_{\mathrm{T}}, \eta)$ and $k_\mu(p_{\mathrm{T}}, \eta)$ are calculated separately for leading and sub-leading leptons, while α is calculated for the leading lepton, ℓ_1. The correction factors are typically within 10% of unity, except in the region $|\eta| < 0.1$ where, because of the lack of coverage by the muon spectrometer, they are up to 50% from unity. For all background estimates based on the flavour-symmetry method, results are computed separately for ee and $\mu\mu$ and then summed to obtain the combined predictions. The resulting estimates from the DF channels are scaled according to the fraction of flavour-symmetric backgrounds in each $e\mu$ control sample, f_{FS} (95% in CR-FS), which is determined by subtracting non-flavour-symmetric backgrounds taken from MC simulation from the data observed in the corresponding $e\mu$ region. In the on-shell case, the result is also scaled by the fraction of events in CR-FS expected to be contained within $81 < m_{\ell\ell} < 101$ GeV, $f_{Z\text{-mass}}$ (38%), which is otherwise set to 100% for the edge regions. The validity of extrapolating in $m_{\ell\ell}$ between CR-FS and SRZ was checked by comparing the $m_{\ell\ell}$ shapes in data and MC simulation in a region similar to VR-S, but with the $m_{\ell\ell}$ requirement relaxed and $H_{\mathrm{T}}^{\mathrm{incl}} > 300$ GeV to obtain a sample with a large number of events. The resulting on-Z fractions in MC simulation were found to agree with data within statistical uncertainties, which are summed in quadrature to assign a systematic uncertainty. In the case of the edge search the full $m_{\ell\ell}$ distribution is validated by applying a flavour-symmetry method to $t\bar{t}$ MC evnets in VR-low, VR-medium and VR-high. This procedure results in good closure, which is further discussed in Sect. 7.5. The difference between the prediction and the observed distribution is used to assign an MC non-closure uncertainty to the estimate.

The flavour-symmetry method in SRZ is further cross-checked by performing a profile likelihood fit [90] of MC yields to data in the Z-mass sidebands ($m_{\ell\ell} \notin [81, 101]$ GeV), the region denoted CRT in Table 3, which is dominated by $t\bar{t}$ (with a purity of $>75\%$) and contains 273 events in data. The other flavour-symmetric processes in this region contribute $\sim$12% (Wt), 10% (WW) and $<1\%$ ($Z \to \tau\tau$). All SM background processes are taken directly from MC simulation in this cross-check, including backgrounds also estimated using the flavour-symmetry method. The normalisation of the dominant $t\bar{t}$ background is a free parameter and is the only parameter affected by the fit. For this cross-check, the contamination from Beyond Standard Model processes in the Z-mass sidebands is assumed to be negligible. The fit results in a scale factor of 0.64 for the $t\bar{t}$ yield predicted by simulation. This result is extrapolated from the Z-mass sidebands to SRZ and gives a prediction of 29 ± 7 events, which is consistent with the nomi-

Table 5 Comparison of the predicted yields for the flavour-symmetric backgrounds in SRZ and VR-S as obtained from the nominal data-driven method using CR-FS and the Z-mass sideband method. The quoted uncertainties include statistical and systematic contributions

Region	Flavour-symmetry	Sideband fit
SRZ	33 ± 4	29 ± 7
VR-S	99 ± 8	92 ± 25

nal flavour-symmetry background estimate of 33 ± 4 in this region.

The sideband fit is repeated at lower $E_{\mathrm{T}}^{\mathrm{miss}}$ in VRT, with the results being propagated to VR-S, so as to test the $m_{\ell\ell}$ extrapolation used in the sideband fit method. The normalisation to data in this region, which is at lower $E_{\mathrm{T}}^{\mathrm{miss}}$ relative to CRT, results in a scale factor of 0.80 for the $t\bar{t}$ yield predicted by simulation. The number of FS events predicted in VR-S using the sideband fit in VRT is compatible with the number estimated by applying the FS method to data in VR-FS. The results of the background estimate in both VR-S and SRZ obtained from the flavour-symmetry method are compared with the values obtained by the sideband fit cross-check in Table 5. The methods result in consistent estimates in both regions. Further results in the edge VRs are discussed in Sect. 7.5.

A potential cause of the low scale factors obtained from the sideband fit at large H_{T} and $E_{\mathrm{T}}^{\mathrm{miss}}$ is mismodelling of the top-quark p_{T} distribution, where measurements of $t\bar{t}$ differential cross sections by the ATLAS and CMS experiments indicate that the top-quark p_{T} distribution predicted by most generators is harder than that observed in data [91,92]. Corrections to the MC predictions according to NNLO calculations provided in Ref. [93] indicate an improvement in the top-quark pair modelling at high H_{T}, which should lead to scale factors closer to unity. With the data-driven method used to estimate $t\bar{t}$ contributions in this analysis, the results do not depend on these corrections. They are therefore not applied to the $t\bar{t}$ MC sample for the sideband-fit cross-check.

7.2 $Z/\gamma^* +$ jets background

The $Z/\gamma^* +$ jets background estimate is based on a data-driven method that uses $\gamma +$ jets events in data to model the $E_{\mathrm{T}}^{\mathrm{miss}}$ distribution of $Z/\gamma^* +$ jets. The $\gamma +$ jets and $Z/\gamma^* +$ jets processes have similar event topologies, with a well-measured object recoiling against a hadronic system, and both tend to have $E_{\mathrm{T}}^{\mathrm{miss}}$ that stems from jet mismeasurements and neutrinos in hadronic decays. In this method, which has been used by CMS in a search in this final state [18], a sample of data events containing at least one photon and no leptons is constructed using the same kinematic selection as each of

the SRs, without the E_T^{miss} and $\Delta\phi(\mathrm{jet}_{12}, \boldsymbol{p}_T^{miss})$ requirements (the CRγ regions defined in Tables 3, 4).

The requirement $\Delta\phi(\mathrm{jet}_{12}, \boldsymbol{p}_T^{miss}) > 0.4$ applied in the SRs suppresses E_T^{miss} from jet mismeasurements and increases the relative contributions to E_T^{miss} from the photon, electrons, and muons. The difference in resolution between photons, electrons, and muons can be significant at high p_T. Therefore, before the $\Delta\phi(\mathrm{jet}_{12}, \boldsymbol{p}_T^{miss}) > 0.4$ requirement is applied, the photon p_T is smeared according to a $Z \to ee$ or $Z \to \mu\mu$ resolution function. The smearing function is derived by comparing the E_T^{miss}-projection along the boson momentum in Z/γ^* + jets and γ + jets MC events in a 1-jet control region with no other event-level kinematic requirements. A deconvolution is applied to avoid including the photon resolution in the Z resolution. For each event, a photon p_T smearing Δp_T is obtained by sampling the smearing function. The photon p_T is shifted by Δp_T, with the parallel component of the E_T^{miss} being correspondingly adjusted by $-\Delta p_T$.

The smeared γ + jets events are then reweighted to match the boson p_T distribution of the Z/γ^* + jets events. This reweighting is applied separately in each region and accounts for small differences between the γ + jets events and Z/γ^* + jets events, which arise mainly from the mass of the Z boson. The reweighting is done using Z/γ^* + jets events in data, and is checked using Z/γ^* + jets MC simulation in an MC closure test, as described further below. Following this smearing and reweighting procedure, the E_T^{miss} of each γ + jets event is recalculated, and the final E_T^{miss} distribution is obtained after applying the $\Delta\phi(\mathrm{jet}_{12}, \boldsymbol{p}_T^{miss}) > 0.4$ requirement. For each SR, the resulting E_T^{miss} distribution is normalised to data in a CRZ with the same requirements except that the SR E_T^{miss} requirement is replaced by $E_T^{miss} < 60$ GeV.

The shape of the Z/γ^* + jets $m_{\ell\ell}$ distribution is extracted from MC simulation and validated by comparing to data in events with lower E_T^{miss} requirements and a veto on b-tagged jets, to suppress the background from $t\bar{t}$. The $m_{\ell\ell}$ distribution is modelled by parameterising the $m_{\ell\ell}$ in Z/γ^* + jets events as a function of the difference between reconstructed and true Z boson p_T in MC simulation. This parameterization ensures that the correlation between lepton momentum mismeasurement and observed $m_{\ell\ell}$ values far from the Z boson mass is preserved. Each photon event is assigned an $m_{\ell\ell}$ via a random sampling of the corresponding distribution, equating photon Δp_T and the difference between true and reconstructed Z boson p_T. The resulting $m_{\ell\ell}$ distribution in γ + jets MC simulation is compared to that extracted from Z/γ^* + jets MC simulation and the difference is assessed as a systematic uncertainty in the background prediction for each $m_{\ell\ell}$ bin.

The full smearing, reweighting, and $m_{\ell\ell}$ assignment procedure is applied to the $V\gamma$ MC sample in parallel with the γ + jets data sample. After applying all corrections to both samples, the $V\gamma$ contribution to the γ + jets data sample is subtracted to remove contamination from backgrounds with real E_T^{miss}. Contamination by events with fake photons in these γ + jets data samples is small, and this contribution is therefore neglected.

In the H_T-inclusive region corresponding to VR-low, there is a non-negligible contribution expected from Z/γ^* + jets events with $p_T^Z < 37$ GeV. Given the photon trigger strategy discussed in Sect. 4, no photons with $p_T < 37$ GeV are included in the event selection. To account for this photon p_T threshold, a boson-p_T correction of up to 50% is applied as a function of E_T^{miss} in VR-low. This correction uses the fraction of Z/γ^* + jets events in a given E_T^{miss} bin expected to have $p_T^Z < 37$ GeV, according to MC simulation. The γ + jets data are then scaled according to this fraction, as a function of E_T^{miss}, to correct for the missing $p_T^Z < 37$ GeV contribution. The correction is found to be negligible in all signal regions.

The distribution of E_T^{miss} obtained in SHERPA Z/γ^* + jets MC simulation is compared to that obtained by applying this background estimation technique to SHERPA γ + jets MC samples. In this check the γ + jets MC simulation is reweighted according to the p_T distribution given by the Z/γ^* + jets MC simulation. The result of this MC closure check is shown in Fig. 3a for events in VRZ (without an upper E_T^{miss} cut), where good agreement between Z/γ^* + jets and corrected γ + jets MC simulation can be seen across the entire E_T^{miss} spectrum. A comparison between the full E_T^{miss} spectrum in data and the Z/γ^* + jets background estimated via the γ + jets method is also shown in Fig. 3b for events in VRZ. The systematic uncertainties associated with this method are described in Sect. 8.

7.3 Fake-lepton background

Semileptonic $t\bar{t}$, $W \to \ell\nu$ and single top (s- and t-channel) events enter the dilepton channels via "fake" leptons. These can include misidentified hadrons, converted photons or non-prompt leptons from b-hadron decays. The extent of this background is estimated using the matrix method, detailed in Ref. [94]. Its contribution in regions with high lepton p_T and dilepton invariant mass is negligible, but in the edge search, where lower-p_T leptons are selected and events can have low $m_{\ell\ell}$, the fake-lepton background can make up to 15% of the total background. In this method a control sample is constructed using baseline leptons, thereby enhancing the probability of selecting a fake lepton due to the looser lepton selection and identification criteria relative to the signal lepton selection. For each relevant CR, VR or SR, the region-specific kinematic requirements are placed upon this sample of baseline leptons. The number of events in this sample in which the selected leptons subsequently pass (N_{pass}) or fail (N_{fail}) the signal lepton requirements in Sect. 5 are
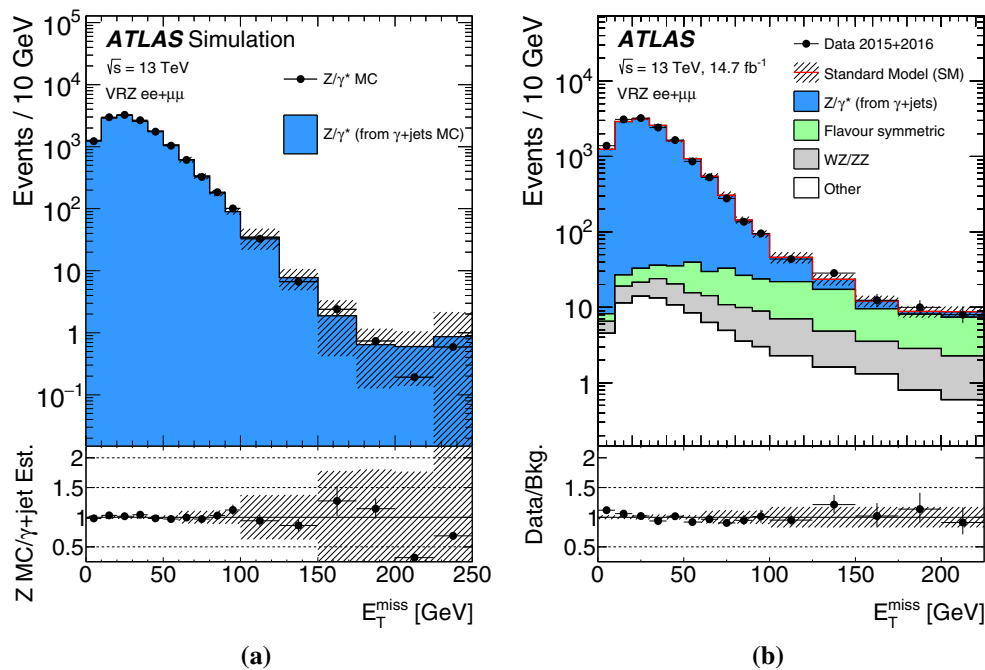
Fig. 3 *Left* the E_T^{miss} spectrum in SHERPA Z/γ^* + jets MC simulation compared to that of the γ + jets background estimation technique applied to SHERPA γ + jets MC simulation in VRZ. The *error bars* on the points indicate the statistical uncertainty of the Z/γ^* + jets MC simulation, and the *hashed uncertainty bands* indicate the statistical and reweighting systematic uncertainties of the γ+jet background method. For this MC comparison the upper E_T^{miss} cut has been removed from VRZ and the overflow is included in the rightmost bin. *Right* the E_T^{miss} spectrum when the method is applied to data in VRZ. Here the flavour-symmetric background is estimated using the data-

driven flavour-symmetry method, and the fake-lepton background is estimated using the data-driven method explained in Sect. 7.3. Rare top and diboson backgrounds are taken from MC simulation. The rare top and data-driven fake-lepton backgrounds are grouped under "other" backgrounds. The *hashed bands* indicate the systematic uncertainty of only the γ + jets and flavour-symmetric backgrounds below 100 GeV and the full uncertainty of the VR-S prediction above 100 GeV. The *bottom panel* of each figure shows the ratio of the observation (*left* in MC simulation; *right* in data) to the prediction

then counted. In the case of a one-lepton selection, the number of fake-lepton events in a given region is then estimated according to:

$$N_{pass}^{fake} = \frac{N_{fail} - (1/\epsilon^{real} - 1) \times N_{pass}}{1/\epsilon^{fake} - 1/\epsilon^{real}}. \qquad (6)$$

Here ϵ^{real} is the relative identification efficiency (from baseline to signal) for genuine, prompt ("real") leptons and ϵ^{fake} is the relative identification efficiency (again from baseline to signal) with which non-prompt leptons or jets might be misidentified as prompt leptons. This principle is then expanded to a dilepton selection by using a four-by-four matrix to account for the various possible real–fake combinations for the two leading leptons in an event.

The real-lepton efficiency, ϵ^{real}, is measured in $Z \rightarrow \ell\ell$ data events using a tag-and-probe method in CR-real, defined in Table 4. In this region the p_T of the leading lepton is required to be >40 GeV, and only events with exactly two SFOS leptons are selected. The fake-lepton efficiency, ϵ^{fake}, is measured in CR-fake, a region enriched with fake leptons by requiring same-sign lepton pairs. The lepton p_T requirements are the same as those in CR-real, with the leading

lepton being tagged as the "real" lepton and the fake efficiency being evaluated based on the sub-leading lepton in the event. An E_T^{miss} requirement of <125 GeV is used to reduce possible contamination from Beyond Standard Model processes. In this region the background due to prompt-lepton production, estimated from MC simulation, is subtracted from the total data contribution. Prompt-lepton production makes up 7% (11%) of the baseline electron (muon) sample and 10% (61%) of the signal electron (muon) sample in CR-fake. From the resulting data sample the fraction of events in which the baseline leptons pass a signal-like selection yields the fake efficiency. Both the real- and fake-lepton efficiencies are binned as a function of lepton p_T and calculated separately for the 2015 and 2016 data sets.

This method is validated by checking the closure in MC simulation and data–background agreement in VR-fake.

7.4 Diboson and rare top processes

The remaining SM background contribution in the SRs is due to WZ/ZZ diboson production and rare top processes ($t\bar{t}Z$,

Table 6 Expected and observed event yields in the four validation regions, VR-S, VR-WZ, VR-ZZ, and VR-3L. The flavour-symmetric, Z/γ^*+jets, and fake-lepton contributions to VR-S are derived using the data-driven estimates described in Sect. 7. All remaining backgrounds, and all backgrounds in the diboson validation regions, are taken from MC simulation. The quoted uncertainties in VR-S include statistical and all systematic contributions. In VR-WZ, VR-ZZ, and VR-3L, the rare top and diboson uncertainties include statistical and all theoretical uncertainties described in Sect. 8. The fake-lepton contribution in these three regions is predominantly due to Z/γ^*+jets, and in this case only the statistical uncertainty is given. The individual uncertainties can be correlated and do not necessarily add up in quadrature to the total systematic uncertainty

	VR-S	VR-WZ	VR-ZZ	VR-3L
Observed events	236	698	132	32
Total expected background events	224 ± 41	622 ± 66	139 ± 25	35 ± 10
Flavour-symmetric ($t\bar{t}$, Wt, WW, $Z \to \tau\tau$)	99 ± 8	–	–	–
WZ/ZZ events	27 ± 13	573 ± 66	139 ± 25	25 ± 10
Rare top events	11 ± 3	14 ± 3	0.44 ± 0.11	9.1 ± 2.3
Z/γ^* + jets events	84 ± 37	–	–	–
Fake-lepton events	4 ± 4	35 ± 6	–	0.6 ± 0.3

Table 7 Expected and observed event yields in the three validation regions, VR-low, VR-medium and VR-high. The quoted uncertainties include statistical and systematic contributions. The individual uncertainties can be correlated and do not necessarily add up in quadrature to the total systematic uncertainty

	VR-low	VR-medium	VR-high
Observed events	16,253	1917	314
Total expected background events	$16{,}500 \pm 700$	1990 ± 150	340 ± 60
Data-driven flavour-symmetry events	$14{,}700 \pm 600$	1690 ± 120	250 ± 50
WZ/ZZ events	250 ± 80	40 ± 19	9 ± 6
Data-driven Z/γ^* + jets (γ + jets) events	1100 ± 400	130 ± 70	50 ± 29
Rare top events	87 ± 23	27 ± 7	6.5 ± 1.8
Data-driven fake-lepton events	270 ± 100	98 ± 35	20 ± 11

$t\bar{t}W$ and $t\bar{t}WW$). The rare top processes compose <5% of the expected SM background in the SRs and are taken directly from MC simulation.

Production of WZ/ZZ dibosons constitutes about 30% of the expected background in SRZ and up to 20% in some edge SR $m_{\ell\ell}$ windows. In SRZ, this background is composed of roughly 70% WZ, about 40% of which is $WZ \to \ell\ell\tau\nu$. This is the largest background contribution that is estimated from MC simulation, and must be carefully validated, especially because these backgrounds contain Z bosons and can thus mimic a signal by producing a peak at $m_{\ell\ell} \approx m_Z$. To validate the MC modelling of these backgrounds, VRs with three leptons (VR-WZ) and four leptons (VR-ZZ) are defined (selection shown in Table 3). In VR-WZ, from the three selected leptons in an event, the SFOS pair with $m_{\ell\ell}$ most consistent with the Z mass is indentified as the Z candidate. The transverse mass of the remaining lepton and the E_T^{miss}, $m_T(\ell_3, E_T^{\mathrm{miss}})$, is then required to be <100 GeV, forming the W candidate. In VR-ZZ an $E_T^{\mathrm{miss}} < 100$ GeV requirement is used to suppress WZ and top processes. The yields and kinematic distributions observed in these regions are well-modelled by MC simulation. In particular, the E_T^{miss}, H_T, jet multiplicity, and boson p_T distributions show good agreement. An additional three-lepton VR (VR-3L) is defined to provide validation of the diboson background in a region of phase space closer to the SR; good agreement is observed in this region as well.

7.5 Results in validation regions

The expected background yields in VR-S are shown in Table 6 and compared with the observed data yield. Agreement between the data and the expected Standard Model background is observed. The expected background yields in the three diboson VRs are also shown in Table 6. The data are consistent with the expected background. Similar information for the edge VRs is provided in Table 7. Data and background estimates are in agreement within uncertainties.

Figure 4 shows the observed and expected $m_{\ell\ell}$ distributions in the same edge VRs. The same background estimation methods are applied to both MC simulation and data. In the MC studies, the flavour-symmetry method of Sect. 7.1 is applied to $t\bar{t}$ MC simulation, and the observed SF $m_{\ell\ell}$ distribution is compared to the prediction based on DF events. In the data studies, the observed SF $m_{\ell\ell}$ distribution is compared to the sum of FS backgrounds from the extended flavour-symmetry method, the Z/γ^* + jets background from the

Fig. 4 Validation of the flavour-symmetry method for the edge search using MC events (*left*) and data (*right*), in the VR-low (*top*), VR-medium (*middle*), and VR-high (*bottom*) regions. In the MC plots the flavour-symmetry estimate from $e\mu$ $t\bar{t}$ MC samples is compared with the observed SF distribution from these MC samples, with the MC statistical uncertainty indicated by the *hashed bands*. In the data plots, all uncertainties in the background prediction are included in the *hashed band*. The rare top and data-driven fake-lepton backgrounds are grouped under "other" backgrounds. The *bottom panel* of each figure shows the ratio of the observation (*left* in MC simulation; *right* in data) to the prediction. In cases where the data point is not accommodated by the scale of this *panel*, a *red arrow* indicates the direction in which the point is out of range. The last bin contains the overflow
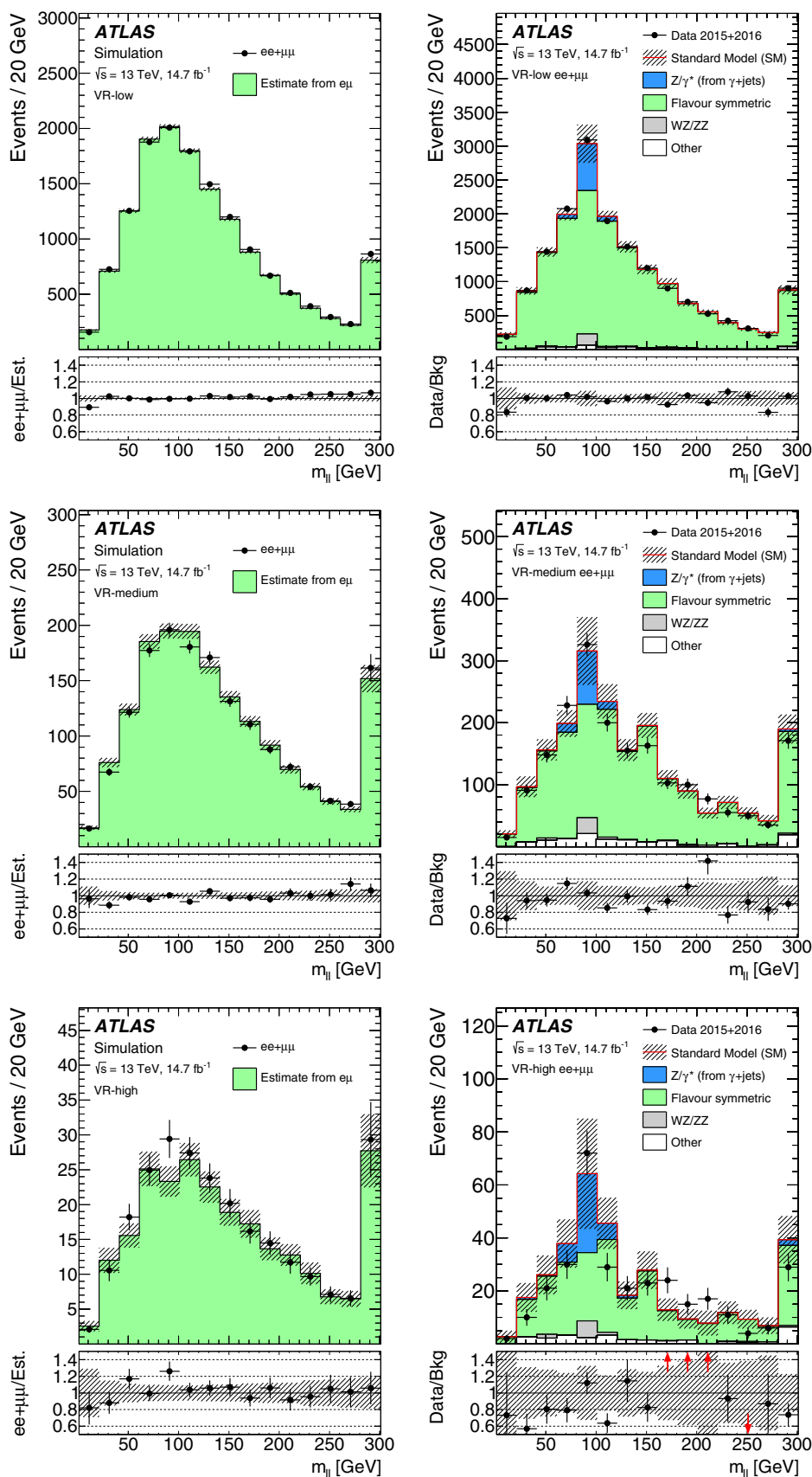
γ + jets method, and the WZ/ZZ diboson, rare top, and fake-lepton backgrounds.

The observed MC closure is good in all validation regions. The data agree with the expected background in the validation regions as well. No significant discrepancies or trends are apparent.

8 Systematic uncertainties

The data-driven background estimates are subject to uncertainties associated with the methods employed and the limited number of events used in their estimation. The dominant uncertainty (10%) for the flavour-symmetry-based background estimate in SRZ is due to the limited number of events in CR-FS. Other systematic uncertainties assigned to this background estimate include those due to MC closure (3%), the measurement of the efficiency correction factors (3%) and the extrapolation in $m_{\ell\ell}$ (1%). In the case of the edge SRs the statistical uncertainty is also the dominant uncertainty in the flavour-symmetric background estimate in the case of SR-high, but for both SR-medium and SR-low the uncertainties from the MC non-closure and efficiency correction factors are comparable in size, or in some cases larger. These uncertainties can contribute up to 5% in SR-low and SR-medium and 10% in SR-high.

Several sources of systematic uncertainty are assessed for the Z/γ^* + jets background. The boson p_{T} reweighting procedure is assigned an uncertainty based on a comparison of the nominal results with those obtained by reweighting using three other kinematic variables, namely H_{T}, Z-boson E_{T} and jet multiplicity. For the smearing function, which is measured using MC events in a 1-jet control region, an uncertainty is derived by comparing the results obtained using the nominal smearing function with those obtained using a smearing function from a 2-jet sample of MC events, and also using a smearing function measured in a 1-jet data sample. An uncertainty of between 40–100% is assigned to account for different reweighting procedures and between 20–100% for the smearing procedure applied to γ + jets events. The smearing uncertainty dominates in SR-high, while the reweighting uncertainty dominates in SR-low and SR-medium, with both being around 60% in SRZ. The full reweighting and smearing procedure is carried out using γ + jets MC events such that an MC non-closure uncertainty can be derived by comparing the resulting γ + jets MC $E_{\mathrm{T}}^{\mathrm{miss}}$ distribution to that in Z/γ^* + jets MC events. The resulting uncertainty of up to 35% is calculated in the VRs, so as to maximise the number of events that contribute. An uncertainty of 16% is assessed for the $V\gamma$ backgrounds, based on data-to-MC agreement in a $V\gamma$-enriched control region. This uncertainty is propagated to the final Z/γ^* + jets estimate following the subtraction of the $V\gamma$ background. In VR-low, a correction is applied to

the $E_{\mathrm{T}}^{\mathrm{miss}}$ distribution in γ + jets events to account for the fraction of Z/γ^* + jets events in this H_{T}-inclusive region expected to have boson p_{T} less than 37 GeV. The full size of this correction (up to 50% for $E_{\mathrm{T}}^{\mathrm{miss}} = 150$ GeV) is applied as a systematic uncertainty. The $m_{\ell\ell}$ distribution assigned to γ + jets MC events is compared to that of Z/γ^* + jets MC events, and the relative difference in a given $m_{\ell\ell}$ bin is assigned as an uncertainty. Finally, the statistical precision of the estimate also enters as a systematic uncertainty of ∼10% in the final background estimate. After applying the correction procedure, differences in the number of b-tagged jets between Z/γ^* + jets and γ + jets are found to be negligible, indicating good agreement in heavy-flavour content.

The uncertainties in the fake-lepton background stem from the number of events in the regions used to measure the real- and fake-lepton efficiencies, the limited size of the inclusive loose-lepton sample, and from varying the region used to measure the fake-lepton efficiency. The nominal fake-lepton efficiency is compared with those measured in a region with b-tagged jets and a region with a b-jet, as well as a region with the prompt-lepton subtraction varied by 20%. Varying the sample composition via b-jet tagging gives the largest uncertainty. The uncertainty for the edge SRs from the statistical component of the lepton efficiencies is 30–45%, and from varying the region for the fake-lepton efficiency it is 50–75%. The uncertainties in SRZ are generally larger due to the small number of events contributing to the estimate in this region.

Theoretical and experimental uncertainties are taken into account for the signal models, as well as background processes that rely on MC simulation. The estimated uncertainty in the luminosity measurement is 2.9% [31,32]. The jet energy scale is subject to uncertainties associated with the jet flavour composition, the pile-up and the jet and event kinematics [81]. Uncertainties in the jet energy resolution are included to account for differences between data and MC simulation [81]. An uncertainty in the $E_{\mathrm{T}}^{\mathrm{miss}}$ soft-term resolution and scale is taken into account [88], and uncertainties due to the lepton energy scales and resolutions, as well as trigger, reconstruction, and identification efficiencies, are also considered.

The WZ/ZZ processes are assigned a cross-section uncertainty of 6% and an additional uncertainty based on comparisons between SHERPA and POWHEG MC samples, which is up to 50% in the SRs. Uncertainties due to the choice of factorisation and renormalisation scales are calculated by varying the nominal values up and down by a factor of two and can be up to 23%. For rare top processes, a 13% PDF and scale variation uncertainty is applied [34] in addition to a 22% cross-section uncertainty [61–63].

For signal models, the nominal cross section and the uncertainty are taken from an envelope of cross-section predictions using different PDF sets and factorisation and renormalisa-

Table 8 Overview of the dominant sources of systematic uncertainty in the total background estimate in the signal regions. The values shown are relative to the total background estimate, shown in %. The systematic uncertainties for the edge search are quoted as a range across the $m_{\ell\ell}$ regions used for statistical interpretations

Source	Relative systematic uncertainty [%]			
	SRZ	SR-low	SR-medium	SR-high
Total systematic uncertainty	17	8–30	6–34	10–45
WZ/ZZ generator uncertainty	13	0–7	0–6	0–10
Flavour symmetry (statistical)	7	3–16	5–16	7–28
WZ/ZZ scale uncertainty	6	0–1	0–1	0–2
Z/γ^* + jets (systematic)	4	0–15	0–25	0–15
Flavour symmetry (systematic)	3	2–23	2–15	4–25
Z/γ^* + jets (statistical)	2	0–3	0–5	0–1
Fake leptons	1	0–17	2–18	2–20

Table 9 Expected and observed event yields in SRZ, inclusively, in the ee channel, and in the $\mu\mu$ channel, along with the discovery p value for zero signal strength ($p(s = 0)$) [97], Gaussian significance, 95% confidence level (CL) observed and expected upper limits on the number of signal events (S^{95}), and the corresponding observed upper limit on the visible cross section ($\langle\epsilon\sigma\rangle^{95}_{\mathrm{obs}}$). For regions in which the data yield is less than expected, the discovery p value is truncated at 0.5 and the significance is set to zero. The flavour-symmetric, Z/γ^* + jets and fake-lepton components are all derived using data-driven estimates described in Sect. 7. All remaining backgrounds are taken from MC simulation. The quoted uncertainties include statistical and systematic contributions. The individual uncertainties can be correlated and do not necessarily add up in quadrature to the total systematic uncertainty

	SRZ	SRZ ee	SRZ $\mu\mu$
Observed events	60	35	25
Total expected background events	53.5 ± 9.3	27.1 ± 5.1	26.8 ± 4.4
Flavour-symmetric ($t\bar{t}$, Wt, WW and $Z \to \tau\tau$) events	33.2 ± 3.9	16.5 ± 2.1	16.7 ± 2.0
Z/γ^* + jets events	3.1 ± 2.8	$1.0^{+1.3}_{-1.0}$	2.1 ± 1.4
WZ/ZZ events	14.2 ± 7.7	7.8 ± 4.3	6.4 ± 3.5
Rare top events	2.9 ± 0.8	1.4 ± 0.4	1.5 ± 0.4
Fake-lepton events	$0.1^{+0.8}_{-0.1}$	$0.5^{+0.7}_{-0.5}$	$0^{+0.2}$
$p(s = 0)$	0.32	0.15	0.5
Significance (σ)	0.47	1.02	0
Observed (expected) S^{95}	$28.2\ (24.5^{+8.9}_{-6.7})$	$22.0\ (15.8^{+6.5}_{-4.5})$	$12.9\ (14.0^{+5.7}_{-3.9})$
$\langle\epsilon\sigma\rangle^{95}_{\mathrm{obs}}$ [fb]	1.9	1.5	0.88

tion scales, as described in Refs. [95,96]. These are calculated at next-to-leading-logarithm accuracy (NLO + NLL) [51–55], and the resulting uncertainties range from 16 to 30%.

A breakdown of the dominant uncertainties in the background prediction in the SRs is provided in Table 8 for the on-shell Z and edge searches. Here these uncertainties are quoted relative to the total background. In the case of the edge regions a range is quoted, taking into account the relative contribution of the given uncertainty in each of the $m_{\ell\ell}$ ranges in SR-low, SR-medium and SR-high. The largest uncertainties in the signal regions are due to the size of the $e\mu$ data sample in CR-FS, used to provide the flavour-symmetric background estimate, the combined systematic uncertainty in the same background, the systematic uncertainty in γ + jets, or, in the case of SRZ, the WZ/ZZ generator uncertainty. The statistical component of the uncertainty from the flavour-symmetry estimate is largest for the edge analysis in SR-medium and SR-high in the highest $m_{\ell\ell}$ regions. In the edge SRs the uncer-

tainty in the WZ/ZZ background tends to be highest in the $m_{\ell\ell}$ ranges that include the Z window. The uncertainty in the fake-lepton background is largest in SR-high, where fake leptons can compose a larger fraction of the background. Experimental uncertainties have a far lower impact on the systematic uncertainty of the total background ($<2\%$).

9 Results

9.1 Results in SRZ

For the on-shell Z search, the expected background and observed yields in the SR are shown in Table 9. A total of 60 events are observed in data with a predicted background of 53.5 ± 9.3 events. There are 35 events observed in data in the ee channel, and 25 events observed in the $\mu\mu$ channel. The probability for the background to produce a fluctua-
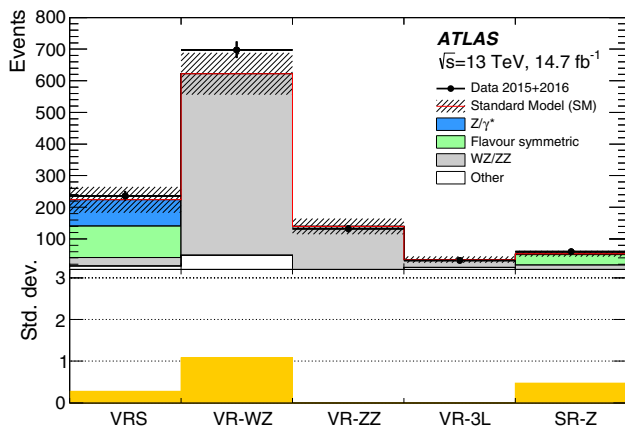
Fig. 5 The expected and observed yields in the validation regions and signal region of the on-shell Z search. The rare top and data-driven fake-lepton backgrounds are grouped under "other" backgrounds. The significance of the difference between the data and the expected background (see *text* for details) is shown in the *bottom plot*; for regions in which the data yield is less than expected, the significance is set to zero. The *hashed uncertainty bands* include the statistical and systematic uncertainties in the background prediction

tion greater than or equal to that observed in the data, called the significance when expressed in terms of the number of standard deviations, corresponds to 0.47σ (details of the significance calculation are presented in Sect. 10). The level of agreement between the observed event yields in data and the background predictions in the VRs, shown previously in Table 6, is also displayed in Fig. 5, along with the results in SRZ.

The dilepton invariant-mass distribution for the $ee + \mu\mu$ and $e\mu$ channels with the kinematic requirements of SRZ, but over the full $m_{\ell\ell}$ range, is shown in Fig. 6. Here the data

are consistent with the expected background over the full $m_{\ell\ell}$ range. The dilepton invariant-mass, jet and b-tagged jet multiplicity, E_T^{miss}, H_T^{incl} and $p_T^{\ell\ell}$ distributions in SRZ are shown in Fig. 7. The shapes of the background distributions in these figures are obtained from MC simulation, where the MC simulation is normalised according to the data-driven estimates in the SR. Here two representative examples of $\tilde{g}$–$\tilde{\chi}_2^0$ on-shell signal models, with $(m(\tilde{g}), m(\tilde{\chi}_2^0)) = (1095, 205)$ GeV and $(m(\tilde{g}), m(\tilde{\chi}_2^0)) = (1240, 960)$ GeV, are overlaid. To demonstrate the modelling of the $Z/\gamma^* +$ jets background in VR-S and SRZ, Fig. 8 shows the minimum $\Delta\phi(jet_{12}, p_T^{miss})$ distribution over the full range, where $\Delta\phi(jet_{12}, p_T^{miss}) > 0.4$ is required in VR-S and SRZ. Here the $Z/\gamma^* +$ jets distribution is modelled using the full data-driven prediction from $\gamma +$ jets. Two of the events in the SR contain a third signal lepton.

9.2 Results in the edge SRs

The integrated yields in the edge signal regions are compared to the expected background in Table 10. To allow for the visualisation of a potential edge, the full $m_{\ell\ell}$ distributions in the three search regions are compared to the expected background in Fig. 9. In addition, the observed $m_{\ell\ell}$ distributions are compared to the predictions from MC simulation in Fig. 10, in which the $t\bar{t}$ background is scaled such that the total MC expected yield matches the data in the $e\mu$ CR. The $t\bar{t}$ normalisation factors are $\mu_{t\bar{t}} = 0.85 \pm 0.03, 0.75 \pm 0.04$, and 0.57 ± 0.07 in SR-low, SR-medium, and SR-high, respectively, where the uncertainty is the data statistical uncertainty. The data-driven flavour-symmetry prediction is used for the quantitative results of the analysis. This prediction does not rely on the $t\bar{t}$ normalisation scale factors discussed above.
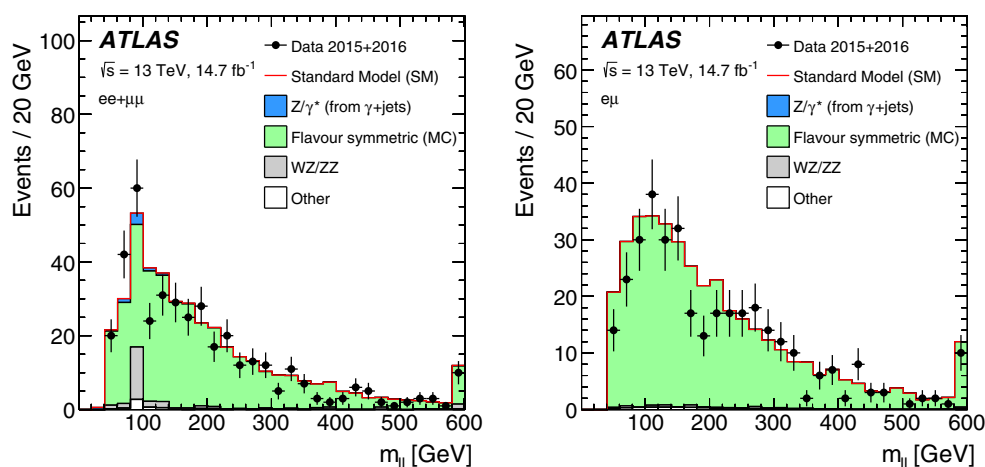
Fig. 6 The dilepton invariant-mass distribution for an SRZ-like selection, but with the Z mass requirement removed, in the same-flavour (*left*) and different-flavour (*right*) channels. With the exception of the $Z/\gamma^* +$ jets background, MC simulation is used to show the expected shapes of the $m_{\ell\ell}$ distributions, with the backgrounds being normalised

according to their SRZ prediction. For the $Z/\gamma^* +$ jets background, the $m_{\ell\ell}$ shape is taken from the $\gamma +$ jets method. The rare top and data-driven fake-lepton backgrounds are grouped under "other" backgrounds. The last bin includes the overflow

Fig. 7 The $m_{\ell\ell}$ (*top left*), $p_T^{\ell\ell}$ (*top right*), E_T^{miss} (*middle left*), H_T^{incl} (*middle right*), jet multiplicity (*bottom left*) and b-tagged jet multiplicity (*bottom right*) distributions in SRZ. Two examples of signal models from the $\tilde{g}-\tilde{\chi}_2^0$ on-shell grid, described in Sect. 4, with $(m(\tilde{g}), m(\tilde{\chi}_2^0)) = (1095, 205)$ GeV and $(m(\tilde{g}), m(\tilde{\chi}_2^0)) = (1240, 960)$ GeV, are overlaid. In the case of the E_T^{miss}, H_T^{incl} and $p_T^{\ell\ell}$ distributions, the last bin contains the overflow. The flavour-symmetric and $Z/\gamma^* +$ jets backgrounds are taken from MC simulation and scaled to match their SRZ data-driven predictions. The rare top and data-driven fake-lepton backgrounds are grouped under "other" backgrounds. The *hashed uncertainty bands* include the statistical and systematic uncertainties in the background prediction
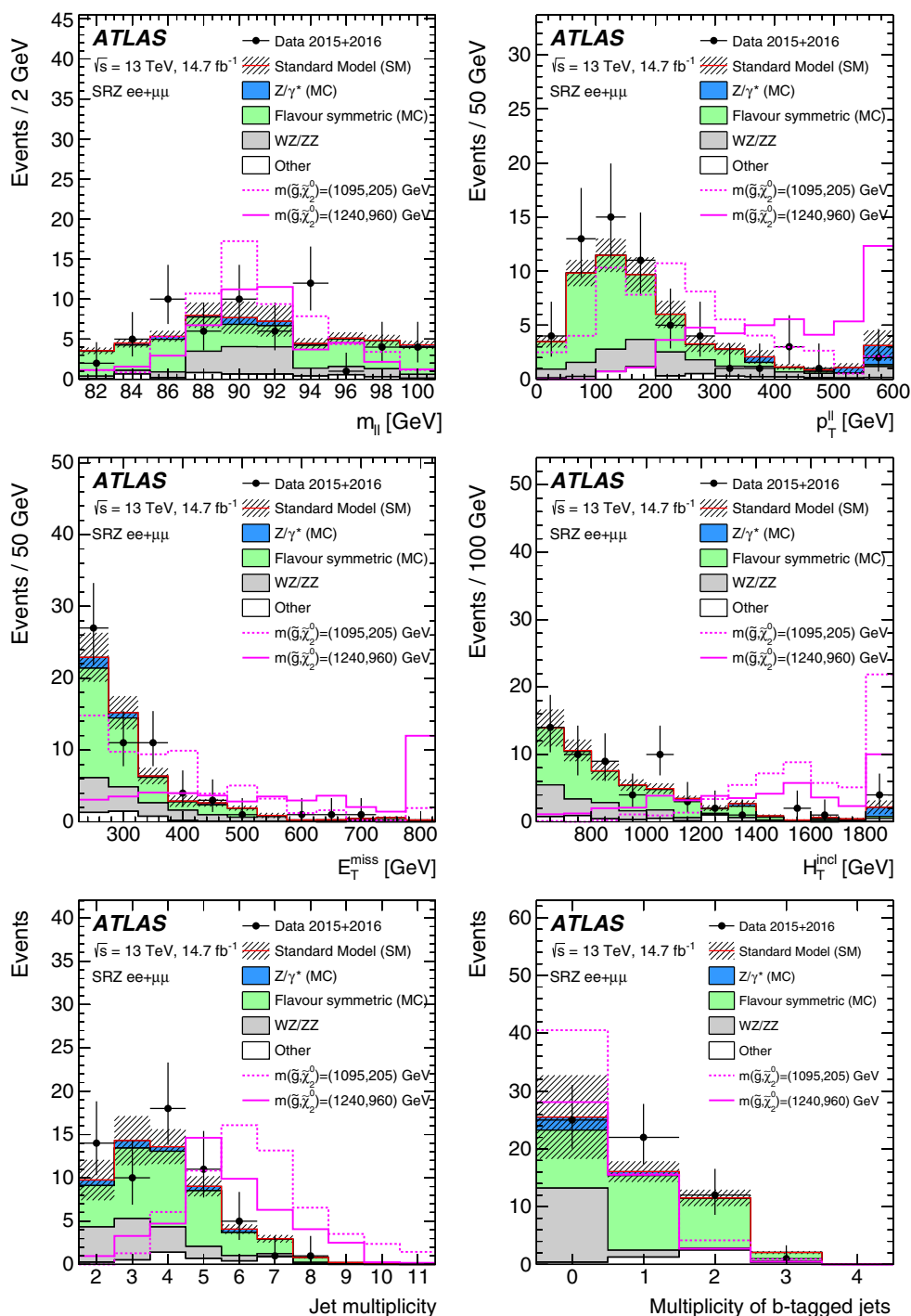
The MC-based cross-check method is used to examine the $m_{\ell\ell}$ distribution in finer bins than can be achieved with the flavour-symmetry method, due to the limited statistical precision of the $e\mu$ CR.

As signal models may produce kinematic endpoints at any value of $m_{\ell\ell}$, any excess must be searched for across the $m_{\ell\ell}$ distribution. To do this a "sliding window" approach is used.

The binning in the SRs, shown in Fig. 9, defines many possible dilepton mass windows. The 24 $m_{\ell\ell}$ ranges (9 for SR-low, 8 for SR-medium, and 7 for SR-high) are chosen because they are the most sensitive for at least one grid point in the signal model parameter space. Some of the ranges overlap. The results in these regions are summarised in Fig. 11, and the expected and observed yields in the combined $ee + \mu\mu$
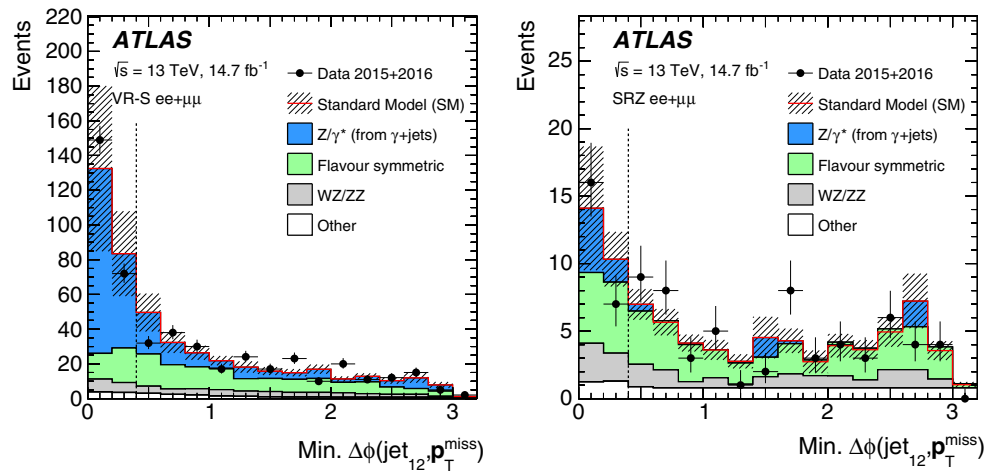
Fig. 8 The min. $\Delta\phi(\mathrm{jet}_{12}, \boldsymbol{p}_{\mathrm{T}}^{\mathrm{miss}})$ distribution in (*left*) VR-S and (*right*) SRZ, where the min. $\Delta\phi(\mathrm{jet}_{12}, \boldsymbol{p}_{\mathrm{T}}^{\mathrm{miss}}) > 0.4$ requirement has been lifted. The *vertical dashed lines* indicate the requirement in each region. The flavour-symmetric and $Z/\gamma^* +$ jets distributions are taken com-

pletely from the data-driven estimate. The rare top and data-driven fake-lepton backgrounds are grouped under "other" backgrounds. The *hashed uncertainty bands* include the statistical and systematic uncertainties in the background prediction

Table 10 Breakdown of the expected background and observed data yields for SR-low, SR-medium and SR-high, integrated over the $m_{\ell\ell}$ spectrum. The flavour-symmetric, $Z/\gamma^* +$ jets and fake-lepton components are all derived using data-driven estimates described in Sect. 7. All remaining backgrounds are taken from MC simulation. The quoted uncertainties include statistical and systematic contributions

	SR-low	SR-medium	SR-high
Observed events	1394	689	212
Total expected background events	1500 ± 100	700 ± 60	171 ± 18
Flavour-symmetric ($t\bar{t}$, Wt, WW and $Z \to \tau\tau$) events	1270 ± 70	584 ± 32	148 ± 14
$Z/\gamma^* +$ jets events	90 ± 50	50 ± 40	3^{+7}_{-3}
WZ/ZZ events	68 ± 31	26 ± 11	7 ± 4
Rare top events	19 ± 5	11.3 ± 3.2	4.2 ± 1.4
Fake-lepton events	59 ± 34	32 ± 19	10 ± 8

channel for all 24 $m_{\ell\ell}$ ranges are presented in Table 11. In SR-low and SR-medium, the data are consistent with the expected background across the full $m_{\ell\ell}$ range. In SR-high the data show a slight excess above the background at low $m_{\ell\ell}$. Of these 24 $m_{\ell\ell}$ ranges, the largest excess is observed in SR-high with $12 < m_{\ell\ell} < 101$ GeV. Here a total of 90 events are observed in data, compared to an expectation of 65 ± 10 events, corresponding to a local significance of 1.7σ.

10 Interpretation

In this section, exclusion limits are shown for the SUSY models detailed in Sect. 3. The asymptotic CL_S prescription [90,98], implemented in the HistFitter program [97], is

used to determine cross-section upper limits at 95% confidence level (CL) for the on-Z search. For the edge search, pseudo-experiments are used to evaluate the cross-section upper limits. A Gaussian model for nuisance parameters is used for all signal and background uncertainties. Exceptions are the statistical uncertainties of the flavour-symmetry method, $\gamma +$ jets method and MC-based backgrounds, all of which are treated as Poissonian nuisance parameters. The different experimental uncertainties are treated as correlated between signal and background events. The theoretical uncertainty of the signal cross section is not accounted for in the limit-setting procedure. Instead, following the initial limit determination, the impact of varying the signal cross section within its uncertainty is evaluated separately and indicated in the exclusion results. Limits are based on the combined $ee + \mu\mu$ results. Possible signal contamination in the CRs is neglected in the limit-setting procedure; the contamination is found to be negligible for signal points near the exclusion boundaries. Far from the exclusion boundary, although the signal contamination can be significant, the number of events appearing in the signal region is large enough that the points are still excluded, due to the relative branching fractions for the signal in the CR and SR. For example, for models with signal contamination of 50% in CR-FS the signal-to-background ratio in SRZ is ~ 10.

The results of the on-shell Z search are interpreted in a simplified model with gluino-pair production, where each gluino decays as $\tilde{g} \to q\bar{q}\tilde{\chi}_2^0$, $\tilde{\chi}_2^0 \to Z\tilde{\chi}_1^0$ and the $\tilde{\chi}_1^0$ mass is set to 1 GeV. The expected and observed exclusion contours for this $\tilde{g}-\tilde{\chi}_2^0$ on-shell grid are shown in the $m(\tilde{g})-m(\tilde{\chi}_2^0)$ plane in Fig. 12. The expected (observed) lower limit on the gluino mass is about 1.35 TeV (1.30 TeV) for a $\tilde{\chi}_2^0$ with a
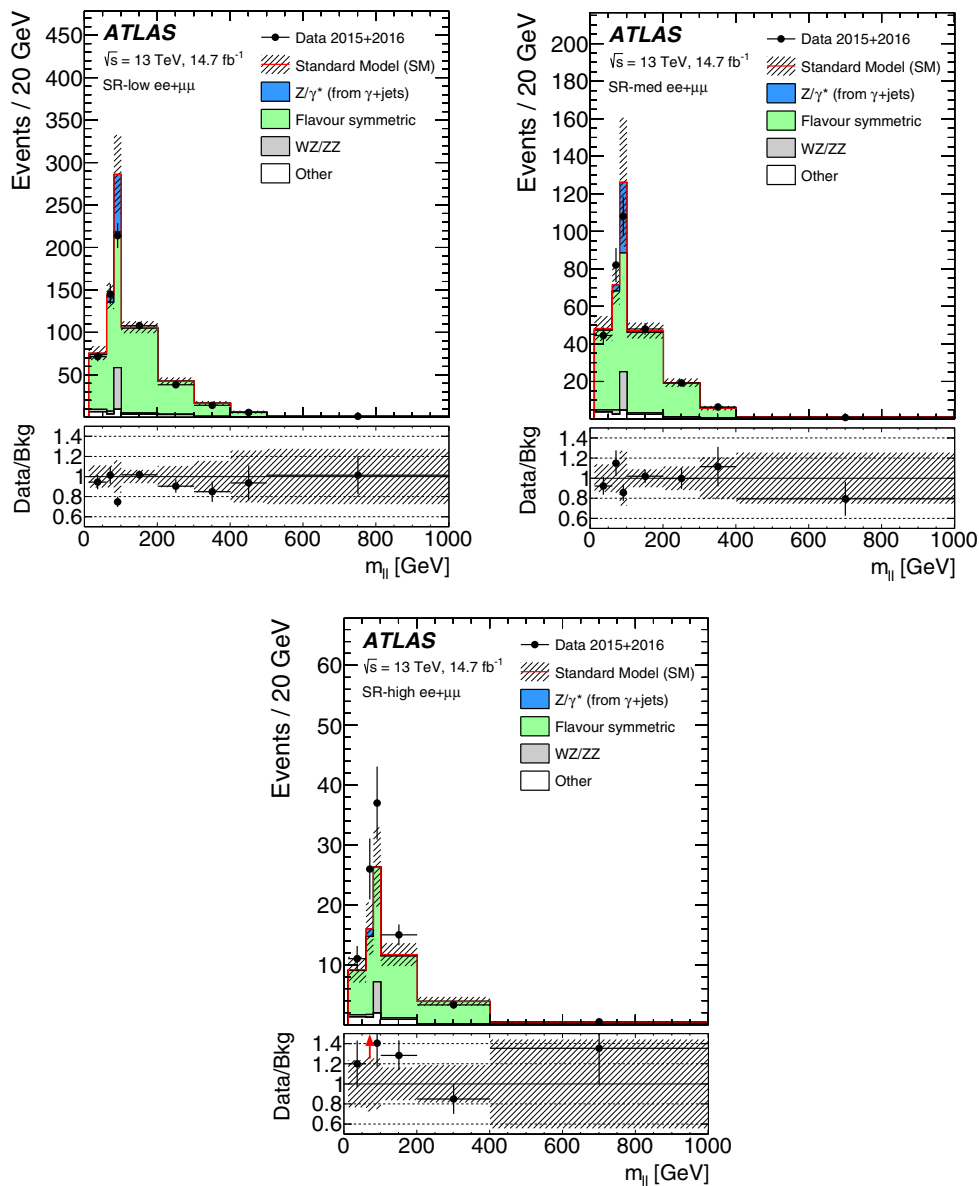
Fig. 9 Expected and observed dilepton mass distributions, with the bin boundaries considered for the interpretation, in (*top left*) SR-low, (*top-right*) SR-medium, and (*bottom*) SR-high of the edge search. These bins, and sets of neighbouring bins, make up the mll windows used for the interpretation. The flavour-symmetric and Z/γ^*+jets distributions are taken completely from the data-driven estimate. The rare top and data-driven fake-lepton backgrounds are grouped under "other" backgrounds. All statistical and systematic uncertainties are included in the *hashed bands*. The ratio of data to predicted background is shown in the *bottom panels*. In cases where the data point is not accommodated by the scale of this *panel*, *a red arrow* indicates the direction in which the point is out of range

mass of 1.1 TeV in this model. The impact of the systematic uncertainties in the background and the experimental uncertainties in the signal, shown with a coloured band, is about 100 GeV on the gluino mass limit. The systematic uncertainty of the signal cross section, shown as dotted lines around the observed contour, has an impact of about 40 GeV. Figure 12 also shows the expected and observed exclusion limits for the $\tilde{q}-\tilde{\chi}_2^0$ on-shell model. This is a simplified model

with squark-pair production, where each squark decays to a quark and a neutralino, with the neutralino subsequently decaying to a Z boson and an LSP with a mass of 1 GeV. In this model, exclusion is expected (observed) for squarks with masses below 1040 GeV (980 GeV) for a $\tilde{\chi}_2^0$ mass of 600 GeV.

Figure 13 shows the expected and observed exclusion contours for the $\tilde{g}-\tilde{\chi}_1^0$ on-shell model, in which the produced
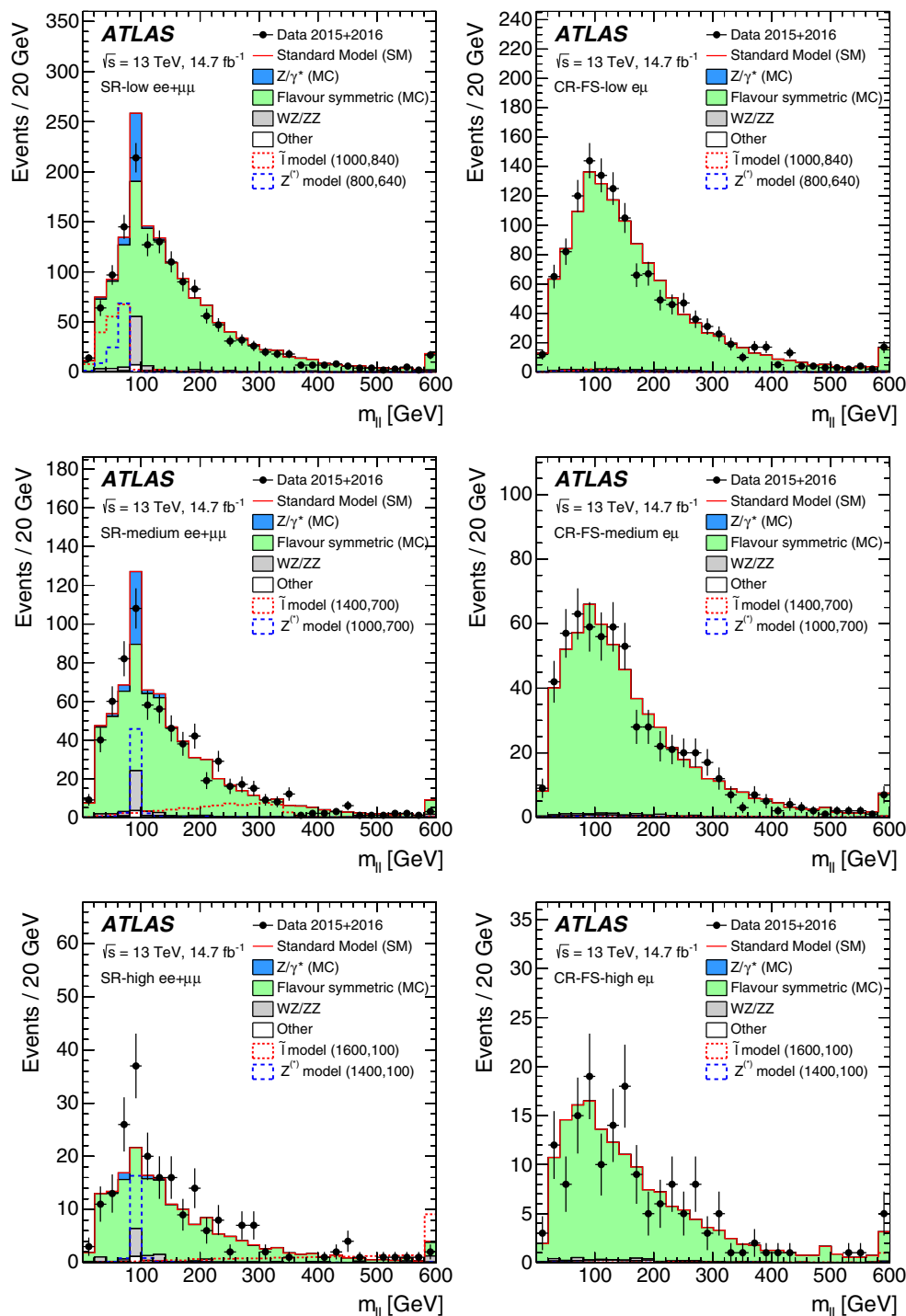
Fig. 10 The dilepton mass distributions in the (*top*) SR-low (*left*) and CR-FS-low (*right*), (*middle*) SR-medium (*left*) and CR-FS-medium (*right*), and (*bottom*) SR-high (*left*) and CR-FS-high (*right*) regions of the edge search. The $t\bar{t}$ MC sample is normalised such that the total MC prediction matches data in the $e\mu$ channel for each region. The $m_{\ell\ell}$ shape and normalisation for the Z/γ^* + jets background is taken from the γ + jets method. The rare top and data-driven fake-lepton backgrounds are grouped under "other" backgrounds. Example signal benchmarks from the slepton and $Z^{(*)}$ models are overlaid on the distributions. The first (second) number in *parentheses* is the gluino (LSP) mass. The overflow is included in the last bin

gluinos follow the same decay chain as in the model above. In this case the mass difference $\Delta m = m(\tilde{\chi}_2^0) - m(\tilde{\chi}_1^0)$ is set to 100 GeV.

The results of the edge search are interpreted in two simplified models with gluino-pair production, in which each gluino decays as $\tilde{g} \rightarrow q\bar{q}\tilde{\chi}_2^0$. For each point in the signal-

Fig. 11 The expected and observed yields in the 24 (overlapping) $m_{\ell\ell}$ ranges of SR-low, SR-medium, and SR-high. The data are compared to the sum of the expected backgrounds. The rare top and data-driven fake-lepton backgrounds are grouped under "other" backgrounds. The significance of the difference between the data and the expected background (see *text* for details) is shown in the *bottom plots*; for regions in which the data yield is less than expected, the significance is set to zero. The *hashed uncertainty bands* include the statistical and systematic uncertainties in the background prediction
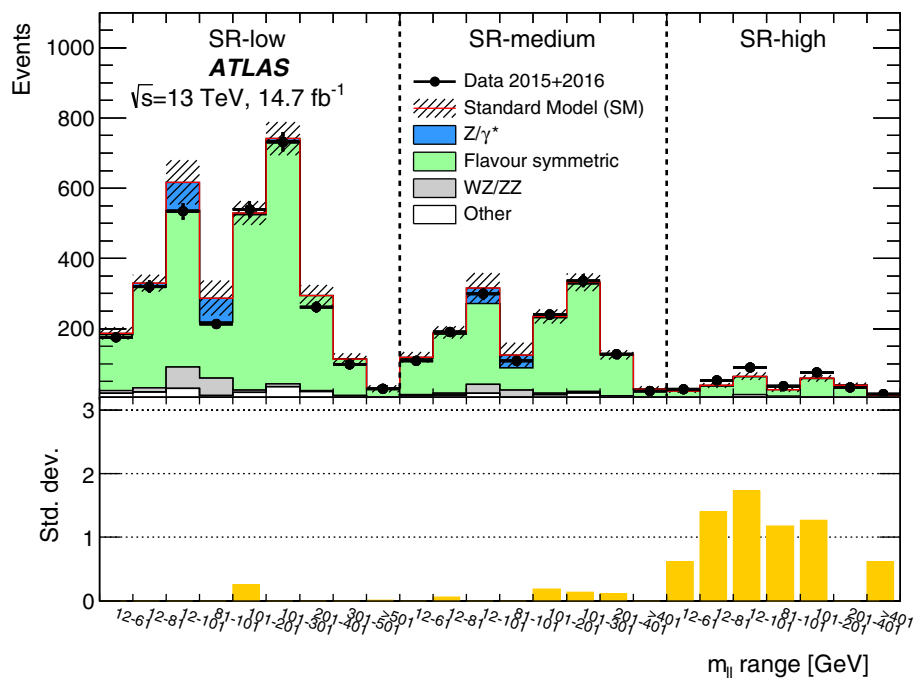
Table 11 Breakdown of the expected background and observed data yields in the edge signal regions. The results are given for SR-low, SR-medium and SR-high in all 24 $m_{\ell\ell}$ ranges. The $m_{\ell\ell}$ range in units of GeV is indicated in the leftmost column of the table. Left to right: the total expected background, with combined statistical and systematic uncertainties, observed data, 95% CL upper limits on the visible cross section ($\langle \epsilon\sigma \rangle_{\mathrm{obs}}^{95}$) and on the number of signal events (S_{obs}^{95}). The sixth column (S_{exp}^{95}) shows the expected 95% CL upper limit on the number of signal events, given the expected number (and $\pm 1\sigma$ excursions) of background events. The last two columns indicate the discovery p value ($p(s = 0)$) [97], and the Gaussian significance ($Z(s = 0)$). For an observed number of events lower than expected, the discovery p value is truncated at 0.5 and the significance is set to zero

Signal region	Total Bkg.	Data	$\langle \epsilon\sigma \rangle_{\mathrm{obs}}^{95}$[fb]	S_{obs}^{95}	S_{exp}^{95}	$p(s=0)$	$Z(s=0)$
SR-low							
12–61	187 ± 18	175	2.68	39.4	48^{+23}_{-14}	0.50	0.00
12–81	330 ± 24	320	3.88	57.1	64^{+30}_{-19}	0.50	0.00
12–101	617 ± 63	534	4.64	68.2	98^{+36}_{-26}	0.50	0.00
81–101	287 ± 50	214	2.73	40.2	62^{+22}_{-16}	0.50	0.00
101–201	529 ± 34	540	6.80	99.9	91^{+52}_{-29}	0.40	0.26
101–301	741 ± 48	732	7.28	107	113^{+53}_{-33}	0.50	0.00
201–401	295 ± 30	262	3.43	50.5	70^{+37}_{-21}	0.50	0.00
301–501	113 ± 17	99	2.37	34.8	46^{+41}_{-16}	0.50	0.00
>501	29 ± 10	29	1.88	27.7	27^{+34}_{-10}	0.50	0.01
SR-medium							
12–61	119 ± 15	109	2.38	35.1	43^{+29}_{-14}	0.50	0.00
12–81	190 ± 18	191	3.57	52.5	51^{+31}_{-15}	0.48	0.06
12–101	315 ± 43	299	5.12	75.3	81^{+29}_{-20}	0.50	0.00
81–101	125 ± 35	108	3.18	46.7	51^{+17}_{-12}	0.50	0.00
101–201	235 ± 20	240	4.26	62.6	58^{+37}_{-19}	0.42	0.19
101–301	332 ± 25	336	4.92	72.3	69^{+39}_{-22}	0.45	0.14
201–401	126 ± 13	128	3.27	48.0	46^{+52}_{-16}	0.46	0.11
>401	28 ± 8	22	1.09	16.1	21^{+19}_{-7}	0.50	0.00
SR-high							
12–61	23 ± 5	27	1.84	27.0	20^{+31}_{-8}	0.27	0.62
12–81	39 ± 7	53	3.32	48.9	26^{+28}_{-10}	0.08	1.40
12–101	65 ± 10	90	4.00	58.8	31^{+17}_{-10}	0.04	1.73
81–101	26 ± 6	37	2.17	31.9	20^{+13}_{-7}	0.12	1.18
101–201	59 ± 9	75	3.68	54.1	31^{+29}_{-11}	0.10	1.27
201–401	39 ± 7	33	1.82	26.7	28^{+14}_{-7}	0.50	0.00
>401	10 ± 5	14	2.04	30.0	21^{+79}_{-10}	0.27	0.62
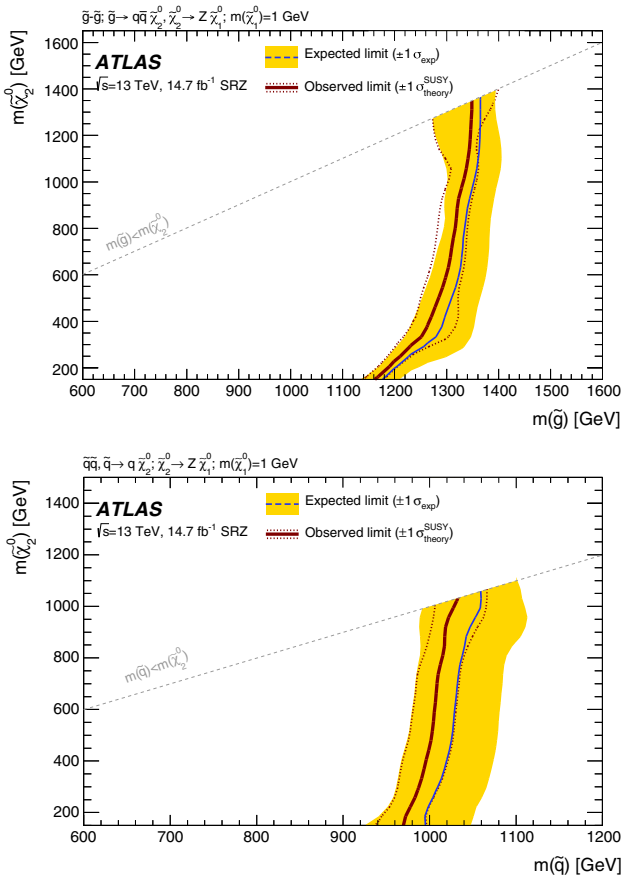
Fig. 12 Expected and observed exclusion contours derived from the results in SRZ for the (*top*) $\tilde{g}$–$\tilde{\chi}_2^0$ on-shell grid and (*bottom*) $\tilde{q}$–$\tilde{\chi}_2^0$ on-shell grid. The *dashed blue line* indicates the expected limits at 95% CL and the *yellow band* shows the 1σ variation of the expected limit as a consequence of the uncertainties in the background prediction and the experimental uncertainties in the signal ($\pm 1\sigma_{\mathrm{exp}}$). The observed limits are shown by the *solid red line*, with the *dotted red lines* indicating the variation resulting from changing the signal cross section within its uncertainty ($\pm 1\sigma_{\mathrm{theory}}^{\mathrm{SUSY}}$)

Fig. 13 Expected and observed exclusion contours derived from the results in SRZ for the $\tilde{g}$–$\tilde{\chi}_1^0$ on-shell grid. The *dashed blue line* indicates the expected limits at 95% CL and the *yellow band* shows the 1σ variation of the expected limit as a consequence of the uncertainties in the background prediction and the experimental uncertainties in the signal ($\pm 1\sigma_{\mathrm{exp}}$). The observed limits are shown by the *solid red line*, with the *dotted red lines* indicating the variation resulting from changing the signal cross section within its uncertainty ($\pm 1\sigma_{\mathrm{theory}}^{\mathrm{SUSY}}$)
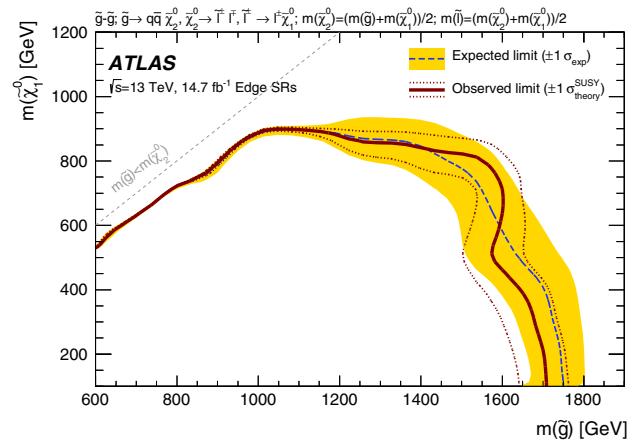
Fig. 14 Expected and observed exclusion contours derived from the results in the edge search SRs for the slepton signal model. The *dashed blue line* indicates the expected limits at 95% CL and the *yellow band* shows the 1σ variation of the expected limit as a consequence of the uncertainties in the background prediction and the experimental uncertainties in the signal ($\pm 1\sigma_{\mathrm{exp}}$). The observed limits are shown by the *solid red lines*, with the *dotted red lines* indicating the variation resulting from changing the signal cross section within its uncertainty ($\pm 1\sigma_{\mathrm{theory}}^{\mathrm{SUSY}}$)

model parameter space, limits on the signal strength are calculated using the $m_{\ell\ell}$ window with the best expected sensitivity. Details of the windows are described in Sect. 9.

The excluded regions in the $m(\tilde{g})$–$m(\tilde{\chi}_1^0)$ plane are presented in Fig. 14 for the slepton model. In this model, pair-produced gluinos each decay as $\tilde{g} \rightarrow q\bar{q}\tilde{\chi}_2^0$, $\tilde{\chi}_2^0 \rightarrow \ell^{\pm}\tilde{\ell}^{\mp}$, $\tilde{\ell}^{\mp} \rightarrow \ell^{\mp}\tilde{\chi}_1^0$. Here, the results exclude gluinos with masses as large as 1.7 TeV, with an expected limit of 1.75 TeV for small $m(\tilde{\chi}_1^0)$. The results probe kinematic endpoints as small as $m_{\ell\ell}^{\max} = m(\tilde{\chi}_2^0) - m(\tilde{\chi}_1^0) = 1/2(m(\tilde{g}) - m(\tilde{\chi}_1^0)) = 50$ GeV.

The $Z^{(*)}$ exclusion limits from the results in the edge SRs are compared with the same limits derived using the results in SRZ in Fig. 15. In this model, pair-produced gluinos each decay as $\tilde{g} \rightarrow q\bar{q}\tilde{\chi}_2^0$, $\tilde{\chi}_2^0 \rightarrow Z^{(*)}\tilde{\chi}_1^0$, and the mass splitting between the $\tilde{\chi}_2^0$ and the $\tilde{\chi}_1^0$ determines whether the Z boson

is produced on-shell. Here the edge limits extend into the more compressed region, whereas the expected SRZ exclusion probes higher $\tilde{\chi}_1^0$ masses in the on-shell regime. At high gluino masses, the edge SRs provide stronger limits. For the $Z^{(*)}$ model, the expected and observed gluino mass limits are 1.4 TeV and 1.34 TeV (1.35 and 1.3 TeV for the on-Z signal region), respectively, for $\tilde{\chi}_1^0$ masses below 400 GeV. The sensitivity in the $Z^{(*)}$ model is smaller than that of the slepton model because the leptonic branching fraction of the Z boson suppresses the signal production rate.
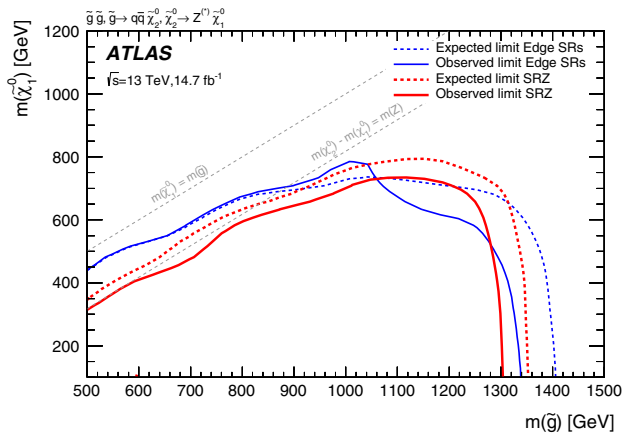
Fig. 15 Expected and observed exclusion contours derived from the results in the edge search SRs and SRZ for the $Z^{(*)}$ model. The *dashed* and *solid blue lines* indicate the expected and observed limits at 95% CL from the results in the edge SRs, while the *thick dashed* and *solid red lines* indicate the expected and observed limits at 95% CL from the results in SRZ

Model-independent upper limits at 95% CL on the number of events that could be attributed to non-SM sources (S^{95}) for SRZ are derived using the CL_S prescription and neglecting possible signal contamination in the CRs. For these upper limits, pseudo-experiments are used rather than the asymptotic approximation. The expected and observed upper limits are given in Table 9. The same information is given for the 24 $m_{\ell\ell}$ ranges of the edge search in Table 11.

11 Conclusion

This paper presents two searches for new phenomena in final states containing a same-flavour opposite-sign lepton (electron or muon) pair, jets, and large missing transverse momentum using 14.7 fb^{-1} of ATLAS data collected during 2015 and 2016 at the LHC at $\sqrt{s} = 13$ TeV. The first search (on-shell Z search) targets lepton pairs consistent with Z boson decay, while the second search (edge search) targets a kinematic endpoint feature in the dilepton mass distribution. For the edge search, a set of 24 mass ranges are considered, with different requirements on E_T^{miss} and H_T, and different kinematic endpoint values in the dilepton invariant-mass distribution. The data in both searches are found to be consistent with the Standard Model prediction. The results are interpreted in simplified models of gluino-pair production and squark-pair production, and exclude gluinos (squarks) with masses as large as 1.7 TeV (980 GeV).

References

1. Y.A. Golfand, E.P. Likhtman, Extension of the algebra of Poincare group generators and violation of p invariance. JETP Lett. **13**, 323–326 (1971)
2. Y.A. Golfand, E.P. Likhtman, Pisma. Zh. Eksp. Teor. Fiz. **13**, 452 (1971)
3. D.V. Volkov, V.P. Akulov, Is the neutrino a goldstone particle? Phys. Lett. B **46**, 109–110 (1973). doi:10.1016/0370-2693(73)90490-5
4. J. Wess, B. Zumino, Supergauge transformations in four-dimensions. Nucl. Phys. B **70**, 39–50 (1974). doi:10.1016/0550-3213(74)90355-1
5. J. Wess, B. Zumino, Supergauge invariant extension of quantum electrodynamics. Nucl. Phys. B **78**, 1 (1974). doi:10.1016/0550-3213(74)90112-6
6. S. Ferrara, B. Zumino, Supergauge invariant Yang–Mills theories. Nucl. Phys. B **79**, 413 (1974). doi:10.1016/0550-3213(74)90559-8
7. A. Salam, J.A. Strathdee, Supersymmetry and nonabelian gauges. Phys. Lett. B **51**, 353–355 (1974). doi:10.1016/0370-2693(74)90226-3
8. N. Sakai, Naturalness in supersymmetric GUTS. Z. Phys. C **11**, 153 (1981). doi:10.1007/BF01573998

9. S. Dimopoulos, S. Raby, F. Wilczek, Supersymmetry and the scale of unification. Phys. Rev. D **24**, 1681–1683 (1981). doi:10.1103/PhysRevD.24.1681

10. L.E. Ibanez, G.G. Ross, Low-energy predictions in supersymmetric grand unified theories. Phys. Lett. B **105**, 439 (1981). doi:10.1016/0370-2693(81)91200-4

11. S. Dimopoulos, H. Georgi, Softly broken supersymmetry and SU(5). Nucl. Phys. B **193**, 150 (1981). doi:10.1016/0550-3213(81)90522-8

12. G.R. Farrar, P. Fayet, Phenomenology of the production, decay, and detection of new hadronic states associated with supersymmetry. Phys. Lett. B **76**, 575–579 (1978). doi:10.1016/0370-2693(78)90858-4

13. H. Goldberg, Constraint on the photino mass from cosmology. Phys. Rev. Lett. **50**, 1419 (1983). doi:10.1103/PhysRevLett.50.1419. [Erratum: Phys. Rev. Lett. 103, 099905 (2009)]

14. J.R. Ellis et al., Supersymmetric relics from the big bang. Nucl. Phys. B **238**, 453–476 (1984). doi:10.1016/0550-3213(84)90461-9

15. M. Dine, W. Fischler, A Phenomenological model of particle physics based on supersymmetry. Phys. Lett. B **110**, 227 (1982). doi:10.1016/0370-2693(82)91241-2

16. L. Alvarez-Gaume, M. Claudson, M.B. Wise, Low-energy supersymmetry. Nucl. Phys. B **207**, 96 (1982). doi:10.1016/0550-3213(82)90138-9

17. C.R. Nappi, B.A. Ovrut, Supersymmetric extension of the SU(3) x SU(2) x U(1) model. Phys. Lett. B **113**, 175 (1982). doi:10.1016/0370-2693(82)90418-X

18. CMS Collaboration, Search for physics beyond the standard model in events with a Z boson, jets, and missing transverse energy in pp collisions at $\sqrt{s} = 7$ TeV. Phys. Lett. B **716**, 260–284 (2012). doi:10.1016/j.physletb.2012.08.026. arXiv:1204.3774 [hep-ex]

19. CMS Collaboration, Search for physics beyond the standard model in events with two leptons, jets, and missing transverse momentum in pp collisions at $\sqrt{s} = 8$ TeV. JHEP **04**, 124 (2015). doi:10.1007/JHEP04(2015)124. arXiv:1502.06031 [hep-ex]

20. ATLAS Collaboration, Search for supersymmetry in events containing a same-flavour opposite-sign dilepton pair, jets, and large missing transverse momentum in $\sqrt{s} = 8$ TeV pp collisions with the ATLAS detector. Eur. Phys. J. C **75**, 318 (2015). doi:10.1140/epjc/s10052-015-3518-2. arXiv:1503.03290 [hep-ex]

21. CMS Collaboration, Search for new physics in final states with two opposite-sign same-flavor leptons, jets and missing transverse momentum in pp collisions at $\sqrt{s} = 13$ TeV. JHEP **12**, 013 (2016). doi:10.1007/JHEP12(2016)013. arXiv:1607.00915 [hep-ex]

22. ATLAS Collaboration, Search for new physics in events with opposite-sign leptons, jets, and missing transverse energy in pp collisions at $\sqrt{s} = 7$ TeV. Phys. Lett. B **718**, 815–840 (2013). doi:10.1016/j.physletb.2012.11.036. arXiv:1206.3949 [hep-ex]

23. ATLAS Collaboration, The ATLAS experiment at the CERN large hadron collider. JINST. **3**, S08003 (2008). doi:10.1088/1748-0221/3/08/S08003

24. ATLAS Collaboration, Early inner detector tracking performance in the 2015 data at $\sqrt{s} = 13$ TeV. ATL-PHYS-PUB-2015-051, 2015. http://cds.cern.ch/record/2110140

25. P. Fayet, Supersymmetry and weak, electromagnetic and strong interactions. Phys. Lett. B **64**, 159 (1976). doi:10.1016/0370-2693(76)90319-1

26. P. Fayet, Spontaneously broken supersymmetric theories of weak, electromagnetic and strong interactions. Phys. Lett. B **69**, 489 (1977). doi:10.1016/0370-2693(77)90852-8

27. M. Cahill-Rowley et al., ATLAS Z+ missing transverse energy excess in the MSSM. Phys. Rev. D **92**, 075029 (2015). doi:10.1103/PhysRevD.92.075029. arXiv:1506.05799 [hep-ph]

28. ATLAS Collaboration, Search for direct top squark pair production in events with a Z boson, b-jets and missing transverse momentum in $\sqrt{s} = 8$ TeV pp collisions with the ATLAS detector. Eur. Phys. J. C **74**, 2883 (2014). doi:10.1140/epjc/s10052-014-2883-6. arXiv:1403.5222 [hep-ex]

29. ATLAS Collaboration, Search for direct top-squark pair production in final states with two leptons in pp collisions at $\sqrt{s} = 8$ TeV with the ATLAS detector. JHEP **06**, 124 (2014). doi:10.1007/JHEP06(2014)124. arXiv:1403.4853 [hep-ex]

30. D. Alves, E. Izaguirre, J. Wacker, Where the sidewalk ends: jets and missing energy search strategies for the 7 TeV LHC. JHEP **10**, 012 (2011). doi:10.1007/JHEP10(2011)012. arXiv:1102.5338 [hep-ph]

31. ATLAS Collaboration, Improved luminosity determination in pp collisions at $\sqrt{s} = 7$ TeV using the ATLAS detector at the LHC. Eur. Phys. J. C **73**, 2518 (2013). doi:10.1140/epjc/s10052-013-2518-3. arXiv:1302.4393 [hep-ex]

32. ATLAS Collaboration, Luminosity determination in pp collisions at $\sqrt{s} = 8$ TeV using the ATLAS detector at the LHC. Eur. Phys. J. C **76**, 653 (2016). doi:10.1140/epjc/s10052-016-4466-1. arXiv:1608.03953 [hep-ex]

33. ATLAS Collaboration, 2015 start-up trigger menu and initial performance assessment of the ATLAS trigger using Run-2 data. ATL-DAQ-PUB-2016-001, 2016. http://cds.cern.ch/record/2136007

34. J. Alwall et al., The automated computation of tree-level and next-to-leading order differential cross sections, and their matching to parton shower simulations. JHEP **07**, 079 (2014). doi:10.1007/JHEP07(2014)079. arXiv:1405.0301 [hep-ph]

35. T. Sjöstrand, S. Mrenna, P. Skands, A brief introduction to PYTHIA 8.1. Comput. Phys. Commun. **178**, 852 (2008). doi:10.1016/j.cpc.2008.01.036. arXiv:0710.3820 [hep-ph]

36. ATLAS Collaboration, ATLAS Pythia 8 tunes to 7 TeV data. ATL-PHYS-PUB-2014-021, 2014. http://cdsweb.cern.ch/record/1966419

37. R.D. Ball et al., Parton distributions with LHC data. Nucl. Phys. B **867**, 244–289 (2013). doi:10.1016/j.nuclphysb.2012.10.003. arXiv:1207.1303 [hep-ph]

38. P. Nason, A new method for combining NLO QCD with shower Monte Carlo algorithms. JHEP **11**, 040 (2004). arXiv:hep-ph/0409146 [hep-ph]

39. S. Frixione, P. Nason, C. Oleari, Matching NLO QCD computations with parton shower simulations: the POWHEG method. JHEP **11**, 070 (2007). arXiv:0709.2092 [hep-ph]

40. S. Alioli et al., A general framework for implementing NLO calculations in shower Monte Carlo programs: the POWHEG BOX. JHEP **06**, 043 (2010). arXiv:1002.2581 [hep-ph]

41. T. Sjöstrand, S. Mrenna, P. Skands, PYTHIA 6.4 physics and manual. JHEP **05**, 026 (2006). doi:10.1088/1126-6708/2006/05/026. arXiv:hep-ph/0603175 [hep-ph]

42. B. Cooper et al., Monte Carlo tuning in the presence of matching. Eur. Phys. J. C **72**, 2078 (2011). doi:10.1140/epjc/s10052-012-2078-y. arXiv:1109.5295 [hep-ph]

43. D.J. Lange, The EvtGen particle decay simulation package. Nucl. Instrum. Methods A **462**, 152 (2001). doi:10.1016/S0168-9002(01)00089-4

44. T. Gleisberg et al., Event generation with Sherpa 1.1. JHEP **02**, 007 (2009). arXiv:0811.4622 [hep-ph]

45. S. Schumann, F. Krauss, A Parton shower algorithm based on Catani–Seymour dipole factorisation. JHEP **03**, 038 (2008). doi:10.1088/1126-6708/2008/03/038. arXiv:0709.1027 [hep-ph]

46. T. Gleisberg, S. Höche, Comix, a new matrix element generator. JHEP **12**, 039 (2008). doi:10.1088/1126-6708/2008/12/039. arXiv:0808.3674 [hep-ph]

47. F. Cascioli, P. Maierhofer, S. Pozzorini, Scattering amplitudes with open loops. Phys. Rev. Lett. **108**, 111601 (2012). doi:10.1103/PhysRevLett.108.111601. arXiv:1111.5206 [hep-ph]

48. S. Höche et al., QCD matrix elements + parton showers: the NLO case. JHEP **04**, 027 (2013). doi:10.1007/JHEP04(2013)027. arXiv:1207.5030 [hep-ph]

49. S. Catani et al., QCD Matrix elements + Parton showers. JHEP **11**, 063 (2001). doi:10.1088/1126-6708/2001/11/063. arXiv:hep-ph/0109231

50. L. Lönnblad, Correcting the colour-dipole cascade model with fixed order matrix elements. JHEP **05**, 046 (2002). doi:10.1088/1126-6708/2002/05/046. arXiv:hep-ph/0112284

51. W. Beenakker et al., Squark and gluino production at hadron colliders. Nucl. Phys. B **492**, 51–103 (1997). doi:10.1016/S0550-3213(97)00084-9. arXiv:hep-ph/9610490 [hep-ph]

52. A. Kulesza, L. Motyka, Threshold resummation for squark–antisquark and gluino-pair production at the LHC. Phys. Rev. Lett. **102**, 111802 (2009). doi:10.1103/PhysRevLett.102.111802. arXiv:0807.2405 [hep-ph]

53. A. Kulesza, L. Motyka, Soft gluon resummation for the production of gluino–gluino and squark–antisquark pairs at the LHC. Phys. Rev. D **80**, 095004 (2009). doi:10.1103/PhysRevD.80.095004. arXiv:0905.4749 [hep-ph]

54. W. Beenakker et al., Soft-gluon resummation for squark and gluino hadroproduction. JHEP **12**, 041 (2009). doi:10.1088/1126-6708/2009/12/041. arXiv:0909.4418 [hep-ph]

55. W. Beenakker et al., Squark and gluino hadroproduction. Int. J. Mod. Phys. A **26**, 2637–2664 (2011). doi:10.1142/S0217751X11053560. arXiv:1105.1110 [hep-ph]

56. ATLAS Collaboration, The ATLAS simulation infrastructure. Eur. Phys. J. C **70**, 823–874 (2010). doi:10.1140/epjc/s10052-010-1429-9. arXiv:1005.4568 [physics.ins-det]

57. S. Agostinelli et al., GEANT4: a simulation toolkit. Nucl. Instrum. Methods A **506**, 250–303 (2003). doi:10.1016/S0168-9002(03)01368-8

58. ATLAS Collaboration, Summary of ATLAS Pythia 8 tunes. ATL-PHYS-PUB-2012-003, 2012. http://cds.cern.ch/record/1474107

59. G. Watt, R.S. Thorne, Study of Monte Carlo approach to experimental uncertainty propagation with MSTW 2008 PDFs. JHEP **08**, 052 (2012). doi:10.1007/JHEP08(2012)052. arXiv:1205.4024 [hep-ph]

60. ATLAS Collaboration, Modelling of the $t\bar{t}H$ and $t\bar{t}V$ ($V = W, Z$) processes for $\sqrt{s} = 13$ TeV ATLAS analyses. ATL-PHYS-PUB-2016-005, 2016. http://cds.cern.ch/record/2120826

61. M.V. Garzelli et al., $t\bar{t}\,W^{+-}$ and $t\bar{t}Z$ Hadroproduction at NLO accuracy in QCD with Parton Shower and Hadronization effects. JHEP **11**, 056 (2012). doi:10.1007/JHEP11(2012)056. arXiv:1208.2665 [hep-ph]

62. J.M. Campbell, R.K. Ellis, $t\bar{t}W$ production and decay at NLO. JHEP **07**, 052 (2012). arXiv:1204.5678 [hep-ph]

63. A. Lazopoulos et al., Next-to-leading order QCD corrections to $t\bar{t}Z$ production at the LHC. Phys Lett. B **666**, 62 (2008). arXiv:0804.2220 [hep-ph]

64. ATLAS Collaboration, Simulation of top quark production for the ATLAS experiment at $\sqrt{s} = 13$ TeV. ATL-PHYS-PUB-2016-004, 2016. http://cds.cern.ch/record/2120417

65. M. Czakon, P. Fiedler, A. Mitov, Total top-quark pair-production cross section at hadron colliders through $O(\alpha_s^4)$. Phys. Rev. Lett. **110**, 252004 (2013). arXiv:1303.6254 [hep-ph]

66. M. Czakon, A. Mitov, Top++: a program for the calculation of the top-pair cross-section at hadron colliders. Comput. Phys. Commun. **185**, 2930 (2014). doi:10.1016/j.cpc.2014.06.021. arXiv:1112.5675 [hep-ph]

67. N. Kidonakis, Two-loop soft anomalous dimensions for single top quark associated production with a W^- or H^-. Phys. Rev. D **82**, 054018 (2010). doi:10.1103/PhysRevD.82.054018. arXiv:1005.4451 [hep-ph]

68. ATLAS Collaboration, Multi-Boson simulation for 13 TeV ATLAS analyses. ATL-PHYS-PUB-2016-002, 2016. http://cds.cern.ch/record/2119986

69. J.M. Campbell, R.K. Ellis, An update on vector boson pair production at hadron colliders. Phys. Rev. D **60**, 113006 (1999). arXiv:hep-ph/9905386 [hep-ph]

70. J.M. Campbell, R.K. Ellis, C. Williams, Vector boson pair production at the LHC. JHEP **07**, 018 (2011). arXiv:1105.0020 [hep-ph]

71. ATLAS Collaboration, Monte Carlo generators for the production of a W or Z/γ^* boson in association with jets at ATLAS in Run 2. ATL-PHYS-PUB-2016-003, 2016. http://cds.cern.ch/record/2120133

72. S. Catani et al., Vector boson production at hadron colliders: a fully exclusive QCD calculation at NNLO. Phys. Rev. Lett. **103**, 082001 (2009). arXiv:0903.2120 [hep-ph]

73. S. Catani, M. Grazzini, An NNLO subtraction formalism in hadron collisions and its application to Higgs boson production at the LHC. Phys. Rev. Lett. **98**, 222002 (2007). arXiv:hep-ph/0703012 [hep-ph]

74. ATLAS Collaboration, Vertex reconstruction performance of the ATLAS detector at $\sqrt{s} = 13$ TeV. ATL-PHYS-PUB-2015-026, 2015. http://cds.cern.ch/record/2037717

75. ATLAS Collaboration, Electron efficiency measurements with the ATLAS detector using the 2012 LHC proton–proton collision data. ATLAS-CONF-2014-032, (2014). https://cds.cern.ch/record/1706245

76. ATLAS Collaboration, Muon reconstruction performance of the ATLAS detector in proton–proton collision data at $\sqrt{s} = 13 TeV$. Eur. Phys. J. C **76**, 292 (2016). doi:10.1140/epjc/s10052-016-4120-y. arXiv:1603.05598 [hep-ex]

77. ATLAS Collaboration, Topological cell clustering in the ATLAS calorimeters and its performance in LHC Run 1. (2016). arXiv:1603.02934 [hep-ex]

78. M. Cacciari, G.P. Salam, G. Soyez, The anti-k_t jet clustering algorithm. JHEP **04**, 063 (2008). doi:10.1088/1126-6708/2008/04/063. arXiv:0802.1189 [hep-ph]

79. M. Cacciari, G.P. Salam, Dispelling the N^3 myth for the Kt jet-finder. Phys. Lett. B **641**, 57–61 (2006). doi:10.1016/j.physletb.2006.08.037. arXiv:hep-ph/0512210

80. ATLAS Collaboration, Jet energy measurement and its systematic uncertainty in proton–proton collisions at $\sqrt{s} = 7TeV$ with the ATLAS detector. Eur. Phys. J. C **75**, 17 (2015). doi:10.1140/epjc/s10052-014-3190-y. arXiv:1406.0076 [hep-ex]

81. ATLAS Collaboration, Jet calibration and systematic uncertainties for jets reconstructed in the ATLAS detector at $\sqrt{s} = 13$ TeV. ATL-PHYS-PUB-2015-015, 2015. http://cds.cern.ch/record/2037613

82. ATLAS Collaboration, Tagging and suppression of pileup jets with the ATLAS detector. ATLAS-CONF-2014-018, 2014. http://cds.cern.ch/record/1700870

83. ATLAS Collaboration, Characterisation and mitigation of beam-induced backgrounds observed in the ATLAS detector during the 2011 proton–proton run. JINST **8**, P07004 (2013). doi:10.1088/1748-0221/8/07/P07004. arXiv:1303.0223 [hep-ex]

84. ATLAS Collaboration, Selection of jets produced in 13 TeV proton–proton collisions with the ATLAS detector. ATLAS-CONF-2015-029, 2015. http://cds.cern.ch/record/2037702

85. ATLAS Collaboration, Performance of b-Jet Identification in the ATLAS experiment. JINST **11**, P04008 (2016). doi:10.1088/1748-0221/11/04/P04008. arXiv:1512.01094 [hep-ex]

86. ATLAS Collaboration, Optimisation of the ATLAS b-tagging performance for the 2016 LHC Run. ATL-PHYS-PUB-2016-012, 2016. http://cds.cern.ch/record/2160731

87. ATLAS Collaboration, Electron and photon energy calibration with the ATLAS detector using LHC Run 1 data. Eur. Phys. J. C **74**, 3071 (2014). doi:10.1140/epjc/s10052-014-3071-4. arXiv:1407.5063 [hep-ex]

88. ATLAS Collaboration, Expected performance of missing transverse momentum reconstruction for the ATLAS detector at $\sqrt{s}$ = 13 TeV. ATL-PHYS-PUB-2015-023, 2015. http://cds.cern.ch/record/2037700

89. ATLAS Collaboration, Performance of missing transverse momentum reconstruction for the ATLAS detector in the first proton–proton collisions at at $\sqrt{s}$ = 13 TeV. ATL-PHYS-PUB-2015-027, 2015. http://cds.cern.ch/record/2037904

90. G. Cowan et al., Asymptotic formulae for likelihood-based tests of new physics. Eur. Phys. J. C **71**, 1554 (2011). doi:10.1140/epjc/s10052-011-1554-0. arXiv:1007.1727 [physics.data-an]

91. ATLAS Collaboration, Measurement of the differential cross-section of highly boosted top quarks as a function of their transverse momentum in $\sqrt{s}$ = 8 TeV proton–proton collisions using the ATLAS detector. Phys. Rev. D **93**, 032009 (2016). doi:10.1103/PhysRevD.93.032009. arXiv:1510.03818 [hep-ex]

92. CMS Collaboration, Measurement of the integrated and differential t-tbar production cross sections for high-p_{T} top quarks in pp collisions at $\sqrt{s}$ = 8 TeV. Phys. Rev. D **94**, 072002 (2016). doi:10.1103/PhysRevD.94.072002. arXiv:1605.00116 [hep-ex]

93. M. Czakon, D. Heymes, A. Mitov. Dynamical scales for multi-TeV top-pair production at the LHC. (2016). arXiv:1606.03350 [hep-ph]

94. ATLAS Collaboration, Search for squarks and gluinos in events with isolated leptons, jets and missing transverse momentum at $\sqrt{s}$ = $8 TeV$ with the ATLAS detector. JHEP **04**, 116 (2015). doi:10.1007/JHEP04(2015)116. arXiv:1501.03555 [hep-ex]

95. M. Krämer et al., Supersymmetry production cross sections in pp collisions at $\sqrt{s}$ = $7 TeV$. (2012). arXiv:1206.2892 [hep-ph]

96. C. Borschensky et al., Squark and gluino production cross sections in pp collisions at $\sqrt{s}$ = 13, 14, 33 and 100 TeV Eur. Phys. J. C **74**, 3174 (2014). doi:10.1140/epjc/s10052-014-3174-y. arXiv:1407.5066 [hep-ph]

97. M. Baak et al., HistFitter software framework for statistical data analysis Eur. Phys. J. C **75**, 153 (2014). doi:10.1140/epjc/s10052-015-3327-7. arXiv:1410.1280 [hep-ex]

98. A. Read, Presentation of search results: the CLs technique. J. Phys. G Nucl. Part. Phys. **28**, 2693–2704 (2002). doi:10.1088/0954-3899/28/10/313

99. ATLAS Collaboration, ATLAS computing acknowledgements 2016–2017. ATL-GEN-PUB-2016-002, 2016. https://cds.cern.ch/record/2202407

ATLAS Collaboration

M. Aaboud[137c], G. Aad[88], B. Abbott[115], J. Abdallah[8], O. Abdinov[12], B. Abeloos[119], O. S. AbouZeid[139], N. L. Abraham[151], H. Abramowicz[155], H. Abreu[154], R. Abreu[118], Y. Abulaiti[148a,148b], B. S. Acharya[167a,167b,a], S. Adachi[157], L. Adamczyk[41a], D. L. Adams[27], J. Adelman[110], T. Adye[133], A. A. Affolder[139], T. Agatonovic-Jovin[14], C. Agheorghiesei[28b], J. A. Aguilar-Saavedra[128a,128f], S. P. Ahlen[24], F. Ahmadov[68,b], G. Aielli[135a,135b], H. Akerstedt[148a,148b], T. P. A. Åkesson[84], A. V. Akimov[98], G. L. Alberghi[22a,22b], J. Albert[172], M. J. Alconada Verzini[74], M. Aleksa[32], I. N. Aleksandrov[68], C. Alexa[28b], G. Alexander[155], T. Alexopoulos[10], M. Alhroob[115], B. Ali[130], M. Aliev[76a,76b], G. Alimonti[94a], J. Alison[33], S. P. Alkire[38], B. M. M. Allbrooke[151], B. W. Allen[118], P. P. Allport[19], A. Aloisio[106a,106b], A. Alonso[39], F. Alonso[74], C. Alpigiani[140], A. A. Alshehri[56], M. Alstaty[88], B. Alvarez Gonzalez[32], D. Álvarez Piqueras[170], M. G. Alviggi[106a,106b], B. T. Amadio[16], Y. Amaral Coutinho[26a], C. Amelung[25], D. Amidei[92], S. P. Amor Dos Santos[128a,128c], A. Amorim[128a,128b], S. Amoroso[32], G. Amundsen[25], C. Anastopoulos[141], L. S. Ancu[52], N. Andari[19], T. Andeen[11], C. F. Anders[60b], J. K. Anders[77], K. J. Anderson[33], A. Andreazza[94a,94b], V. Andrei[60a], S. Angelidakis[9], I. Angelozzi[109], A. Angerami[38], F. Anghinolfi[32], A. V. Anisenkov[111,c], N. Anjos[13], A. Annovi[126a,126b], C. Antel[60a], M. Antonelli[50], A. Antonov[100,*], D. J. Antrim[166], F. Anulli[134a], M. Aoki[69], L. Aperio Bella[19], G. Arabidze[93], Y. Arai[69], J. P. Araque[128a], V. Araujo Ferraz[26a], A. T. H. Arce[48], F. A. Arduh[74], J.-F. Arguin[97], S. Argyropoulos[66], M. Arik[20a], A. J. Armbruster[145], L. J. Armitage[79], O. Arnaez[32], H. Arnold[51], M. Arratia[30], O. Arslan[23], A. Artamonov[99], G. Artoni[122], S. Artz[86], S. Asai[157], N. Asbah[45], A. Ashkenazi[155], B. Åsman[148a,148b], L. Asquith[151], K. Assamagan[27], R. Astalos[146a], M. Atkinson[169], N. B. Atlay[143], K. Augsten[130], G. Avolio[32], B. Axen[16], M. K. Ayoub[119], G. Azuelos[97,d], M. A. Baak[32], A. E. Baas[60a], M. J. Baca[19], H. Bachacou[138], K. Bachas[76a,76b], M. Backes[122], M. Backhaus[32], P. Bagiacchi[134a,134b], P. Bagnaia[134a,134b], Y. Bai[35a], J. T. Baines[133], M. Bajic[39], O. K. Baker[179], E. M. Baldin[111,c], P. Balek[175], T. Balestri[150], F. Balli[138], W. K. Balunas[124], E. Banas[42], Sw. Banerjee[176,e], A. A. E. Bannoura[178], L. Barak[32], E. L. Barberio[91], D. Barberis[53a,53b], M. Barbero[88], T. Barillari[103], M-S Barisits[32], T. Barklow[145], N. Barlow[30], S. L. Barnes[87], B. M. Barnett[133], R. M. Barnett[16], Z. Barnovska-Blenessy[36a], A. Baroncelli[136a], G. Barone[25], A. J. Barr[122], L. Barranco Navarro[170], F. Barreiro[85], J. Barreiro Guimarães da Costa[35a], R. Bartoldus[145], A. E. Barton[75], P. Bartos[146a], A. Basalaev[125], A. Bassalat[119,f], R. L. Bates[56], S. J. Batista[161], J. R. Batley[30], M. Battaglia[139], M. Bauce[134a,134b], F. Bauer[138], H. S. Bawa[145,g], J. B. Beacham[113], M. D. Beattie[75], T. Beau[83], P. H. Beauchemin[165], P. Bechtle[23], H. P. Beck[18,h], K. Becker[122], M. Becker[86], M. Beckingham[173], C. Becot[112], A. J. Beddall[20d], A. Beddall[20b], V. A. Bednyakov[68], M. Bedognetti[109], C. P. Bee[150], L. J. Beemster[109], T. A. Beermann[32], M. Begel[27], J. K. Behr[45], A. S. Bell[81], G. Bella[155], L. Bellagamba[22a], A. Bellerive[31], M. Bellomo[89], K. Belotskiy[100], O. Beltramello[32], N. L. Belyaev[100], O. Benary[155,*], D. Benchekroun[137a], M. Bender[102], K. Bendtz[148a,148b], N. Benekos[10], Y. Benhammou[155], E. Benhar Noccioli[179], J. Benitez[66], D. P. Benjamin[48], J. R. Bensinger[25], S. Bentvelsen[109], L. Beresford[122], M. Beretta[50], D. Berge[109], E. Bergeaas Kuutmann[168], N. Berger[5], J. Beringer[16], S. Berlendis[58], N. R. Bernard[89], C. Bernius[112], F. U. Bernlochner[23], T. Berry[80], P. Berta[131],

C. Bertella[86], G. Bertoli[148a,148b], F. Bertolucci[126a,126b], I. A. Bertram[75], C. Bertsche[45], D. Bertsche[115], G. J. Besjes[39], O. Bessidskaia Bylund[148a,148b], M. Bessner[45], N. Besson[138], C. Betancourt[51], A. Bethani[58], S. Bethke[103], A. J. Bevan[79], R. M. Bianchi[127], M. Bianco[32], O. Biebel[102], D. Biedermann[17], R. Bielski[87], N. V. Biesuz[126a,126b], M. Biglietti[136a], J. Bilbao De Mendizabal[52], T. R. V. Billoud[97], H. Bilokon[50], M. Bindi[57], A. Bingul[20b], C. Bini[134a,134b], S. Biondi[22a,22b], T. Bisanz[57], D. M. Bjergaard[48], C. W. Black[152], J. E. Black[145], K. M. Black[24], D. Blackburn[140], R. E. Blair[6], T. Blazek[146a], I. Bloch[45], C. Blocker[25], A. Blue[56], W. Blum[86,*], U. Blumenschein[57], S. Blunier[34a], G. J. Bobbink[109], V. S. Bobrovnikov[111,c], S. S. Bocchetta[84], A. Bocci[48], C. Bock[102], M. Boehler[51], D. Boerner[178], J. A. Bogaerts[32], D. Bogavac[102], A. G. Bogdanchikov[111], C. Bohm[148a], V. Boisvert[80], P. Bokan[14], T. Bold[41a], A. S. Boldyrev[101], M. Bomben[83], M. Bona[79], M. Boonekamp[138], A. Borisov[132], G. Borissov[75], J. Bortfeldt[32], D. Bortoletto[122], V. Bortolotto[62a,62b,62c], K. Bos[109], D. Boscherini[22a], M. Bosman[13], J. D. Bossio Sola[29], J. Boudreau[127], J. Bouffard[2], E. V. Bouhova-Thacker[75], D. Boumediene[37], C. Bourdarios[119], S. K. Boutle[56], A. Boveia[113], J. Boyd[32], I. R. Boyko[68], J. Bracinik[19], A. Brandt[8], G. Brandt[57], O. Brandt[60a], U. Bratzler[158], B. Brau[89], J. E. Brau[118], W. D. Breaden Madden[56], K. Brendlinger[124], A. J. Brennan[91], L. Brenner[109], R. Brenner[168], S. Bressler[175], T. M. Bristow[49], D. Britton[56], D. Britzger[45], F. M. Brochu[30], I. Brock[23], R. Brock[93], G. Brooijmans[38], T. Brooks[80], W. K. Brooks[34b], J. Brosamer[16], E. Brost[110], J. H Broughton[19], P. A. Bruckman de Renstrom[42], D. Bruncko[146b], A. Bruni[22a], G. Bruni[22a], L. S. Bruni[109], BH Brunt[30], M. Bruschi[22a], N. Bruscino[23], P. Bryant[33], L. Bryngemark[84], T. Buanes[15], Q. Buat[144], P. Buchholz[143], A. G. Buckley[56], I. A. Budagov[68], F. Buehrer[51], M. K. Bugge[121], O. Bulekov[100], D. Bullock[8], H. Burckhart[32], S. Burdin[77], C. D. Burgard[51], A. M. Burger[5], B. Burghgrave[110], K. Burka[42], S. Burke[133], I. Burmeister[46], J. T. P. Burr[122], E. Busato[37], D. Büscher[51], V. Büscher[86], P. Bussey[56], J. M. Butler[24], C. M. Buttar[56], J. M. Butterworth[81], P. Butti[109], W. Buttinger[27], A. Buzatu[35c], A. R. Buzykaev[111,c], S. Cabrera Urbán[170], D. Caforio[130], V. M. Cairo[40a,40b], O. Cakir[4a], N. Calace[52], P. Calafiura[16], A. Calandri[88], G. Calderini[83], P. Calfayan[64], G. Callea[40a,40b], L. P. Caloba[26a], S. Calvente Lopez[85], D. Calvet[37], S. Calvet[37], T. P. Calvet[88], R. Camacho Toro[33], S. Camarda[32], P. Camarri[135a,135b], D. Cameron[121], R. Caminal Armadans[169], C. Camincher[58], S. Campana[32], M. Campanelli[81], A. Camplani[94a,94b], A. Campoverde[143], V. Canale[106a,106b], A. Canepa[163a], M. Cano Bret[36c], J. Cantero[116], T. Cao[155], M. D. M. Capeans Garrido[32], I. Caprini[28b], M. Caprini[28b], M. Capua[40a,40b], R. M. Carbone[38], R. Cardarelli[135a], F. Cardillo[51], I. Carli[131], T. Carli[32], G. Carlino[106a], B. T. Carlson[127], L. Carminati[94a,94b], R. M. D. Carney[148a,148b], S. Caron[108], E. Carquin[34b], G. D. Carrillo-Montoya[32], J. R. Carter[30], J. Carvalho[128a,128c], D. Casadei[19], M. P. Casado[13,i], M. Casolino[13], D. W. Casper[166], R. Castelijn[109], A. Castelli[109], V. Castillo Gimenez[170], N. F. Castro[128a,j], A. Catinaccio[32], J. R. Catmore[121], A. Cattai[32], J. Caudron[23], V. Cavaliere[169], E. Cavallaro[13], D. Cavalli[94a], M. Cavalli-Sforza[13], V. Cavasinni[126a,126b], F. Ceradini[136a,136b], L. Cerda Alberich[170], A. S. Cerqueira[26b], A. Cerri[151], L. Cerrito[135a,135b], F. Cerutti[16], A. Cervelli[18], S. A. Cetin[20c], A. Chafaq[137a], D. Chakraborty[110], S. K. Chan[59], Y. L. Chan[62a], P. Chang[169], J. D. Chapman[30], D. G. Charlton[19], A. Chatterjee[52], C. C. Chau[161], C. A. Chavez Barajas[151], S. Che[113], S. Cheatham[167a,167c], A. Chegwidden[93], S. Chekanov[6], S. V. Chekulaev[163a], G. A. Chelkov[68,k], M. A. Chelstowska[32], C. Chen[67], H. Chen[27], S. Chen[35b], S. Chen[157], X. Chen[35c], Y. Chen[70], H. C. Cheng[92], H. J. Cheng[35a], Y. Cheng[33], A. Cheplakov[68], E. Cheremushkina[132], R. Cherkaoui El Moursli[137d], V. Chernyatin[27,*], E. Cheu[7], L. Chevalier[138], V. Chiarella[50], G. Chiarelli[126a,126b], G. Chiodini[76a], A. S. Chisholm[32], A. Chitan[28b], Y. H. Chiu[172], M. V. Chizhov[68], K. Choi[64], A. R. Chomont[37], S. Chouridou[9], B. K. B. Chow[102], V. Christodoulou[81], D. Chromek-Burckhart[32], J. Chudoba[129], A. J. Chuinard[90], J. J. Chwastowski[42], L. Chytka[117], A. K. Ciftci[4a], D. Cinca[46], V. Cindro[78], I. A. Cioara[23], A. Ciocca[22a,22b], A. Ciocio[16], F. Cirotto[106a,106b], Z. H. Citron[175], M. Citterio[94a], M. Ciubancan[28b], A. Clark[52], B. L. Clark[59], M. R. Clark[38], P. J. Clark[49], R. N. Clarke[16], C. Clement[148a,148b], Y. Coadou[88], M. Cobal[167a,167c], A. Coccaro[52], J. Cochran[67], L. Colasurdo[108], B. Cole[38], A. P. Colijn[109], J. Collot[58], T. Colombo[166], P. Conde Muiño[128a,128b], E. Coniavitis[51], S. H. Connell[147b], I. A. Connelly[80], V. Consorti[51], S. Constantinescu[28b], G. Conti[32], F. Conventi[106a,l], M. Cooke[16], B. D. Cooper[81], A. M. Cooper-Sarkar[122], F. Cormier[171], K. J. R. Cormier[161], T. Cornelissen[178], M. Corradi[134a,134b], F. Corriveau[90,m], A. Cortes-Gonzalez[32], G. Cortiana[103], G. Costa[94a], M. J. Costa[170], D. Costanzo[141], G. Cottin[30], G. Cowan[80], B. E. Cox[87], K. Cranmer[112], S. J. Crawley[56], G. Cree[31], S. Crépé-Renaudin[58], F. Crescioli[83], W. A. Cribbs[148a,148b], M. Crispin Ortuzar[122], M. Cristinziani[23], V. Croft[108], G. Crosetti[40a,40b], A. Cueto[85], T. Cuhadar Donszelmann[141], J. Cummings[179], M. Curatolo[50], J. Cúth[86], H. Czirr[143], P. Czodrowski[3], G. D'amen[22a,22b], S. D'Auria[56], M. D'Onofrio[77], M. J. Da Cunha Sargedas De Sousa[128a,128b], C. Da Via[87], W. Dabrowski[41a], T. Dado[146a], T. Dai[92], O. Dale[15], F. Dallaire[97], C. Dallapiccola[89], M. Dam[39], J. R. Dandoy[124], N. P. Dang[51], A. C. Daniells[19], N. S. Dann[87], M. Danninger[171], M. Dano Hoffmann[138], V. Dao[51], G. Darbo[53a], S. Darmora[8], J. Dassoulas[3], A. Dattagupta[118], T. Daubney[45], W. Davey[23], C. David[45], T. Davidek[131], M. Davies[155], P. Davison[81], E. Dawe[91], I. Dawson[141], K. De[8], R. de Asmundis[106a], A. De Benedetti[115], S. De Castro[22a,22b], S. De Cecco[83], N. De Groot[108], P. de Jong[109], H. De la Torre[93], F. De Lorenzi[67], A. De Maria[57], D. De Pedis[134a], A. De Salvo[134a], U. De Sanctis[151], A. De Santo[151], J. B. De Vivie De Regie[119],

W. J. Dearnaley[75], R. Debbe[27], C. Debenedetti[139], D. V. Dedovich[68], N. Dehghanian[3], I. Deigaard[109], M. Del Gaudio[40a,40b], J. Del Peso[85], T. Del Prete[126a,126b], D. Delgove[119], F. Deliot[138], C. M. Delitzsch[52], A. Dell'Acqua[32], L. Dell'Asta[24], M. Dell'Orso[126a,126b], M. Della Pietra[106a,l], D. della Volpe[52], M. Delmastro[5], P. A. Delsart[58], D. A. DeMarco[161], S. Demers[179], M. Demichev[68], A. Demilly[83], S. P. Denisov[132], D. Denysiuk[138], D. Derendarz[42], J. E. Derkaoui[137c], F. Derue[83], P. Dervan[77], K. Desch[23], C. Deterre[45], K. Dette[46], P. O. Deviveiros[32], A. Dewhurst[133], S. Dhaliwal[25], A. Di Ciaccio[135a,135b], L. Di Ciaccio[5], W. K. Di Clemente[124], C. Di Donato[106a,106b], A. Di Girolamo[32], B. Di Girolamo[32], B. Di Micco[136a,136b], R. Di Nardo[32], K. F. Di Petrillo[59], A. Di Simone[51], R. Di Sipio[161], D. Di Valentino[31], C. Diaconu[88], M. Diamond[161], F. A. Dias[49], M. A. Diaz[34a], E. B. Diehl[92], J. Dietrich[17], S. Díez Cornell[45], A. Dimitrievska[14], J. Dingfelder[23], P. Dita[28b], S. Dita[28b], F. Dittus[32], F. Djama[88], T. Djobava[54b], J. I. Djuvsland[60a], M. A. B. do Vale[26c], D. Dobos[32], M. Dobre[28b], C. Doglioni[84], J. Dolejsi[131], Z. Dolezal[131], M. Donadelli[26d], S. Donati[126a,126b], P. Dondero[123a,123b], J. Donini[37], J. Dopke[133], A. Doria[106a], M. T. Dova[74], A. T. Doyle[56], E. Drechsler[57], M. Dris[10], Y. Du[36b], J. Duarte-Campderros[155], E. Duchovni[175], G. Duckeck[102], O. A. Ducu[97,n], D. Duda[109], A. Dudarev[32], A. Chr. Dudder[86], E. M. Duffield[16], L. Duflot[119], M. Dührssen[32], M. Dumancic[175], A. K. Duncan[56], M. Dunford[60a], H. Duran Yildiz[4a], M. Düren[55], A. Durglishvili[54b], D. Duschinger[47], B. Dutta[45], M. Dyndal[45], C. Eckardt[45], K. M. Ecker[103], R. C. Edgar[92], N. C. Edwards[49], T. Eifert[32], G. Eigen[15], K. Einsweiler[16], T. Ekelof[168], M. El Kacimi[137b], V. Ellajosyula[88], M. Ellert[168], S. Elles[5], F. Ellinghaus[178], A. A. Elliot[172], N. Ellis[32], J. Elmsheuser[27], M. Elsing[32], D. Emeliyanov[133], Y. Enari[157], O. C. Endner[86], J. S. Ennis[173], J. Erdmann[46], A. Ereditato[18], G. Ernis[178], J. Ernst[2], M. Ernst[27], S. Errede[169], E. Ertel[86], M. Escalier[119], H. Esch[46], C. Escobar[127], B. Esposito[50], A. I. Etienvre[138], E. Etzion[155], H. Evans[64], A. Ezhilov[125], M. Ezzi[137d], F. Fabbri[22a,22b], L. Fabbri[22a,22b], G. Facini[33], R. M. Fakhrutdinov[132], S. Falciano[134a], R. J. Falla[81], J. Faltova[32], Y. Fang[35a], M. Fanti[94a,94b], A. Farbin[8], A. Farilla[136a], C. Farina[127], E. M. Farina[123a,123b], T. Farooque[93], S. Farrell[16], S. M. Farrington[173], P. Farthouat[32], F. Fassi[137d], P. Fassnacht[32], D. Fassouliotis[9], M. Faucci Giannelli[80], A. Favareto[53a,53b], W. J. Fawcett[122], L. Fayard[119], O. L. Fedin[125,o], W. Fedorko[171], S. Feigl[121], L. Feligioni[88], C. Feng[36b], E. J. Feng[32], H. Feng[92], A. B. Fenyuk[132], L. Feremenga[8], P. Fernandez Martinez[170], S. Fernandez Perez[13], J. Ferrando[45], A. Ferrari[168], P. Ferrari[109], R. Ferrari[123a], D. E. Ferreira de Lima[60b], A. Ferrer[170], D. Ferrere[52], C. Ferretti[92], F. Fiedler[86], A. Filipčič[78], M. Filipuzzi[45], F. Filthaut[108], M. Fincke-Keeler[172], K. D. Finelli[152], M. C. N. Fiolhais[128a,128c], L. Fiorini[170], A. Fischer[2], C. Fischer[13], J. Fischer[178], W. C. Fisher[93], N. Flaschel[45], I. Fleck[143], P. Fleischmann[92], G. T. Fletcher[141], R. R. M. Fletcher[124], T. Flick[178], B. M. Flierl[102], L. R. Flores Castillo[62a], M. J. Flowerdew[103], G. T. Forcolin[87], A. Formica[138], A. Forti[87], A. G. Foster[19], D. Fournier[119], H. Fox[75], S. Fracchia[13], P. Francavilla[83], M. Franchini[22a,22b], D. Francis[32], L. Franconi[121], M. Franklin[59], M. Frate[166], M. Fraternali[123a,123b], D. Freeborn[81], S. M. Fressard-Batraneanu[32], D. Froidevaux[32], J. A. Frost[122], C. Fukunaga[158], E. Fullana Torregrosa[86], T. Fusayasu[104], J. Fuster[170], C. Gabaldon[58], O. Gabizon[154], A. Gabrielli[22a,22b], A. Gabrielli[16], G. P. Gach[41a], S. Gadatsch[32], G. Gagliardi[53a,53b], L. G. Gagnon[97], P. Gagnon[64], C. Galea[108], B. Galhardo[128a,128c], E. J. Gallas[122], B. J. Gallop[133], P. Gallus[130], G. Galster[39], K. K. Gan[113], S. Ganguly[37], J. Gao[36a], Y. Gao[77], Y. S. Gao[145,g], F. M. Garay Walls[49], C. García[170], J. E. García Navarro[170], M. Garcia-Sciveres[16], R. W. Gardner[33], N. Garelli[145], V. Garonne[121], A. Gascon Bravo[45], K. Gasnikova[45], C. Gatti[50], A. Gaudiello[53a,53b], G. Gaudio[123a], L. Gauthier[97], I. L. Gavrilenko[98], C. Gay[171], G. Gaycken[23], E. N. Gazis[10], Z. Gecse[171], C. N. P. Gee[133], Ch. Geich-Gimbel[23], M. Geisen[86], M. P. Geisler[60a], K. Gellerstedt[148a,148b], C. Gemme[53a], M. H. Genest[58], C. Geng[36a,p], S. Gentile[134a,134b], C. Gentsos[156], S. George[80], D. Gerbaudo[13], A. Gershon[155], S. Ghasemi[143], M. Ghneimat[23], B. Giacobbe[22a], S. Giagu[134a,134b], P. Giannetti[126a,126b], S. M. Gibson[80], M. Gignac[171], M. Gilchriese[16], T. P. S. Gillam[30], D. Gillberg[31], G. Gilles[178], D. M. Gingrich[3,d], N. Giokaris[9,*], M. P. Giordani[167a,167c], F. M. Giorgi[22a], P. F. Giraud[138], P. Giromini[59], D. Giugni[94a], F. Giuli[122], C. Giuliani[103], M. Giulini[60b], B. K. Gjelsten[121], S. Gkaitatzis[156], I. Gkialas[156], E. L. Gkougkousis[139], L. K. Gladilin[101], C. Glasman[85], J. Glatzer[13], P. C. F. Glaysher[49], A. Glazov[45], M. Goblirsch-Kolb[25], J. Godlewski[42], S. Goldfarb[91], T. Golling[52], D. Golubkov[132], A. Gomes[128a,128b,128d], R. Gonçalo[128a], R. Goncalves Gama[26a], J. Goncalves Pinto Firmino Da Costa[138], G. Gonella[51], L. Gonella[19], A. Gongadze[68], S. González de la Hoz[170], S. Gonzalez-Sevilla[52], L. Goossens[32], P. A. Gorbounov[99], H. A. Gordon[27], I. Gorelov[107], B. Gorini[32], E. Gorini[76a,76b], A. Gorišek[78], A. T. Goshaw[48], C. Gössling[46], M. I. Gostkin[68], C. R. Goudet[119], D. Goujdami[137b], A. G. Goussiou[140], N. Govender[147b,q], E. Gozani[154], L. Graber[57], I. Grabowska-Bold[41a], P. O. J. Gradin[58], P. Grafström[22a,22b], J. Gramling[52], E. Gramstad[121], S. Grancagnolo[17], V. Gratchev[125], P. M. Gravila[28d], H. M. Gray[32], E. Graziani[136a], Z. D. Greenwood[82,r], C. Grefe[23], K. Gregersen[81], I. M. Gregor[45], P. Grenier[145], K. Grevtsov[5], J. Griffiths[8], A. A. Grillo[139], K. Grimm[75], S. Grinstein[13,s], Ph. Gris[37], J.-F. Grivaz[119], S. Groh[86], E. Gross[175], J. Grosse-Knetter[57], G. C. Grossi[82], Z. J. Grout[81], L. Guan[92], W. Guan[176], J. Guenther[65], F. Guescini[163a], D. Guest[166], O. Gueta[155], B. Gui[113], E. Guido[53a,53b], T. Guillemin[5], S. Guindon[2], U. Gul[56], C. Gumpert[32], J. Guo[36c], W. Guo[92], Y. Guo[36a], R. Gupta[43], S. Gupta[122], G. Gustavino[134a,134b], P. Gutierrez[115], N. G. Gutierrez Ortiz[81], C. Gutschow[81], C. Guyot[138], C. Gwenlan[122], C. B. Gwilliam[77], A. Haas[112],

C. Haber[16], H. K. Hadavand[8], N. Haddad[137d], A. Hadef[88], S. Hageböck[23], M. Hagihara[164], H. Hakobyan[180,*], M. Haleem[45], J. Haley[116], G. Halladjian[93], G. D. Hallewell[88], K. Hamacher[178], P. Hamal[117], K. Hamano[172], A. Hamilton[147a], G. N. Hamity[141], P. G. Hamnett[45], L. Han[36a], S. Han[35a], K. Hanagaki[69,t], K. Hanawa[157], M. Hance[139], B. Haney[124], P. Hanke[60a], R. Hanna[138], J. B. Hansen[39], J. D. Hansen[39], M. C. Hansen[23], P. H. Hansen[39], K. Hara[164], A. S. Hard[176], T. Harenberg[178], F. Hariri[119], S. Harkusha[95], R. D. Harrington[49], P. F. Harrison[173], F. Hartjes[109], N. M. Hartmann[102], M. Hasegawa[70], Y. Hasegawa[142], A. Hasib[49], S. Hassani[138], S. Haug[18], R. Hauser[93], L. Hauswald[47], M. Havranek[130], C. M. Hawkes[19], R. J. Hawkings[32], D. Hayakawa[159], D. Hayden[93], C. P. Hays[122], J. M. Hays[79], H. S. Hayward[77], S. J. Haywood[133], S. J. Head[19], T. Heck[86], V. Hedberg[84], L. Heelan[8], S. Heim[124], T. Heim[16], B. Heinemann[45], J. J. Heinrich[102], L. Heinrich[112], C. Heinz[55], J. Hejbal[129], L. Helary[32], S. Hellman[148a,148b], C. Helsens[32], J. Henderson[122], R. C. W. Henderson[75], Y. Heng[176], S. Henkelmann[171], A. M. Henriques Correia[32], S. Henrot-Versille[119], G. H. Herbert[17], H. Herde[25], V. Herget[177], Y. Hernández Jiménez[147c], G. Herten[51], R. Hertenberger[102], L. Hervas[32], T. C. Herwig[124], G. G. Hesketh[81], N. P. Hessey[109], J. W. Hetherly[43], E. Higón-Rodriguez[170], E. Hill[172], J. C. Hill[30], K. H. Hiller[45], S. J. Hillier[19], I. Hinchliffe[16], E. Hines[124], M. Hirose[51], D. Hirschbuehl[178], O. Hladik[129], X. Hoad[49], J. Hobbs[150], N. Hod[163a], M. C. Hodgkinson[141], P. Hodgson[141], A. Hoecker[32], M. R. Hoeferkamp[107], F. Hoenig[102], D. Hohn[23], T. R. Holmes[16], M. Homann[46], S. Honda[164], T. Honda[69], T. M. Hong[127], B. H. Hooberman[169], W. H. Hopkins[118], Y. Horii[105], A. J. Horton[144], J.-Y. Hostachy[58], S. Hou[153], A. Hoummada[137a], J. Howarth[45], J. Hoya[74], M. Hrabovsky[117], I. Hristova[17], J. Hrivnac[119], T. Hryn'ova[5], A. Hrynevich[96], P. J. Hsu[63], S.-C. Hsu[140], Q. Hu[36a], S. Hu[36c], Y. Huang[35a], Z. Hubacek[130], F. Hubaut[88], F. Huegging[23], T. B. Huffman[122], E. W. Hughes[38], G. Hughes[75], M. Huhtinen[32], P. Huo[150], N. Huseynov[68,b], J. Huston[93], J. Huth[59], G. Iacobucci[52], G. Iakovidis[27], I. Ibragimov[143], L. Iconomidou-Fayard[119], Z. Idrissi[137d], P. Iengo[32], O. Igonkina[109,u], T. Iizawa[174], Y. Ikegami[69], M. Ikeno[69], Y. Ilchenko[11,v], D. Iliadis[156], N. Ilic[145], G. Introzzi[123a,123b], P. Ioannou[9,*], M. Iodice[136a], K. Iordanidou[38], V. Ippolito[59], N. Ishijima[120], M. Ishino[157], M. Ishitsuka[159], C. Issever[122], S. Istin[20a], F. Ito[164], J. M. Iturbe Ponce[87], R. Iuppa[162a,162b], H. Iwasaki[69], J. M. Izen[44], V. Izzo[106a], S. Jabbar[3], P. Jackson[1], V. Jain[2], K. B. Jakobi[86], K. Jakobs[51], S. Jakobsen[32], T. Jakoubek[129], D. O. Jamin[116], D. K. Jana[82], R. Jansky[65], J. Janssen[23], M. Janus[57], P. A. Janus[41a], G. Jarlskog[84], N. Javadov[68,b], T. Javůrek[51], M. Javurkova[51], F. Jeanneau[138], L. Jeanty[16], J. Jejelava[54a,w], G.-Y. Jeng[152], P. Jenni[51,x], C. Jeske[173], S. Jézéquel[5], H. Ji[176], J. Jia[150], H. Jiang[67], Y. Jiang[36a], Z. Jiang[145], S. Jiggins[81], J. Jimenez Pena[170], S. Jin[35a], A. Jinaru[28b], O. Jinnouchi[159], H. Jivan[147c], P. Johansson[141], K. A. Johns[7], C. A. Johnson[64], W. J. Johnson[140], K. Jon-And[148a,148b], G. Jones[173], R. W. L. Jones[75], S. Jones[7], T. J. Jones[77], J. Jongmanns[60a], P. M. Jorge[128a,128b], J. Jovicevic[163a], X. Ju[176], A. Juste Rozas[13,s], M. K. Köhler[175], A. Kaczmarska[42], M. Kado[119], H. Kagan[113], M. Kagan[145], S. J. Kahn[88], T. Kaji[174], E. Kajomovitz[48], C. W. Kalderon[84], A. Kaluza[86], S. Kama[43], A. Kamenshchikov[132], N. Kanaya[157], S. Kaneti[30], L. Kanjir[78], V. A. Kantserov[100], J. Kanzaki[69], B. Kaplan[112], L. S. Kaplan[176], A. Kapliy[33], D. Kar[147c], K. Karakostas[10], A. Karamaoun[3], N. Karastathis[10], M. J. Kareem[57], E. Karentzos[10], S. N. Karpov[68], Z. M. Karpova[68], K. Karthik[112], V. Kartvelishvili[75], A. N. Karyukhin[132], K. Kasahara[164], L. Kashif[176], R. D. Kass[113], A. Kastanas[149], Y. Kataoka[157], C. Kato[157], A. Katre[52], J. Katzy[45], K. Kawade[105], K. Kawagoe[73], T. Kawamoto[157], G. Kawamura[57], V. F. Kazanin[111,c], R. Keeler[172], R. Kehoe[43], J. S. Keller[45], J. J. Kempster[80], H. Keoshkerian[161], O. Kepka[129], B. P. Kerševan[78], S. Kersten[178], R. A. Keyes[90], M. Khader[169], F. Khalil-zada[12], A. Khanov[116], A. G. Kharlamov[111,c], T. Kharlamova[111,c], T. J. Khoo[52], V. Khovanskiy[99], E. Khramov[68], J. Khubua[54b,y], S. Kido[70], C. R. Kilby[80], H. Y. Kim[8], S. H. Kim[164], Y. K. Kim[33], N. Kimura[156], O. M. Kind[17], B. T. King[77], M. King[170], D. Kirchmeier[47], J. Kirk[133], A. E. Kiryunin[103], T. Kishimoto[157], D. Kisielewska[41a], K. Kiuchi[164], O. Kivernyk[138], E. Kladiva[146b], T. Klapdor-Kleingrothaus[51], M. H. Klein[38], M. Klein[77], U. Klein[77], K. Kleinknecht[86], P. Klimek[110], A. Klimentov[27], R. Klingenberg[46], T. Klioutchnikova[32], E.-E. Kluge[60a], P. Kluit[109], S. Kluth[103], J. Knapik[42], E. Kneringer[65], E. B. F. G. Knoops[88], A. Knue[103], A. Kobayashi[157], D. Kobayashi[159], T. Kobayashi[157], M. Kobel[47], M. Kocian[145], P. Kodys[131], T. Koffas[31], E. Koffeman[109], N. M. Köhler[103], T. Koi[145], H. Kolanoski[17], M. Kolb[60b], I. Koletsou[5], A. A. Komar[98,*], Y. Komori[157], T. Kondo[69], N. Kondrashova[36c], K. Köneke[51], A. C. König[108], T. Kono[69,z], R. Konoplich[112,aa], N. Konstantinidis[81], R. Kopeliansky[64], S. Koperny[41a], A. K. Kopp[51], K. Korcyl[42], K. Kordas[156], A. Korn[81], A. A. Korol[111,c], I. Korolkov[13], E. V. Korolkova[141], O. Kortner[103], S. Kortner[103], T. Kosek[131], V. V. Kostyukhin[23], A. Kotwal[48], A. Koulouris[10], A. Kourkoumeli-Charalampidi[123a,123b], C. Kourkoumelis[9], V. Kouskoura[27], A. B. Kowalewska[42], R. Kowalewski[172], T. Z. Kowalski[41a], C. Kozakai[157], W. Kozanecki[138], A. S. Kozhin[132], V. A. Kramarenko[101], G. Kramberger[78], D. Krasnopevtsev[100], M. W. Krasny[83], A. Krasznahorkay[32], A. Kravchenko[27], M. Kretz[60c], J. Kretzschmar[77], K. Kreutzfeldt[55], P. Krieger[161], K. Krizka[33], K. Kroeninger[46], H. Kroha[103], J. Kroll[124], J. Kroseberg[23], J. Krstic[14], U. Kruchonak[68], H. Krüger[23], N. Krumnack[67], M. C. Kruse[48], M. Kruskal[24], T. Kubota[91], H. Kucuk[81], S. Kuday[4b], J. T. Kuechler[178], S. Kuehn[51], A. Kugel[60c], F. Kuger[177], T. Kuhl[45], V. Kukhtin[68], R. Kukla[138], Y. Kulchitsky[95], S. Kuleshov[34b], M. Kuna[134a,134b], T. Kunigo[71], A. Kupco[129], O. Kuprash[155], H. Kurashige[70], L. L. Kurchaninov[163a], Y. A. Kurochkin[95], M. G. Kurth[35a], V. Kus[129],

E. S. Kuwertz[172], M. Kuze[159], J. Kvita[117], T. Kwan[172], D. Kyriazopoulos[141], A. La Rosa[103], J. L. La Rosa Navarro[26d], L. La Rotonda[40a,40b], C. Lacasta[170], F. Lacava[134a,134b], J. Lacey[31], H. Lacker[17], D. Lacour[83], E. Ladygin[68], R. Lafaye[5], B. Laforge[83], T. Lagouri[179], S. Lai[57], S. Lammers[64], W. Lampl[7], E. Lançon[27], U. Landgraf[51], M. P. J. Landon[79], M. C. Lanfermann[52], V. S. Lang[60a], J. C. Lange[13], A. J. Lankford[166], F. Lanni[27], K. Lantzsch[23], A. Lanza[123a], A. Lapertosa[53a,53b], S. Laplace[83], C. Lapoire[32], J. F. Laporte[138], T. Lari[94a], F. Lasagni Manghi[22a,22b], M. Lassnig[32], P. Laurelli[50], W. Lavrijsen[16], A. T. Law[139], P. Laycock[77], T. Lazovich[59], M. Lazzaroni[94a,94b], B. Le[91], O. Le Dortz[83], E. Le Guirriec[88], E. P. Le Quilleuc[138], M. LeBlanc[172], T. LeCompte[6], F. Ledroit-Guillon[58], C. A. Lee[27], S. C. Lee[153], L. Lee[1], B. Lefebvre[90], G. Lefebvre[83], M. Lefebvre[172], F. Legger[102], C. Leggett[16], A. Lehan[77], G. Lehmann Miotto[32], X. Lei[7], W. A. Leight[31], A. G. Leister[179], M. A. L. Leite[26d], R. Leitner[131], D. Lellouch[175], B. Lemmer[57], K. J. C. Leney[81], T. Lenz[23], B. Lenzi[32], R. Leone[7], S. Leone[126a,126b], C. Leonidopoulos[49], S. Leontsinis[10], G. Lerner[151], C. Leroy[97], A. A. J. Lesage[138], C. G. Lester[30], M. Levchenko[125], J. Levêque[5], D. Levin[92], L. J. Levinson[175], M. Levy[19], D. Lewis[79], M. Leyton[44], B. Li[36a,p], C. Li[36a], H. Li[150], L. Li[48], L. Li[36c], Q. Li[35a], S. Li[48], X. Li[87], Y. Li[143], Z. Liang[35a], B. Liberti[135a], A. Liblong[161], P. Lichard[32], K. Lie[169], J. Liebal[23], W. Liebig[15], A. Limosani[152], S. C. Lin[153,ab], T. H. Lin[86], B. E. Lindquist[150], A. E. Lionti[52], E. Lipeles[124], A. Lipniacka[15], M. Lisovyi[60b], T. M. Liss[169], A. Lister[171], A. M. Litke[139], B. Liu[153,ac], H. Liu[92], H. Liu[27], J. Liu[36b], J. B. Liu[36a], K. Liu[88], L. Liu[169], M. Liu[36a], Y. L. Liu[36a], Y. Liu[36a], M. Livan[123a,123b], A. Lleres[58], J. Llorente Merino[35a], S. L. Lloyd[79], F. Lo Sterzo[153], E. M. Lobodzinska[45], P. Loch[7], F. K. Loebinger[87], K. M. Loew[25], A. Loginov[179,*], T. Lohse[17], K. Lohwasser[45], M. Lokajicek[129], B. A. Long[24], J. D. Long[169], R. E. Long[75], L. Longo[76a,76b], K. A. Looper[113], J. A. Lopez[34b], D. Lopez Mateos[59], B. Lopez Paredes[141], I. Lopez Paz[13], A. Lopez Solis[83], J. Lorenz[102], N. Lorenzo Martinez[64], M. Losada[21], P. J. Lösel[102], X. Lou[35a], A. Lounis[119], J. Love[6], P. A. Love[75], H. Lu[62a], N. Lu[92], H. J. Lubatti[140], C. Luci[134a,134b], A. Lucotte[58], C. Luedtke[51], F. Luehring[64], W. Lukas[65], L. Luminari[134a], O. Lundberg[148a,148b], B. Lund-Jensen[149], P. M. Luzi[83], D. Lynn[27], R. Lysak[129], E. Lytken[84], V. Lyubushkin[68], H. Ma[27], L. L. Ma[36b], Y. Ma[36b], G. Maccarrone[50], A. Macchiolo[103], C. M. Macdonald[141], B. Maček[78], J. Machado Miguens[124,128b], D. Madaffari[88], R. Madar[37], H. J. Maddocks[168], W. F. Mader[47], A. Madsen[45], J. Maeda[70], S. Maeland[15], T. Maeno[27], A. Maevskiy[101], E. Magradze[57], J. Mahlstedt[109], C. Maiani[119], C. Maidantchik[26a], A. A. Maier[103], T. Maier[102], A. Maio[128a,128b,128d], S. Majewski[118], Y. Makida[69], N. Makovec[119], B. Malaescu[83], Pa. Malecki[42], V. P. Maleev[125], F. Malek[58], U. Mallik[66], D. Malon[6], C. Malone[30], S. Maltezos[10], S. Malyukov[32], J. Mamuzic[170], G. Mancini[50], L. Mandelli[94a], I. Mandić[78], J. Maneira[128a,128b], L. Manhaes de Andrade Filho[26b], J. Manjarres Ramos[163b], A. Mann[102], A. Manousos[32], B. Mansoulie[138], J. D. Mansour[35a], R. Mantifel[90], M. Mantoani[57], S. Manzoni[94a,94b], L. Mapelli[32], G. Marceca[29], L. March[52], G. Marchiori[83], M. Marcisovsky[129], M. Marjanovic[14], D. E. Marley[92], F. Marroquim[26a], S. P. Marsden[87], Z. Marshall[16], S. Marti-Garcia[170], T. A. Martin[173], V. J. Martin[49], B. Martin dit Latour[15], M. Martinez[13,s], V. I. Martinez Outschoorn[169], S. Martin-Haugh[133], V. S. Martoiu[28b], A. C. Martyniuk[81], A. Marzin[32], L. Masetti[86], T. Mashimo[157], R. Mashinistov[98], J. Masik[87], A. L. Maslennikov[111,c], L. Massa[22a,22b], P. Mastrandrea[5], A. Mastroberardino[40a,40b], T. Masubuchi[157], P. Mättig[178], J. Mattmann[86], J. Maurer[28b], S. J. Maxfield[77], D. A. Ma ximov[111,c], R. Mazini[153], I. Maznas[156], S. M. Mazza[94a,94b], N. C. Mc Fadden[107], G. Mc Goldrick[161], S. P. Mc Kee[92], A. McCarn[92], R. L. McCarthy[150], T. G. McCarthy[103], L. I. McClymont[81], E. F. McDonald[91], J. A. Mcfayden[81], G. Mchedlidze[57], S. J. McMahon[133], P. C. McNamara[91], R. A. McPherson[172,m], M. Medinnis[45], S. Meehan[140], S. Mehlhase[102], A. Mehta[77], K. Meier[60a], C. Meineck[102], B. Meirose[44], D. Melini[170,ad], B. R. Mellado Garcia[147c], M. Melo[146a], F. Meloni[18], S. B. Menary[87], L. Meng[77], X. T. Meng[92], A. Mengarelli[22a,22b], S. Menke[103], E. Meoni[165], S. Mergelmeyer[17], P. Mermod[52], L. Merola[106a,106b], C. Meroni[94a], F. S. Merritt[33], A. Messina[134a,134b], J. Metcalfe[6], A. S. Mete[166], C. Meyer[124], J.-P. Meyer[138], J. Meyer[109], H. Meyer Zu Theenhausen[60a], F. Miano[151], R. P. Middleton[133], S. Miglioranzi[53a,53b], L. Mijović[49], G. Mikenberg[175], M. Mikestikova[129], M. Mikuž[78], M. Milesi[91], A. Milic[27], D. W. Miller[33], C. Mills[49], A. Milov[175], D. A. Milstead[148a,148b], A. A. Minaenko[132], Y. Minami[157], I. A. Minashvili[68], A. I. Mincer[112], B. Mindur[41a], M. Mineev[68], Y. Minegishi[157], Y. Ming[176], L. M. Mir[13], K. P. Mistry[124], T. Mitani[174], J. Mitrevski[102], V. A. Mitsou[170], A. Miucci[18], P. S. Miyagawa[141], A. Mizukami[69], J. U. Mjörnmark[84], M. Mlynarikova[131], T. Moa[148a,148b], K. Mochizuki[97], P. Mogg[51], S. Mohapatra[38], S. Molander[148a,148b], R. Moles-Valls[23], R. Monden[71], M. C. Mondragon[93], K. Mönig[45], J. Monk[39], E. Monnier[88], A. Montalbano[150], J. Montejo Berlingen[32], F. Monticelli[74], S. Monzani[94a,94b], R. W. Moore[3], N. Morange[119], D. Moreno[21], M. Moreno Llácer[57], P. Morettini[53a], S. Morgenstern[32], D. Mori[144], T. Mori[157], M. Morii[59], M. Morinaga[157], V. Morisbak[121], S. Moritz[86], A. K. Morley[152], G. Mornacchi[32], J. D. Morris[79], S. S. Mortensen[39], L. Morvaj[150], P. Moschovakos[10], M. Mosidze[54b], H. J. Moss[141], J. Moss[145,ae], K. Motohashi[159], R. Mount[145], E. Mountricha[27], E. J. W. Moyse[89], S. Muanza[88], R. D. Mudd[19], F. Mueller[103], J. Mueller[127], R. S. P. Mueller[102], T. Mueller[30], D. Muenstermann[75], P. Mullen[56], G. A. Mullier[18], F. J. Munoz Sanchez[87], J. A. Murillo Quijada[19], W. J. Murray[173,133], H. Musheghyan[57], M. Muškinja[78], A. G. Myagkov[132,af], M. Myska[130], B. P. Nachman[16], O. Nackenhorst[52], K. Nagai[122],

R. Nagai[69,z], K. Nagano[69], Y. Nagasaka[61], K. Nagata[164], M. Nagel[51], E. Nagy[88], A. M. Nairz[32], Y. Nakahama[105], K. Nakamura[69], T. Nakamura[157], I. Nakano[114], R. F. Naranjo Garcia[45], R. Narayan[11], D. I. Narrias Villar[60a], I. Naryshkin[125], T. Naumann[45], G. Navarro[21], R. Nayyar[7], H. A. Neal[92], P. Yu. Nechaeva[98], T. J. Neep[87], A. Negri[123a,123b], M. Negrini[22a], S. Nektarijevic[108], C. Nellist[119], A. Nelson[166], S. Nemecek[129], P. Nemethy[112], A. A. Nepomuceno[26a], M. Nessi[32,ag], M. S. Neubauer[169], M. Neumann[178], R. M. Neves[112], P. Nevski[27], P. R. Newman[19], T. Nguyen Manh[97], R. B. Nickerson[122], R. Nicolaidou[138], J. Nielsen[139], V. Nikolaenko[132,af], I. Nikolic-Audit[83], K. Nikolopoulos[19], J. K. Nilsen[121], P. Nilsson[27], Y. Ninomiya[157], A. Nisati[134a], R. Nisius[103], T. Nobe[157], Y. Noguchi[71], M. Nomachi[120], I. Nomidis[31], T. Nooney[79], S. Norberg[115], M. Nordberg[32], N. Norjoharuddeen[122], O. Novgorodova[47], S. Nowak[103], M. Nozaki[69], L. Nozka[117], K. Ntekas[166], E. Nurse[81], F. Nuti[91], D. C. O'Neil[144], A. A. O'Rourke[45], V. O'Shea[56], F. G. Oakham[31,d], H. Oberlack[103], T. Obermann[23], J. Ocariz[83], A. Ochi[70], I. Ochoa[38], J. P. Ochoa-Ricoux[34a], S. Oda[73], S. Odaka[69], H. Ogren[64], A. Oh[87], S. H. Oh[48], C. C. Ohm[16], H. Ohman[168], H. Oide[53a,53b], H. Okawa[164], Y. Okumura[157], T. Okuyama[69], A. Olariu[28b], L. F. Oleiro Seabra[128a], S. A. Olivares Pino[49], D. Oliveira Damazio[27], A. Olszewski[42], J. Olszowska[42], A. Onofre[128a,128e], K. Onogi[105], P. U. E. Onyisi[11,v], M. J. Oreglia[33], Y. Oren[155], D. Orestano[136a,136b], N. Orlando[62b], R. S. Orr[161], B. Osculati[53a,53b,*], R. Ospanov[87], G. Otero y Garzon[29], H. Otono[73], M. Ouchrif[137c], F. Ould-Saada[121], A. Ouraou[138], K. P. Oussoren[109], Q. Ouyang[35a], M. Owen[56], R. E. Owen[19], V. E. Ozcan[20a], N. Ozturk[8], K. Pachal[144], A. Pacheco Pages[13], L. Pacheco Rodriguez[138], C. Padilla Aranda[13], S. Pagan Griso[16], M. Paganini[179], F. Paige[27], P. Pais[89], K. Pajchel[121], G. Palacino[64], S. Palazzo[40a,40b], S. Palestini[32], M. Palka[41b], D. Pallin[37], E. St. Panagiotopoulou[10], I. Panagoulias[10], C. E. Pandini[83], J. G. Panduro Vazquez[80], P. Pani[148a,148b], S. Panitkin[27], D. Pantea[28b], L. Paolozzi[52], Th. D. Papadopoulou[10], K. Papageorgiou[156], A. Paramonov[6], D. Paredes Hernandez[179], A. J. Parker[75], M. A. Parker[30], K. A. Parker[141], F. Parodi[53a,53b], J. A. Parsons[38], U. Parzefall[51], V. R. Pascuzzi[161], E. Pasqualucci[134a], S. Passaggio[53a], Fr. Pastore[80], S. Pataraia[178], J. R. Pater[87], T. Pauly[32], J. Pearce[172], B. Pearson[115], L. E. Pedersen[39], S. Pedraza Lopez[170], R. Pedro[128a,128b], S. V. Peleganchuk[111,c], O. Penc[129], C. Peng[35a], H. Peng[36a], J. Penwell[64], B. S. Peralva[26b], M. M. Perego[138], D. V. Perepelitsa[27], E. Perez Codina[163a], L. Perini[94a,94b], H. Pernegger[32], S. Perrella[106a,106b], R. Peschke[45], V. D. Peshekhonov[68], K. Peters[45], R. F. Y. Peters[87], B. A. Petersen[32], T. C. Petersen[39], E. Petit[58], A. Petridis[1], C. Petridou[156], P. Petroff[119], E. Petrolo[134a], M. Petrov[122], F. Petrucci[136a,136b], N. E. Pettersson[89], A. Peyaud[138], R. Pezoa[34b], P. W. Phillips[133], G. Piacquadio[150], E. Pianori[173], A. Picazio[89], E. Piccaro[79], M. Piccinini[22a,22b], M. A. Pickering[122], R. Piegaia[29], J. E. Pilcher[33], A. D. Pilkington[87], A. W. J. Pin[87], M. Pinamonti[167a,167c,ah], J. L. Pinfold[3], S. Pires[83], H. Pirumov[45], M. Pitt[175], L. Plazak[146a], M.-A. Pleier[27], V. Pleskot[86], E. Plotnikova[68], D. Pluth[67], R. Poettgen[148a,148b], L. Poggioli[119], D. Pohl[23], G. Polesello[123a], A. Poley[45], A. Policicchio[40a,40b], R. Polifka[32], A. Polini[22a], C. S. Pollard[56], V. Polychronakos[27], K. Pommès[32], L. Pontecorvo[134a], B. G. Pope[93], G. A. Popeneciu[28c], A. Poppleton[32], S. Pospisil[130], K. Potamianos[16], I. N. Potrap[68], C. J. Potter[30], C. T. Potter[118], G. Poulard[32], J. Poveda[32], V. Pozdnyakov[68], M. E. Pozo Astigarraga[32], P. Pralavorio[88], A. Pranko[16], S. Prell[67], D. Price[87], L. E. Price[6], M. Primavera[76a], S. Prince[90], K. Prokofiev[62c], F. Prokoshin[34b], S. Protopopescu[27], J. Proudfoot[6], M. Przybycien[41a], D. Puddu[136a,136b], M. Purohit[27,ai], P. Puzo[119], J. Qian[92], G. Qin[56], Y. Qin[87], A. Quadt[57], W. B. Quayle[167a,167b], M. Queitsch-Maitland[45], D. Quilty[56], S. Raddum[121], V. Radeka[27], V. Radescu[122], S. K. Radhakrishnan[150], P. Radloff[118], P. Rados[91], F. Ragusa[94a,94b], G. Rahal[181], J. A. Raine[87], S. Rajagopalan[27], M. Rammensee[32], C. Rangel-Smith[168], M. G. Ratti[94a,94b], D. M. Rauch[45], F. Rauscher[102], S. Rave[86], T. Ravenscroft[56], I. Ravinovich[175], M. Raymond[32], A. L. Read[121], N. P. Readioff[77], M. Reale[76a,76b], D. M. Rebuzzi[123a,123b], A. Redelbach[177], G. Redlinger[27], R. Reece[139], R. G. Reed[147c], K. Reeves[44], L. Rehnisch[17], J. Reichert[124], A. Reiss[86], C. Rembser[32], H. Ren[35a], M. Rescigno[134a], S. Resconi[94a], E. D. Resseguie[124], O. L. Rezanova[111,c], P. Reznicek[131], R. Rezvani[97], R. Richter[103], S. Richter[81], E. Richter-Was[41b], O. Ricken[23], M. Ridel[83], P. Rieck[103], C. J. Riegel[178], J. Rieger[57], O. Rifki[115], M. Rijssenbeek[150], A. Rimoldi[123a,123b], M. Rimoldi[18], L. Rinaldi[22a], G. Ripellino[149], B. Ristić[52], E. Ritsch[32], I. Riu[13], F. Rizatdinova[116], E. Rizvi[79], C. Rizzi[13], R. T. Roberts[87], S. H. Robertson[90,m], A. Robichaud-Veronneau[90], D. Robinson[30], J. E. M. Robinson[45], A. Robson[56], C. Roda[126a,126b], Y. Rodina[88,aj], A. Rodriguez Perez[13], D. Rodriguez Rodriguez[170], S. Roe[32], C. S. Rogan[59], O. Røhne[121], J. Roloff[59], A. Romaniouk[100], M. Romano[22a,22b], S. M. Romano Saez[37], E. Romero Adam[170], N. Rompotis[77], M. Ronzani[51], L. Roos[83], E. Ros[170], S. Rosati[134a], K. Rosbach[51], P. Rose[139], N.-A. Rosien[57], V. Rossetti[148a,148b], E. Rossi[106a,106b], L. P. Rossi[53a], J. H. N. Rosten[30], R. Rosten[140], M. Rotaru[28b], I. Roth[175], J. Rothberg[140], D. Rousseau[119], A. Rozanov[88], Y. Rozen[154], X. Ruan[147c], F. Rubbo[145], M. S. Rudolph[161], F. Rühr[51], A. Ruiz-Martinez[31], Z. Rurikova[51], N. A. Rusakovich[68], A. Ruschke[102], H. L. Russell[140], J. P. Rutherfoord[7], N. Ruthmann[32], Y. F. Ryabov[125], M. Rybar[169], G. Rybkin[119], S. Ryu[6], A. Ryzhov[132], G. F. Rzehorz[57], A. F. Saavedra[152], G. Sabato[109], S. Sacerdoti[29], H. F-W. Sadrozinski[139], R. Sadykov[68], F. Safai Tehrani[134a], P. Saha[110], M. Sahinsoy[60a], M. Saimpert[138], T. Saito[157], H. Sakamoto[157], Y. Sakurai[174], G. Salamanna[136a,136b], J. E. Salazar Loyola[34b], D. Salek[109], P. H. Sales De Bruin[140], D. Salihagic[103], A. Salnikov[145], J. Salt[170], D. Salvatore[40a,40b], F. Salvatore[151], A. Salvucci[62a,62b,62c], A. Salzburger[32], D. Sammel[51],

D. Sampsonidis[156], J. Sánchez[170], V. Sanchez Martinez[170], A. Sanchez Pineda[106a,106b], H. Sandaker[121], R. L. Sandbach[79], M. Sandhoff[178], C. Sandoval[21], D. P. C. Sankey[133], M. Sannino[53a,53b], A. Sansoni[50], C. Santoni[37], R. Santonico[135a,135b], H. Santos[128a], I. Santoyo Castillo[151], K. Sapp[127], A. Sapronov[68], J. G. Saraiva[128a,128d], B. Sarrazin[23], O. Sasaki[69], K. Sato[164], E. Sauvan[5], G. Savage[80], P. Savard[161,d], N. Savic[103], C. Sawyer[133], L. Sawyer[82,r], J. Saxon[33], C. Sbarra[22a], A. Sbrizzi[22a,22b], T. Scanlon[81], D. A. Scannicchio[166], M. Scarcella[152], V. Scarfone[40a,40b], J. Schaarschmidt[140], P. Schacht[103], B. M. Schachtner[102], D. Schaefer[32], L. Schaefer[124], R. Schaefer[45], J. Schaeffer[86], S. Schaepe[23], S. Schaetzel[60b], U. Schäfer[86], A. C. Schaffer[119], D. Schaile[102], R. D. Schamberger[150], V. Scharf[60a], V. A. Schegelsky[125], D. Scheirich[131], M. Schernau[166], C. Schiavi[53a,53b], S. Schier[139], C. Schillo[51], M. Schioppa[40a,40b], S. Schlenker[32], K. R. Schmidt-Sommerfeld[103], K. Schmieden[32], C. Schmitt[86], S. Schmitt[45], S. Schmitz[86], B. Schneider[163a], U. Schnoor[51], L. Schoeffel[138], A. Schoening[60b], B. D. Schoenrock[93], E. Schopf[23], M. Schott[86], J. F. P. Schouwenberg[108], J. Schovancova[8], S. Schramm[52], M. Schreyer[177], N. Schuh[86], A. Schulte[86], M. J. Schultens[23], H.-C. Schultz-Coulon[60a], H. Schulz[17], M. Schumacher[51], B. A. Schumm[139], Ph. Schune[138], A. Schwartzman[145], T. A. Schwarz[92], H. Schweiger[87], Ph. Schwemling[138], R. Schwienhorst[93], J. Schwindling[138], T. Schwindt[23], G. Sciolla[25], F. Scuri[126a,126b], F. Scutti[91], J. Searcy[92], P. Seema[23], S. C. Seidel[107], A. Seiden[139], F. Seifert[130], J. M. Seixas[26a], G. Sekhniaidze[106a], K. Sekhon[92], S. J. Sekula[43], N. Semprini-Cesari[22a,22b], C. Serfon[121], L. Serin[119], L. Serkin[167a,167b], M. Sessa[136a,136b], R. Seuster[172], H. Severini[115], T. Sfiligoj[78], F. Sforza[32], A. Sfyrla[52], E. Shabalina[57], N. W. Shaikh[148a,148b], L. Y. Shan[35a], R. Shang[169], J. T. Shank[24], M. Shapiro[16], P. B. Shatalov[99], K. Shaw[167a,167b], S. M. Shaw[87], A. Shcherbakova[148a,148b], C. Y. Shehu[151], Y. Shen[115], P. Sherwood[81], L. Shi[153,ak], S. Shimizu[70], C. O. Shimmin[166], M. Shimojima[104], S. Shirabe[73], M. Shiyakova[68,al], J. Shlomi[175], A. Shmeleva[98], D. Shoaleh Saadi[97], M. J. Shochet[33], S. Shojaii[94a], D. R. Shope[115], S. Shrestha[113], E. Shulga[100], M. A. Shupe[7], P. Sicho[129], A. M. Sickles[169], P. E. Sidebo[149], E. Sideras Haddad[147c], O. Sidiropoulou[177], D. Sidorov[116], A. Sidoti[22a,22b], F. Siegert[47], Dj. Sijacki[14], J. Silva[128a,128d], S. B. Silverstein[148a], V. Simak[130], Lj. Simic[14], S. Simion[119], E. Simioni[86], B. Simmons[81], M. Simon[86], P. Sinervo[161], N. B. Sinev[118], M. Sioli[22a,22b], G. Siragusa[177], I. Siral[92], S. Yu. Sivoklokov[101], J. Sjölin[148a,148b], M. B. Skinner[75], P. Skubic[115], M. Slater[19], T. Slavicek[130], M. Slawinska[109], K. Sliwa[165], R. Slovak[131], V. Smakhtin[175], B. H. Smart[5], L. Smestad[15], J. Smiesko[146a], S. Yu. Smirnov[100], Y. Smirnov[100], L. N. Smirnova[101,am], O. Smirnova[84], J. W. Smith[57], M. N. K. Smith[38], R. W. Smith[38], M. Smizanska[75], K. Smolek[130], A. A. Snesarev[98], I. M. Snyder[118], S. Snyder[27], R. Sobie[172,m], F. Socher[47], A. Soffer[155], D. A. Soh[153], G. Sokhrannyi[78], C. A. Solans Sanchez[32], M. Solar[130], E. Yu. Soldatov[100], U. Soldevila[170], A. A. Solodkov[132], A. Soloshenko[68], O. V. Solovyanov[132], V. Solovyev[125], P. Sommer[51], H. Son[165], H. Y. Song[36a,an], A. Sood[16], A. Sopczak[130], V. Sopko[130], V. Sorin[13], D. Sosa[60b], C. L. Sotiropoulou[126a,126b], R. Soualah[167a,167c], A. M. Soukharev[111,c], D. South[45], B. C. Sowden[80], S. Spagnolo[76a,76b], M. Spalla[126a,126b], M. Spangenberg[173], F. Spanò[80], D. Sperlich[17], F. Spettel[103], T. M. Spieker[60a], R. Spighi[22a], G. Spigo[32], L. A. Spiller[91], M. Spousta[131], R. D. St. Denis[56,*], A. Stabile[94a], R. Stamen[60a], S. Stamm[17], E. Stanecka[42], R. W. Stanek[6], C. Stanescu[136a], M. Stanescu-Bellu[45], M. M. Stanitzki[45], S. Stapnes[121], E. A. Starchenko[132], G. H. Stark[33], J. Stark[58], P. Staroba[129], P. Starovoitov[60a], S. Stärz[32], R. Staszewski[42], P. Steinberg[27], B. Stelzer[144], H. J. Stelzer[32], O. Stelzer-Chilton[163a], H. Stenzel[55], G. A. Stewart[56], J. A. Stillings[23], M. C. Stockton[90], M. Stoebe[90], G. Stoicea[28b], P. Stolte[57], S. Stonjek[103], A. R. Stradling[8], A. Straessner[47], M. E. Stramaglia[18], J. Strandberg[149], S. Strandberg[148a,148b], A. Strandlie[121], M. Strauss[115], P. Strizenec[146b], R. Ströhmer[177], D. M. Strom[118], R. Stroynowski[43], A. Strubig[108], S. A. Stucci[27], B. Stugu[15], N. A. Styles[45], D. Su[145], J. Su[127], S. Suchek[60a], Y. Sugaya[120], M. Suk[130], V. V. Sulin[98], S. Sultansoy[4c], T. Sumida[71], S. Sun[59], X. Sun[3], K. Suruliz[151], C. J. E. Suster[152], M. R. Sutton[151], S. Suzuki[69], M. Svatos[129], M. Swiatlowski[33], S. P. Swift[2], I. Sykora[146a], T. Sykora[131], D. Ta[51], K. Tackmann[45], J. Taenzer[155], A. Taffard[166], R. Tafirout[163a], N. Taiblum[155], H. Takai[27], R. Takashima[72], T. Takeshita[142], Y. Takubo[69], M. Talby[88], A. A. Talyshev[111,c], J. Tanaka[157], M. Tanaka[159], R. Tanaka[119], S. Tanaka[69], R. Tanioka[70], B. B. Tannenwald[113], S. Tapia Araya[34b], S. Tapprogge[86], S. Tarem[154], G. F. Tartarelli[94a], P. Tas[131], M. Tasevsky[129], T. Tashiro[71], E. Tassi[40a,40b], A. Tavares Delgado[128a,128b], Y. Tayalati[137d], A. C. Taylor[107], G. N. Taylor[91], P. T. E. Taylor[91], W. Taylor[163b], F. A. Teischinger[32], P. Teixeira-Dias[80], K. K. Temming[51], D. Temple[144], H. Ten Kate[32], P. K. Teng[153], J. J. Teoh[120], F. Tepel[178], S. Terada[69], K. Terashi[157], J. Terron[85], S. Terzo[13], M. Testa[50], R. J. Teuscher[161,m], T. Theveneaux-Pelzer[88], J. P. Thomas[19], J. Thomas-Wilsker[80], P. D. Thompson[19], A. S. Thompson[56], L. A. Thomsen[179], E. Thomson[124], M. J. Tibbetts[16], R. E. Ticse Torres[88], V. O. Tikhomirov[98,ao], Yu. A. Tikhonov[111,c], S. Timoshenko[100], P. Tipton[179], S. Tisserant[88], K. Todome[159], S. Todorova-Nova[5], J. Tojo[73], S. Tokár[146a], K. Tokushuku[69], E. Tolley[59], L. Tomlinson[87], M. Tomoto[105], L. Tompkins[145,ap], K. Toms[107], B. Tong[59], P. Tornambe[51], E. Torrence[118], H. Torres[144], E. Torró Pastor[140], J. Toth[88,aq], F. Touchard[88], D. R. Tovey[141], T. Trefzger[177], A. Tricoli[27], I. M. Trigger[163a], S. Trincaz-Duvoid[83], M. F. Tripiana[13], W. Trischuk[161], B. Trocmé[58], A. Trofymov[45], C. Troncon[94a], M. Trottier-McDonald[16], M. Trovatelli[172], L. Truong[167a,167c], M. Trzebinski[42], A. Trzupek[42], J. C.-L. Tseng[122], P. V. Tsiareshka[95], G. Tsipolitis[10], N. Tsirintanis[9], S. Tsiskaridze[13], V. Tsiskaridze[51], E. G. Tskhadadze[54a], K. M. Tsui[62a],

I. I. Tsukerman[99], V. Tsulaia[16], S. Tsuno[69], D. Tsybychev[150], Y. Tu[62b], A. Tudorache[28b], V. Tudorache[28b], T. T. Tulbure[28a], A. N. Tuna[59], S. A. Tupputi[22a,22b], S. Turchikhin[68], D. Turgeman[175], I. Turk Cakir[4b,ar], R. Turra[94a,94b], P. M. Tuts[38], G. Ucchielli[22a,22b], I. Ueda[69], M. Ughetto[148a,148b], F. Ukegawa[164], G. Unal[32], A. Undrus[27], G. Unel[166], F. C. Ungaro[91], Y. Unno[69], C. Unverdorben[102], J. Urban[146b], P. Urquijo[91], P. Urrejola[86], G. Usai[8], J. Usui[69], L. Vacavant[88], V. Vacek[130], B. Vachon[90], C. Valderanis[102], E. Valdes Santurio[148a,148b], N. Valencic[109], S. Valentinetti[22a,22b], A. Valero[170], L. Valery[13], S. Valkar[131], J. A. Valls Ferrer[170], W. Van Den Wollenberg[109], P. C. Van Der Deijl[109], H. van der Graaf[109], N. van Eldik[154], P. van Gemmeren[6], J. Van Nieuwkoop[144], I. van Vulpen[109], M. C. van Woerden[109], M. Vanadia[134a,134b], W. Vandelli[32], R. Vanguri[124], A. Vaniachine[160], P. Vankov[109], G. Vardanyan[180], R. Vari[134a], E. W. Varnes[7], T. Varol[43], D. Varouchas[83], A. Vartapetian[8], K. E. Varvell[152], J. G. Vasquez[179], G. A. Vasquez[34b], F. Vazeille[37], T. Vazquez Schroeder[90], J. Veatch[57], V. Veeraraghavan[7], L. M. Veloce[161], F. Veloso[128a,128c], S. Veneziano[134a], A. Ventura[76a,76b], M. Venturi[172], N. Venturi[161], A. Venturini[25], V. Vercesi[123a], M. Verducci[134a,134b], W. Verkerke[109], J. C. Vermeulen[109], M. C. Vetterli[144,d], O. Viazlo[84], I. Vichou[169,*], T. Vickey[141], O. E. Vickey Boeriu[141], G. H. A. Viehhauser[122], S. Viel[16], L. Vigani[122], M. Villa[22a,22b], M. Villaplana Perez[94a,94b], E. Vilucchi[50], M. G. Vincter[31], V. B. Vinogradov[68], A. Vishwakarma[45], C. Vittori[22a,22b], I. Vivarelli[151], S. Vlachos[10], M. Vlasak[130], M. Vogel[178], P. Vokac[130], G. Volpi[126a,126b], M. Volpi[91], H. von der Schmitt[103], E. von Toerne[23], V. Vorobel[131], K. Vorobev[100], M. Vos[170], R. Voss[32], J. H. Vossebeld[77], N. Vranjes[14], M. Vranjes Milosavljevic[14], V. Vrba[130], M. Vreeswijk[109], R. Vuillermet[32], I. Vukotic[33], P. Wagner[23], W. Wagner[178], H. Wahlberg[74], S. Wahrmund[47], J. Wakabayashi[105], J. Walder[75], R. Walker[102], W. Walkowiak[143], V. Wallangen[148a,148b], C. Wang[35b], C. Wang[36b,as], F. Wang[176], H. Wang[16], H. Wang[3], J. Wang[45], J. Wang[152], K. Wang[90], Q. Wang[115], R. Wang[6], S. M. Wang[153], T. Wang[38], W. Wang[36a], C. Wanotayaroj[118], A. Warburton[90], C. P. Ward[30], D. R. Wardrope[81], A. Washbrook[49], P. M. Watkins[19], A. T. Watson[19], M. F. Watson[19], G. Watts[140], S. Watts[87], B. M. Waugh[81], S. Webb[86], M. S. Weber[18], S. W. Weber[177], S. A. Weber[31], J. S. Webster[6], A. R. Weidberg[122], B. Weinert[64], J. Weingarten[57], C. Weiser[51], H. Weits[109], P. S. Wells[32], T. Wenaus[27], T. Wengler[32], S. Wenig[32], N. Wermes[23], M. D. Werner[67], P. Werner[32], M. Wessels[60a], J. Wetter[165], K. Whalen[118], N. L. Whallon[140], A. M. Wharton[75], A. White[8], M. J. White[1], R. White[34b], D. Whiteson[166], F. J. Wickens[133], W. Wiedenmann[176], M. Wielers[133], C. Wiglesworth[39], L. A. M. Wiik-Fuchs[23], A. Wildauer[103], F. Wilk[87], H. G. Wilkens[32], H. H. Williams[124], S. Williams[109], C. Willis[93], S. Willocq[89], J. A. Wilson[19], I. Wingerter-Seez[5], F. Winklmeier[118], O. J. Winston[151], B. T. Winter[23], M. Wittgen[145], M. Wobisch[82,r], T. M. H. Wolf[109], R. Wolff[88], M. W. Wolter[42], H. Wolters[128a,128c], S. D. Worm[133], B. K. Wosiek[42], J. Wotschack[32], M. J. Woudstra[87], K. W. Wozniak[42], M. Wu[58], M. Wu[33], S. L. Wu[176], X. Wu[52], Y. Wu[92], T. R. Wyatt[87], B. M. Wynne[49], S. Xella[39], Z. Xi[92], D. Xu[35a], L. Xu[27], B. Yabsley[152], S. Yacoob[147a], D. Yamaguchi[159], Y. Yamaguchi[120], A. Yamamoto[69], S. Yamamoto[157], T. Yamanaka[157], K. Yamauchi[105], Y. Yamazaki[70], Z. Yan[24], H. Yang[36c], H. Yang[176], Y. Yang[153], Z. Yang[15], W.-M. Yao[16], Y. C. Yap[83], Y. Yasu[69], E. Yatsenko[5], K. H. Yau Wong[23], J. Ye[43], S. Ye[27], I. Yeletskikh[68], E. Yildirim[86], K. Yorita[174], R. Yoshida[6], K. Yoshihara[124], C. Young[145], C. J. S. Young[32], S. Youssef[24], D. R. Yu[16], J. Yu[8], J. Yu[67], L. Yuan[70], S. P. Y. Yuen[23], I. Yusuff[30,at], B. Zabinski[42], G. Zacharis[10], R. Zaidan[13], A. M. Zaitsev[132,af], N. Zakharchuk[45], J. Zalieckas[15], A. Zaman[150], S. Zambito[59], D. Zanzi[91], C. Zeitnitz[178], M. Zeman[130], A. Zemla[41a], J. C. Zeng[169], Q. Zeng[145], O. Zenin[132], T. Ženiš[146a], D. Zerwas[119], D. Zhang[92], F. Zhang[176], G. Zhang[36a,an], H. Zhang[35b], J. Zhang[6], L. Zhang[51], L. Zhang[36a], M. Zhang[169], R. Zhang[23], R. Zhang[36a,as], X. Zhang[36b], Y. Zhang[35a], Z. Zhang[119], X. Zhao[43], Y. Zhao[36b,au], Z. Zhao[36a], A. Zhemchugov[68], J. Zhong[122], B. Zhou[92], C. Zhou[176], L. Zhou[43], M. Zhou[35a], M. Zhou[150], N. Zhou[35c], C. G. Zhu[36b], H. Zhu[35a], J. Zhu[92], Y. Zhu[36a], X. Zhuang[35a], K. Zhukov[98], A. Zibell[177], D. Zieminska[64], N. I. Zimine[68], C. Zimmermann[86], S. Zimmermann[51], Z. Zinonos[103], M. Zinser[86], M. Ziolkowski[143], L. Živković[14], G. Zobernig[176], A. Zoccoli[22a,22b], M. zur Nedden[17], L. Zwalinski[32]

1 Department of Physics, University of Adelaide, Adelaide, SA, Australia

2 Physics Department, SUNY Albany, Albany, NY, USA

3 Department of Physics, University of Alberta, Edmonton, AB, Canada

4 (a)Department of Physics, Ankara University, Ankara, Turkey; (b)Istanbul Aydin University, Istanbul, Turkey; (c)Division of Physics, TOBB University of Economics and Technology, Ankara, Turkey

5 LAPP, CNRS/IN2P3 and Université Savoie Mont Blanc, Annecy-le-Vieux, France

6 High Energy Physics Division, Argonne National Laboratory, Argonne, IL, USA

7 Department of Physics, University of Arizona, Tucson, AZ, USA

8 Department of Physics, The University of Texas at Arlington, Arlington, TX, USA

9 Physics Department, National and Kapodistrian University of Athens, Athens, Greece

10 Physics Department, National Technical University of Athens, Zografou, Greece

11 Department of Physics, The University of Texas at Austin, Austin, TX, USA

[12] Institute of Physics, Azerbaijan Academy of Sciences, Baku, Azerbaijan

[13] Institut de Física d'Altes Energies (IFAE), The Barcelona Institute of Science and Technology, Barcelona, Spain

[14] Institute of Physics, University of Belgrade, Belgrade, Serbia

[15] Department for Physics and Technology, University of Bergen, Bergen, Norway

[16] Physics Division, Lawrence Berkeley National Laboratory and University of California, Berkeley, CA, USA

[17] Department of Physics, Humboldt University, Berlin, Germany

[18] Albert Einstein Center for Fundamental Physics and Laboratory for High Energy Physics, University of Bern, Bern, Switzerland

[19] School of Physics and Astronomy, University of Birmingham, Birmingham, UK

[20] [a]Department of Physics, Bogazici University, Istanbul, Turkey; [b]Department of Physics Engineering, Gaziantep University, Gaziantep, Turkey; [c]Istanbul Bilgi University, Faculty of Engineering and Natural Sciences, Istanbul, Turkey; [d]Bahcesehir University, Faculty of Engineering and Natural Sciences, Istanbul, Turkey

[21] Centro de Investigaciones, Universidad Antonio Narino, Bogota, Colombia

[22] [a]INFN Sezione di Bologna, Bologna, Italy; [b]Dipartimento di Fisica e Astronomia, Università di Bologna, Bologna, Italy

[23] Physikalisches Institut, University of Bonn, Bonn, Germany

[24] Department of Physics, Boston University, Boston, MA, USA

[25] Department of Physics, Brandeis University, Waltham, MA, USA

[26] [a]Universidade Federal do Rio De Janeiro COPPE/EE/IF, Rio de Janeiro, Brazil; [b]Electrical Circuits Department, Federal University of Juiz de Fora (UFJF), Juiz de Fora, Brazil; [c]Federal University of Sao Joao del Rei (UFSJ), Sao Joao del Rei, Brazil; [d]Instituto de Fisica, Universidade de Sao Paulo, Sao Paulo, Brazil

[27] Physics Department, Brookhaven National Laboratory, Upton, NY, USA

[28] [a]Transilvania University of Brasov, Brasov, Romania; [b]Horia Hulubei National Institute of Physics and Nuclear Engineering, Bucharest, Romania; [c]Physics Department, National Institute for Research and Development of Isotopic and Molecular Technologies, Cluj Napoca, Romania; [d]West University in Timisoara, Timisoara, Romania

[29] Departamento de Física, Universidad de Buenos Aires, Buenos Aires, Argentina

[30] Cavendish Laboratory, University of Cambridge, Cambridge, UK

[31] Department of Physics, Carleton University, Ottawa, ON, Canada

[32] CERN, Geneva, Switzerland

[33] Enrico Fermi Institute, University of Chicago, Chicago, IL, USA

[34] [a]Departamento de Física, Pontificia Universidad Católica de Chile, Santiago, Chile; [b]Departamento de Física, Universidad Técnica Federico Santa María, Valparaiso, Chile

[35] [a]Institute of High Energy Physics, Chinese Academy of Sciences, Beijing, China; [b]Department of Physics, Nanjing University, Jiangsu, China; [c]Physics Department, Tsinghua University, Beijing 100084, China

[36] [a]Department of Modern Physics, University of Science and Technology of China, Anhui, China; [b]School of Physics, Shandong University, Shandong, China; [c]Department of Physics and Astronomy, Shanghai Key Laboratory for Particle Physics and Cosmology, Shanghai Jiao Tong University (also affiliated with PKU-CHEP), Shanghai, China

[37] Laboratoire de Physique Corpusculaire, Université Clermont Auvergne niversité Blaise Pascal, CNRS/IN2P3, Clermont-Ferrand, France

[38] Nevis Laboratory, Columbia University, Irvington, NY, USA

[39] Niels Bohr Institute, University of Copenhagen, Copenhagen, Denmark

[40] [a]INFN Gruppo Collegato di Cosenza, Laboratori Nazionali di Frascati, Frascati, Italy; [b]Dipartimento di Fisica, Università della Calabria, Rende, Italy

[41] [a]Faculty of Physics and Applied Computer Science, AGH University of Science and Technology, Krakow, Poland; [b]Marian Smoluchowski Institute of Physics, Jagiellonian University, Kraków, Poland

[42] Institute of Nuclear Physics, Polish Academy of Sciences, Kraków, Poland

[43] Physics Department, Southern Methodist University, Dallas, TX, USA

[44] Physics Department, University of Texas at Dallas, Richardson, TX, USA

[45] DESY, Hamburg and Zeuthen, Germany

[46] Lehrstuhl für Experimentelle Physik IV, Technische Universität Dortmund, Dortmund, Germany

[47] Institut für Kern-und Teilchenphysik, Technische Universität Dresden, Dresden, Germany

[48] Department of Physics, Duke University, Durham, NC, USA

[49] SUPA-School of Physics and Astronomy, University of Edinburgh, Edinburgh, UK

[50] INFN Laboratori Nazionali di Frascati, Frascati, Italy

[51] Fakultät für Mathematik und Physik, Albert-Ludwigs-Universität, Freiburg, Germany

[52] Departement de Physique Nucleaire et Corpusculaire, Université de Genève, Geneva, Switzerland

[53] [a]INFN Sezione di Genova, Genoa, Italy; [b]Dipartimento di Fisica, Università di Genova, Genoa, Italy

[54] [a]E. Andronikashvili Institute of Physics, Iv. Javakhishvili Tbilisi State University, Tbilisi, Georgia; [b]High Energy Physics Institute, Tbilisi State University, Tbilisi, Georgia

[55] II Physikalisches Institut, Justus-Liebig-Universität Giessen, Giessen, Germany

[56] SUPA-School of Physics and Astronomy, University of Glasgow, Glasgow, UK

[57] II Physikalisches Institut, Georg-August-Universität, Göttingen, Germany

[58] Laboratoire de Physique Subatomique et de Cosmologie, Université Grenoble-Alpes, CNRS/IN2P3, Grenoble, France

[59] Laboratory for Particle Physics and Cosmology, Harvard University, Cambridge, MA, USA

[60] [a]Kirchhoff-Institut für Physik, Ruprecht-Karls-Universität Heidelberg, Heidelberg, Germany; [b]Physikalisches Institut, Ruprecht-Karls-Universität Heidelberg, Heidelberg, Germany; [c]ZITI Institut für technische Informatik, Ruprecht-Karls-Universität Heidelberg, Mannheim, Germany

[61] Faculty of Applied Information Science, Hiroshima Institute of Technology, Hiroshima, Japan

[62] [a]Department of Physics, The Chinese University of Hong Kong, Shatin, NT, Hong Kong; [b]Department of Physics, The University of Hong Kong, Hong Kong, China; [c]Department of Physics and Institute for Advanced Study, The Hong Kong University of Science and Technology, Clear Water Bay, Kowloon, Hong Kong, China

[63] Department of Physics, National Tsing Hua University, Hsinchu, Taiwan, Taiwan

[64] Department of Physics, Indiana University, Bloomington, IN, USA

[65] Institut für Astro- und Teilchenphysik, Leopold-Franzens-Universität, Innsbruck, Austria

[66] University of Iowa, Iowa City, IA, USA

[67] Department of Physics and Astronomy, Iowa State University, Ames, IA, USA

[68] Joint Institute for Nuclear Research, JINR Dubna, Dubna, Russia

[69] KEK, High Energy Accelerator Research Organization, Tsukuba, Japan

[70] Graduate School of Science, Kobe University, Kobe, Japan

[71] Faculty of Science, Kyoto University, Kyoto, Japan

[72] Kyoto University of Education, Kyoto, Japan

[73] Department of Physics, Kyushu University, Fukuoka, Japan

[74] Instituto de Física La Plata, Universidad Nacional de La Plata and CONICET, La Plata, Argentina

[75] Physics Department, Lancaster University, Lancaster, UK

[76] [a]INFN Sezione di Lecce, Lecce, Italy; [b]Dipartimento di Matematica e Fisica, Università del Salento, Lecce, Italy

[77] Oliver Lodge Laboratory, University of Liverpool, Liverpool, UK

[78] Department of Experimental Particle Physics, Jožef Stefan Institute and Department of Physics, University of Ljubljana, Ljubljana, Slovenia

[79] School of Physics and Astronomy, Queen Mary University of London, London, UK

[80] Department of Physics, Royal Holloway University of London, Surrey, UK

[81] Department of Physics and Astronomy, University College London, London, UK

[82] Louisiana Tech University, Ruston, LA, USA

[83] Laboratoire de Physique Nucléaire et de Hautes Energies, UPMC and Université Paris-Diderot and CNRS/IN2P3, Paris, France

[84] Fysiska institutionen, Lunds universitet, Lund, Sweden

[85] Departamento de Fisica Teorica C-15, Universidad Autonoma de Madrid, Madrid, Spain

[86] Institut für Physik, Universität Mainz, Mainz, Germany

[87] School of Physics and Astronomy, University of Manchester, Manchester, UK

[88] CPPM, Aix-Marseille Université and CNRS/IN2P3, Marseille, France

[89] Department of Physics, University of Massachusetts, Amherst, MA, USA

[90] Department of Physics, McGill University, Montreal, QC, Canada

[91] School of Physics, University of Melbourne, Melbourne, VIC, Australia

[92] Department of Physics, The University of Michigan, Ann Arbor, MI, USA

[93] Department of Physics and Astronomy, Michigan State University, East Lansing, MI, USA

[94] [a]INFN Sezione di Milano, Milan, Italy; [b]Dipartimento di Fisica, Università di Milano, Milan, Italy

[95] B.I. Stepanov Institute of Physics, National Academy of Sciences of Belarus, Minsk, Republic of Belarus

[96] Research Institute for Nuclear Problems of Byelorussian State University, Minsk, Republic of Belarus

[97] Group of Particle Physics, University of Montreal, Montreal, QC, Canada

[98] P.N. Lebedev Physical Institute of the Russian Academy of Sciences, Moscow, Russia

[99] Institute for Theoretical and Experimental Physics (ITEP), Moscow, Russia

[100] National Research Nuclear University MEPhI, Moscow, Russia

[101] D.V. Skobeltsyn Institute of Nuclear Physics, M.V. Lomonosov Moscow State University, Moscow, Russia

[102] Fakultät für Physik, Ludwig-Maximilians-Universität München, Munich, Germany

[103] Max-Planck-Institut für Physik (Werner-Heisenberg-Institut), Munich, Germany

[104] Nagasaki Institute of Applied Science, Nagasaki, Japan

[105] Graduate School of Science and Kobayashi-Maskawa Institute, Nagoya University, Nagoya, Japan

[106] (a)INFN Sezione di Napoli, Naples, Italy; (b)Dipartimento di Fisica, Università di Napoli, Naples, Italy

[107] Department of Physics and Astronomy, University of New Mexico, Albuquerque, NM, USA

[108] Institute for Mathematics, Astrophysics and Particle Physics, Radboud University Nijmegen/Nikhef, Nijmegen, The Netherlands

[109] Nikhef National Institute for Subatomic Physics and University of Amsterdam, Amsterdam, The Netherlands

[110] Department of Physics, Northern Illinois University, DeKalb, IL, USA

[111] Budker Institute of Nuclear Physics, SB RAS, Novosibirsk, Russia

[112] Department of Physics, New York University, New York, NY, USA

[113] Ohio State University, Columbus, OH, USA

[114] Faculty of Science, Okayama University, Okayama, Japan

[115] Homer L. Dodge Department of Physics and Astronomy, University of Oklahoma, Norman, OK, USA

[116] Department of Physics, Oklahoma State University, Stillwater, OK, USA

[117] Palacký University, RCPTM, Olomouc, Czech Republic

[118] Center for High Energy Physics, University of Oregon, Eugene, OR, USA

[119] LAL, Univ. Paris-Sud, CNRS/IN2P3, Université Paris-Saclay, Orsay, France

[120] Graduate School of Science, Osaka University, Osaka, Japan

[121] Department of Physics, University of Oslo, Oslo, Norway

[122] Department of Physics, Oxford University, Oxford, UK

[123] (a)INFN Sezione di Pavia, Pavia, Italy; (b)Dipartimento di Fisica, Università di Pavia, Pavia, Italy

[124] Department of Physics, University of Pennsylvania, Philadelphia, PA, USA

[125] National Research Centre "Kurchatov Institute" B.P.Konstantinov Petersburg Nuclear Physics Institute, St. Petersburg, Russia

[126] (a)INFN Sezione di Pisa, Pisa, Italy; (b)Dipartimento di Fisica E. Fermi, Università di Pisa, Pisa, Italy

[127] Department of Physics and Astronomy, University of Pittsburgh, Pittsburgh, PA, USA

[128] (a)Laboratório de Instrumentação e Física Experimental de Partículas-LIP, Lisbon, Portugal; (b)Faculdade de Ciências, Universidade de Lisboa, Lisbon, Portugal; (c)Department of Physics, University of Coimbra, Coimbra, Portugal; (d)Centro de Física Nuclear da Universidade de Lisboa, Lisbon, Portugal; (e)Departamento de Fisica, Universidade do Minho, Braga, Portugal; (f)Departamento de Fisica Teorica y del Cosmos and CAFPE, Universidad de Granada, Granada, Spain

[129] Institute of Physics, Academy of Sciences of the Czech Republic, Prague, Czech Republic

[130] Czech Technical University in Prague, Prague, Czech Republic

[131] Faculty of Mathematics and Physics, Charles University in Prague, Prague, Czech Republic

[132] State Research Center Institute for High Energy Physics (Protvino), NRC KI, Russia

[133] Particle Physics Department, Rutherford Appleton Laboratory, Didcot, UK

[134] (a)INFN Sezione di Roma, Rome, Italy; (b)Dipartimento di Fisica, Sapienza Università di Roma, Rome, Italy

[135] (a)INFN Sezione di Roma Tor Vergata, Rome, Italy; (b)Dipartimento di Fisica, Università di Roma Tor Vergata, Rome, Italy

[136] (a)INFN Sezione di Roma Tre, Rome, Italy; (b)Dipartimento di Matematica e Fisica, Università Roma Tre, Rome, Italy

[137] (a)Faculté des Sciences Ain Chock, Réseau Universitaire de Physique des Hautes Energies-Université Hassan II, Casablanca, Morocco; (b)Faculté des Sciences Semlalia, Université Cadi Ayyad, LPHEA-Marrakech, Marrakech, Morocco; (c)Faculté des Sciences, Université Mohamed Premier and LPTPM, Oujda, Morocco; (d)Faculté des Sciences, Université Mohammed V, Rabat, Morocco

[138] DSM/IRFU (Institut de Recherches sur les Lois Fondamentales de l'Univers), CEA Saclay (Commissariat à l'Energie Atomique et aux Energies Alternatives), Gif-sur-Yvette, France

[139] Santa Cruz Institute for Particle Physics, University of California Santa Cruz, Santa Cruz, CA, USA

[140] Department of Physics, University of Washington, Seattle, WA, USA

[141] Department of Physics and Astronomy, University of Sheffield, Sheffield, UK

[142] Department of Physics, Shinshu University, Nagano, Japan

[143] Fachbereich Physik, Universität Siegen, Siegen, Germany

[144] Department of Physics, Simon Fraser University, Burnaby, BC, Canada

[145] SLAC National Accelerator Laboratory, Stanford, CA, USA

[146] (a)Faculty of Mathematics, Physics and Informatics, Comenius University, Bratislava, Slovak Republic; (b)Department of Subnuclear Physics, Institute of Experimental Physics of the Slovak Academy of Sciences, Kosice, Slovak Republic

[147] (a)Department of Physics, University of Cape Town, Cape Town, South Africa; (b)Department of Physics, University of Johannesburg, Johannesburg, South Africa; (c)School of Physics, University of the Witwatersrand, Johannesburg, South Africa

[148] (a)Department of Physics, Stockholm University, Stockholm, Sweden; (b)The Oskar Klein Centre, Stockholm, Sweden

[149] Physics Department, Royal Institute of Technology, Stockholm, Sweden

[150] Departments of Physics and Astronomy and Chemistry, Stony Brook University, Stony Brook, NY, USA

[151] Department of Physics and Astronomy, University of Sussex, Brighton, UK

[152] School of Physics, University of Sydney, Sydney, NSW, Australia

[153] Institute of Physics, Academia Sinica, Taipei, Taiwan

[154] Department of Physics, Technion: Israel Institute of Technology, Haifa, Israel

[155] Raymond and Beverly Sackler School of Physics and Astronomy, Tel Aviv University, Tel Aviv, Israel

[156] Department of Physics, Aristotle University of Thessaloniki, Thessaloniki, Greece

[157] International Center for Elementary Particle Physics and Department of Physics, The University of Tokyo, Tokyo, Japan

[158] Graduate School of Science and Technology, Tokyo Metropolitan University, Tokyo, Japan

[159] Department of Physics, Tokyo Institute of Technology, Tokyo, Japan

[160] Tomsk State University, Tomsk, Russia

[161] Department of Physics, University of Toronto, Toronto, ON, Canada

[162] (a)INFN-TIFPA, Povo, Italy; (b)University of Trento, Trento, Italy

[163] (a)TRIUMF, Vancouver, BC, Canada; (b)Department of Physics and Astronomy, York University, Toronto, ON, Canada

[164] Faculty of Pure and Applied Sciences, and Center for Integrated Research in Fundamental Science and Engineering, University of Tsukuba, Tsukuba, Japan

[165] Department of Physics and Astronomy, Tufts University, Medford, MA, USA

[166] Department of Physics and Astronomy, University of California Irvine, Irvine, CA, USA

[167] (a)INFN Gruppo Collegato di Udine, Sezione di Trieste, Udine, Italy; (b)ICTP, Trieste, Italy; (c)Dipartimento di Chimica Fisica e Ambiente, Università di Udine, Udine, Italy

[168] Department of Physics and Astronomy, University of Uppsala, Uppsala, Sweden

[169] Department of Physics, University of Illinois, Urbana, IL, USA

[170] Instituto de Fisica Corpuscular (IFIC) and Departamento de Fisica Atomica, Molecular y Nuclear and Departamento de Ingeniería Electrónica and Instituto de Microelectrónica de Barcelona (IMB-CNM), University of Valencia and CSIC, Valencia, Spain

[171] Department of Physics, University of British Columbia, Vancouver, BC, Canada

[172] Department of Physics and Astronomy, University of Victoria, Victoria, BC, Canada

[173] Department of Physics, University of Warwick, Coventry, UK

[174] Waseda University, Tokyo, Japan

[175] Department of Particle Physics, The Weizmann Institute of Science, Rehovot, Israel

[176] Department of Physics, University of Wisconsin, Madison, WI, USA

[177] Fakultät für Physik und Astronomie, Julius-Maximilians-Universität, Würzburg, Germany

[178] Fakultät für Mathematik und Naturwissenschaften, Fachgruppe Physik, Bergische Universität Wuppertal, Wuppertal, Germany

[179] Department of Physics, Yale University, New Haven, CT, USA

[180] Yerevan Physics Institute, Yerevan, Armenia

[181] Centre de Calcul de l'Institut National de Physique Nucléaire et de Physique des Particules (IN2P3), Villeurbanne, France

[a] Also at Department of Physics, King's College London, London, UK

[b] Also at Institute of Physics, Azerbaijan Academy of Sciences, Baku, Azerbaijan

[c] Also at Novosibirsk State University, Novosibirsk, Russia

[d] Also at TRIUMF, Vancouver, BC, Canada

[e] Also at Department of Physics and Astronomy, University of Louisville, Louisville, KY, USA

[f] Also at Physics Department, An-Najah National University, Nablus, Palestine

[g] Also at Department of Physics, California State University, Fresno, CA, USA

[h] Also at Department of Physics, University of Fribourg, Fribourg, Switzerland

[i] Also at Departament de Fisica de la Universitat Autonoma de Barcelona, Barcelona, Spain

[j] Also at Departamento de Fisica e Astronomia, Faculdade de Ciencias, Universidade do Porto, Porto, Portugal

[k] Also at Tomsk State University, Tomsk, Russia

[l] Also at Universita di Napoli Parthenope, Naples, Italy

[m] Also at Institute of Particle Physics (IPP), Victoria, BC, Canada

[n] Also at Horia Hulubei National Institute of Physics and Nuclear Engineering, Bucharest, Romania

[o] Also at Department of Physics, St. Petersburg State Polytechnical University, St. Petersburg, Russia

[p] Also at Department of Physics, The University of Michigan, Ann Arbor, MI, USA

[q] Also at Centre for High Performance Computing, CSIR Campus, Rosebank, Cape Town, South Africa

[r] Also at Louisiana Tech University, Ruston, LA, USA

[s] Also at Institucio Catalana de Recerca i Estudis Avancats, ICREA, Barcelona, Spain

[t] Also at Graduate School of Science, Osaka University, Osaka, Japan

[u] Also at Institute for Mathematics, Astrophysics and Particle Physics, Radboud University Nijmegen/Nikhef, Nijmegen, The Netherlands

[v] Also at Department of Physics, The University of Texas at Austin, Austin, TX, USA

[w] Also at Institute of Theoretical Physics, Ilia State University, Tbilisi, Georgia

[x] Also at CERN, Geneva, Switzerland

[y] Also at Georgian Technical University (GTU), Tbilisi, Georgia

[z] Also at Ochadai Academic Production, Ochanomizu University, Tokyo, Japan

[aa] Also at Manhattan College, New York, NY, USA

[ab] Also at Academia Sinica Grid Computing, Institute of Physics, Academia Sinica, Taipei, Taiwan

[ac] Also at School of Physics, Shandong University, Shandong, China

[ad] Also at Departamento de Fisica Teorica y del Cosmos and CAFPE, Universidad de Granada, Granada (Spain), Portugal

[ae] Also at Department of Physics, California State University, Sacramento CA, United States of America

[af] Also at Moscow Institute of Physics and Technology, State University, Dolgoprudny, Russia

[ag] Also at Also at Departement de Physique Nucleaire et Corpusculaire, Université de Genève, Geneva, Switzerland

[ah] Also at International School for Advanced Studies (SISSA), Trieste, Italy

[ai] Also at Department of Physics and Astronomy, University of South Carolina, Columbia, SC, USA

[aj] Also at Institut de Física d'Altes Energies (IFAE), The Barcelona Institute of Science and Technology, Barcelona, Spain

[ak] Also at School of Physics, Sun Yat-sen University, Guangzhou, China

[al] Also at Institute for Nuclear Research and Nuclear Energy (INRNE) of the Bulgarian Academy of Sciences, Sofia, Bulgaria

[am] Also at Faculty of Physics, M.V. Lomonosov Moscow State University, Moscow, Russia

[an] Also at Institute of Physics, Academia Sinica, Taipei, Taiwan

[ao] Also at National Research Nuclear University MEPhI, Moscow, Russia

[ap] Also at Department of Physics, Stanford University, Stanford, CA, USA

[aq] Also at Institute for Particle and Nuclear Physics, Wigner Research Centre for Physics, Budapest, Hungary

[ar] Also at Giresun University, Faculty of Engineering, Turkey

[as] Also at CPPM, Aix-Marseille Université and CNRS/IN2P3, Marseille, France

[at] Also at University of Malaya, Department of Physics, Kuala Lumpur, Malaysia

[au] Also at LAL, Univ. Paris-Sud, CNRS/IN2P3, Université Paris-Saclay, Orsay, France

* Deceased